8-19-1991

Computational analysis of space transfer vehicle engine turbopump diffuser design for deep-throttling

Gordon J. Wissinger

COMPUTATIONAL ANALYSIS OF SPACE TRANSFER VEHICLE ENGINE TURBOPUMP DIFFUSER DESIGN FOR DEEP-THROTTLING

by

Gordon J. Wissinger

A Thesis Submitted
in
Partial Fulfillment
of the
Requirements of the Degree of
MASTER OF SCIENCE
in
Mechanical Engineering

Approved by:

Dr. A. Ogut Thesis Advisor (RIT)

Dr. J. S. Torok (RIT)

Mr. J. Veres (NASA Lewis Research Center)

Dr. C. Haines (Department Head, RIT)

Department of Mechanical Engineering
College of Engineering
Rochester Institute of Technology
Rochester, NY 14623
1991

COMPUTATIONAL ANALYSIS OF SPACE TRANSFER VEHICLE ENGINE TURBOPUMP DIFFUSER DESIGN FOR DEEP-THROTTLING

I, Gordon J. Wissinger, herby grant permission to the Wallace Memorial Library of RIT to reproduce my thesis in whole or in part. Any reproduction will not be for commercial use of profit.

August 19, 1991

Dedication

I would like to dedicate this work to the memory of my Grandfather, **Charles R. Mehaffie**. Without his inspiration, I would not have persued Engineering as a career.

Acknowledgements

I would like to thank my family, John and Alice Wissinger, for making the dream possible by allowing me to attend college and to put forth my best effort towards attaing my goals. Their support during the course of my education was uplifting and needed at times.

Aug 1991

ABSTRACT

Space Transfer Vehicles (STV) are expected to perform missions (orbital transfer, Lunar/Mars transfer and descents) which will require deep-engine throttling thrust capability. To accomplish this, turbopumps which can efficiently provide a wide range of flow outputs are needed. The current state-of-the-art cryogenic fuel and oxidizer turbopump designs do not perform efficiently at off-design flow rates mainly due to stall and flow separation in the diffuser. This thesis examines how boundary layer control techniques can be used to control, reduce or eliminate diffuser flow separation.

A finite element based code, FIDAP, was used to study flow in a diffuser by developing a 2-D diffuser model and establishing conditions for flow separation. Various rates of suction (removing decelerating fluid particles) and blowing (reenergizing decelerating fluid particles) were tested for their effectiveness in suppressing or eliminating the flow separation at an off-design flow rate.

The results showed that FIDAP can be used effectively to model boundary layer control by suction and blowing in a diffuser operating at 60% of design flow. Suction was implemented at various flow rates through the top of the diffuser and shown to be effective at a rate of 15% in counteracting the incidence effects at the inlet of the diffuser and reduce the region of flow separation. Blowing was also shown to be effective in reenergizing the boundary layer to reduce the region of flow separation.

Table of Contents

List of Figures

List of Tables

List of Symbols

A_i	=	Coefficient Matrix
A	=	Area
A	=	Differential operator of order 2m
AR	=	Area ratio
B_i	=	Coefficient Matrix
B_i	=	Boundary operator of order n
B_{ij}	=	Element stiffness matrix
B_t	=	Throat blockage
C_i	=	Coefficient Matrix
c	=	Speed of sound
c_1, c_2	=	Empirical constants
c_μ	=	Empirical constant = 0.09
c_p	=	Pressure recovery coefficient
$c_{p\ ideal}$	=	Ideal pressure recovery coefficient
D_i	=	Coefficient Matrix
D_H	=	Hydraulic diameter of diffuser
Δt	=	Change in time
E	=	empirical constant
e	=	Energy
F_i	=	Coefficient Matrix
F	=	Body force term
F	=	Forcing term
G	=	Coefficient Matrix
g_j	=	Boundary condition
I	=	Turbulent intensity
k	=	Turbulent kinetic energy
k^*	=	Dimensionless kinetic energy
K_{ij}	=	Global stiffnes matrix
L_{ij}	=	Coefficient Matrix
L	=	Wall length of diffuser
l(v)	=	Weak form of boundary terms
l_t	=	Turbulent eddy length
M	=	Coefficient Matrix

M_p^{-1}	=	Coefficient Matrix
m	=	Mass flow rate of fluid
M_t	=	Mach number
N	=	Coefficient Matrix
N	=	Axial length of diffuser
P	=	Pressure
p	=	Fluid Pressure
p^*	=	Dimensionless pressure
q	=	Heat flux
Re	=	Reynolds number
T	=	Temperature
t	=	Time
U	=	Global displacement
U	=	Velocity
u	=	Local displacement
u^*	=	Dimensionless velocity
u^*	=	Friction velocity
u^+	=	Dimensionless velocity
u_i	=	Fluid velocity in the i direction
u_t	=	Turbulent eddy velocity
v	=	fluid speed
v	=	test function
v	=	Volume of finite element
v_t	=	Throat velocity
W	=	Diffuser width
x	=	Distance measure
x^*	=	Dimensionless length
y^+	=	Dimensionless normal distance from the wall
2Θ	=	Divergence of diffuser
β	=	
δ^*	=	Momentum boundary layer thickness
$d\Omega^i$	=	Boundary of Ω
ε	=	Penalty parameter
ε	=	Turbulent dissipation
ε^*	=	Dimensionless dissipation

Φ	=	Local basis function
Φ, Ψ, υ	=	column vectors of interpolation funcitons
η	=	Efficiency
η	=	Instantaneous value of N
η	=	Time average of N
κ	=	von Karman constant
μ	=	Absolute fluid viscosity
μ_t	=	Eddy viscosity
N	=	Generic variable
ν	=	Kinematic fluid viscosity
Θ	=	Incidence angle at inlet to diffuser
ρ	=	Fluid density
$\rho u_i' u_j'$	=	Reynolds stress term
σ_ε	=	Turbulent Schmidt number
σ_k	=	Turbulent Prantl number
T	=	Temperature
τ	=	Total shear stress
τ^*	=	Shear stress at the wall
τ_{ij}	=	Viscous stress tensor
Ω	=	Domain
Ψ	=	Global basis function

1 INTRODUCTION

1-1.0 Justification of Work

At the present time, there is a need for throttling thrust capabilities for the NASA Space Transfer Vehicles (STV) in order for them the perform orbital transfer missions and Lunar/Mars transfer and descent. This capability can be attained by designing a high performance liquid hydrogen (LH2) turbopump which can efficiently output a wide range of flow rates and provide the necessary deep engine throttling capability.

The current designs of high pressure, multistage turbopumps with radial vaned diffusers do not provide this capability at off-design flow conditions. The lower flow rates present in this configuration lead to poor diffuser performance (ie. flow separation and diffuser stall) due to impeller discharge effects, increased boundary layer blockage and lack of turbulence intensity in the diffuser. This project investigates possibilities of increasing the diffuser performance at off design flow rates without significantly altering the geometry of the diffuser.

The goal of the project at Rochester Institute of Technology is to develop a pump test station based on the Pratt and Whitney AETB test bed engine turbopump and MK 49-F High Pressure LH2 Turbopump to investigate ways to increase pump efficiency. In order to reduce the amount of actual testing required, 2- and 3-D models have been developed using a finite element based code, FIDAP (Fluid Dynamics Analysis Package). These numerical models will be used to gain a

better understanding of the resulting flow patterns and to test the effectiveness of boundary layer control by suction and blowing.

This thesis presents the results of the 2-D computational work.

1-2.0 Goal of Work

The function of a diffuser is to convert inlet dynamic pressure (kinetic energy) to a static pressure rise. This is done by decelerating the fluid by means of a gradual increase of the cross-sectional area. It is desirable to recover as large a part of the inlet dynamic pressure as possible under a steady flow condition. However, the diffuser performs in an adverse pressure gradient field which limits its efficiency. In an incompressible viscous flow field, the existence of this pressure gradient often leads to stall and flow separation.

The separation occurs when the pressure rise in the main flow is severe enough to bring the boundary layer to rest. Usually, a vortex (stall region) forms just downstream of this stationary point, with near-wall flow reversing direction against the wall. If the flow does not reattach itself, but continues as a high-velocity jet flow away from the wall, the jet dissipates into turbulent mixing and the diffusion process for pressure recovery by and large comes to an end.

The goal of this work is to provide insight into the effectiveness of boundary layer control devices (ie suction and blowing) for the prevention or reduction of stall in a diffuser. In order to justify the added cost it must also be demonstrated that

these techniques allow a pressure recovery that is significantly higher than in a diffuser without controls. These objectives can be achieved by experimental testing, 2- and 3-D numerical modeling, or the combination of both.

Due to the relatively low computer requirements on storage space and computational time, a 2-D finite element model will be used to provide a selective range of suction and blowing rates that most effectively reduce stall. These results will be used in a more extensive 3-D model, allowing it to attain better results in a shorter period of time. The results from the 3-D model will then be used as a basis for the experimental work to be done in a test station.

1-3.0 Description of the System

The MK 49-F High Pressure LH2 Turbopump that was developed for NASA is shown in Figure 1.1. It is a three-stage, centrifugal, high pressure turbopump developed for the Orbital Transfer Vehicle rocket engine. The developer, Rocketdyne, simplified this pump to a single stage water tester (Figure 1.2) to run performance tests [1].* The specific area of interest for this work is the diffuser crossover section where the pressure recovery occurs. The inset of Figure 1.2 shows the individual diffuser under investigation.

---

* Numbers in square brackets refer to references listed at the end of the thesis.

Figure 1.1 - MK 49-F High-Pressure LH2 Turbopump

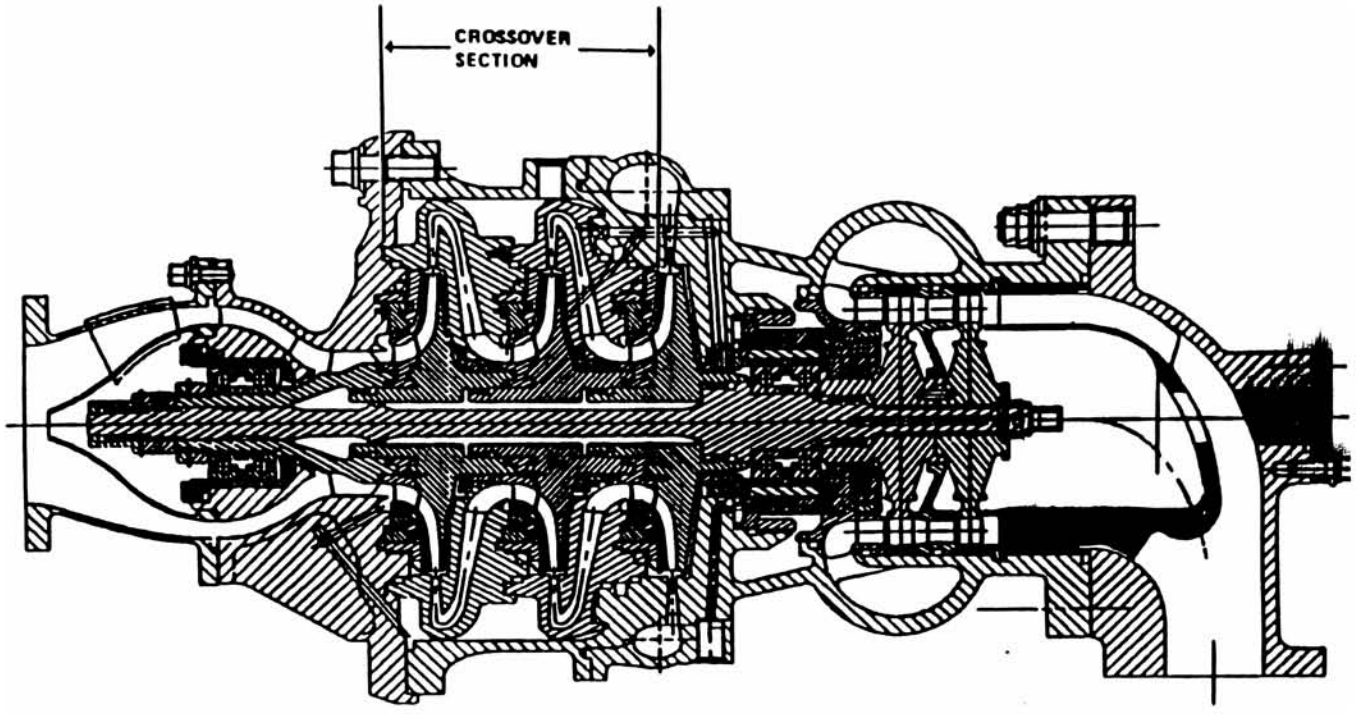

Figure 1.2 - Rocketdyne Water Tester

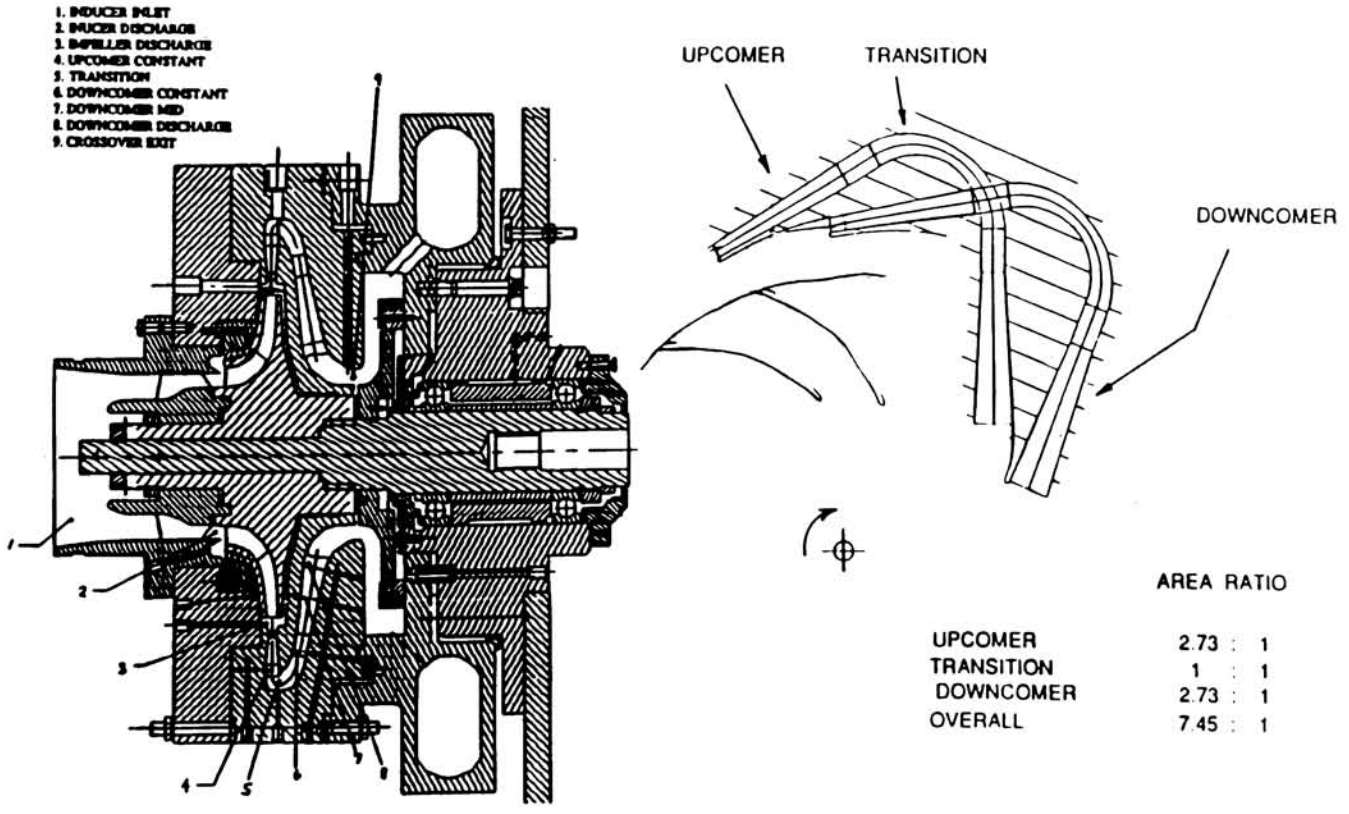

From Figure 1.2, it can be seen that the fluid leaves the impeller blades and enters a vaneless diffuser. From there the fluid enters the upcomer diffuser where the majority of the pressure recovery takes place. Due to the impeller exit effects, the inlet flow to the upcomer diffuser enters at a certain incidence angle which changes as the flow rate changes (Table 1.1). The fluid then travels through a constant area turning channel to the downcomer diffuser to finish the diffusion process.

Table 1.1
Incidence Angles for Rocketdyne Mark-49F Water Tester
(From CPAC)

Percent of Inlet Flow	Incidence Angle (deg)
50	4.82
60	4.19
70	3.55
80	2.89
90	2.19
100	1.49
110	0.77
120	0.02
130	-0.75
140	-1.54

The test station configuration is shown in Figure 1.3. This rig was designed to investigate possible remedies to flow separation and is based on the MK 49-F LH2 turbopump and the Rocketdyne water tester. It is a closed loop water system with the capability of varying the incidence angle at the inlet to the diffuser to mimic actual flow conditions that are present in the pump. It will be run

at various flow rates to produce stall conditions, then the boundary layer control devices will be installed to test the effectiveness of these devices for reducing or eliminating stall.

At the present time, a 3-D model of the experimental diffuser is being generated using FIDAP. As a precursor, a 2-D model was generated (Figure 1.4) to obtain a smaller set of test conditions for this more extensive model. It should be noted that this is not simply a cross section of the 3-D model, nor does it maintain the 3-D area ratio. This diffuser design was chosen because it allowed flow separation while maintaining turbulent flow for testing of boundary layer control devices.

Figure 1.5 shows the 2-D diffuser with slits added for suction and blowing. A total of 14 slits are available for use. The inflow and/or outflow of fluids through these slits is controlled by the boundary conditions imposed in the FIDAP input file. As will be seen in the results, all of these holes are not used at all times.

Results from the Rocketdyne water tester indicate that the inlet mass flow rates of less than 76% of design produced the onset of stall. To guarantee stall as well as to push the desirable lower limit of throttling-thrust capability, a flow rate of 60% of design was chosen as the basis of the tests. The simplification of the model to two-dimensions prohibited the direct transfer of the inlet flow rates while maintaining separation, so a Reynolds number of 10,000 was chosen. In order to maintain applicability to the actual turbopump, the incidence angle of 4.19 degrees present at 60% of design flow rate was used in the tests.

Figure 1.3 - RIT Test Bed Configuration

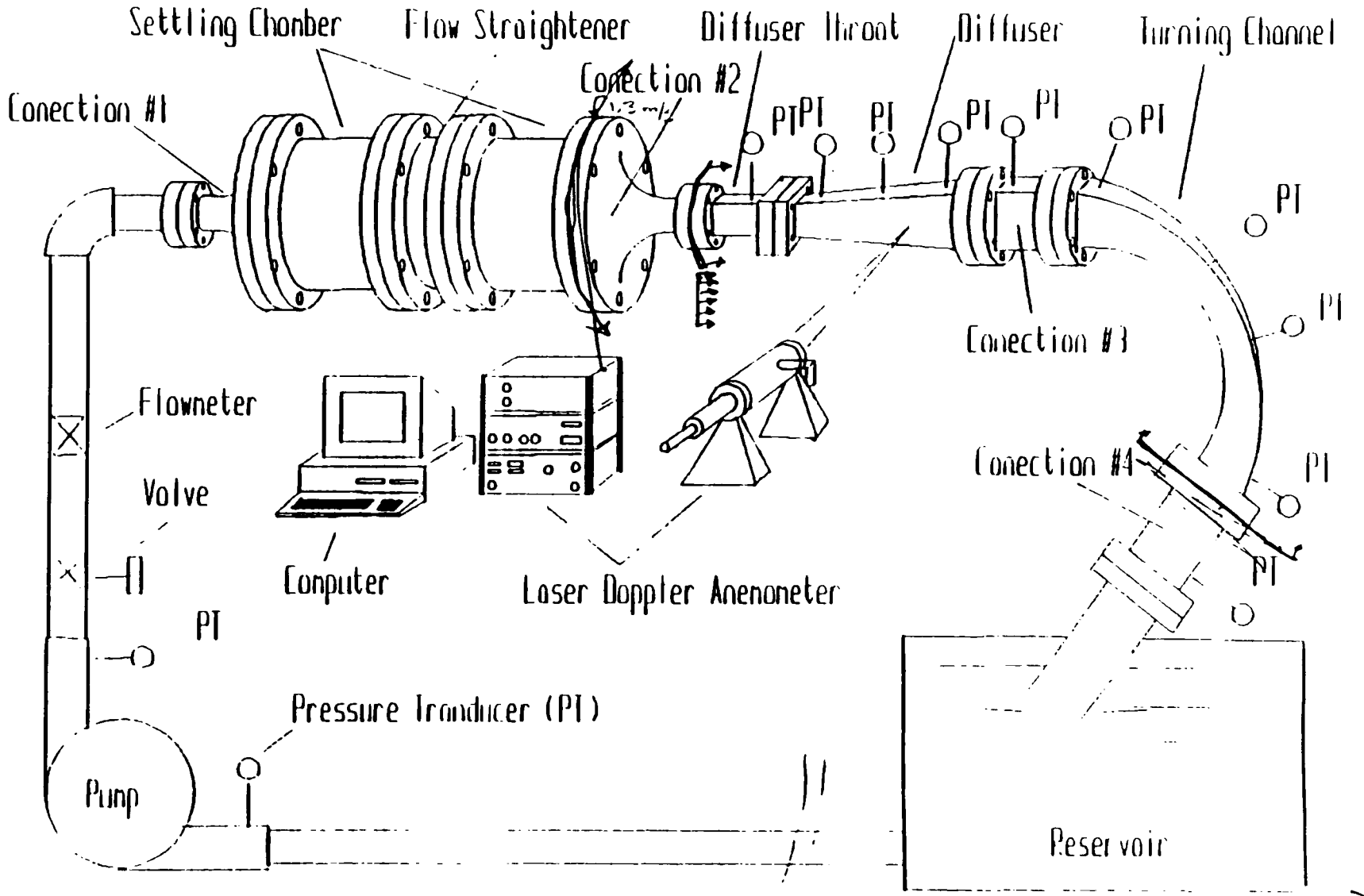

Figure 1.4 - 2-D Diffuser and Turning Channel

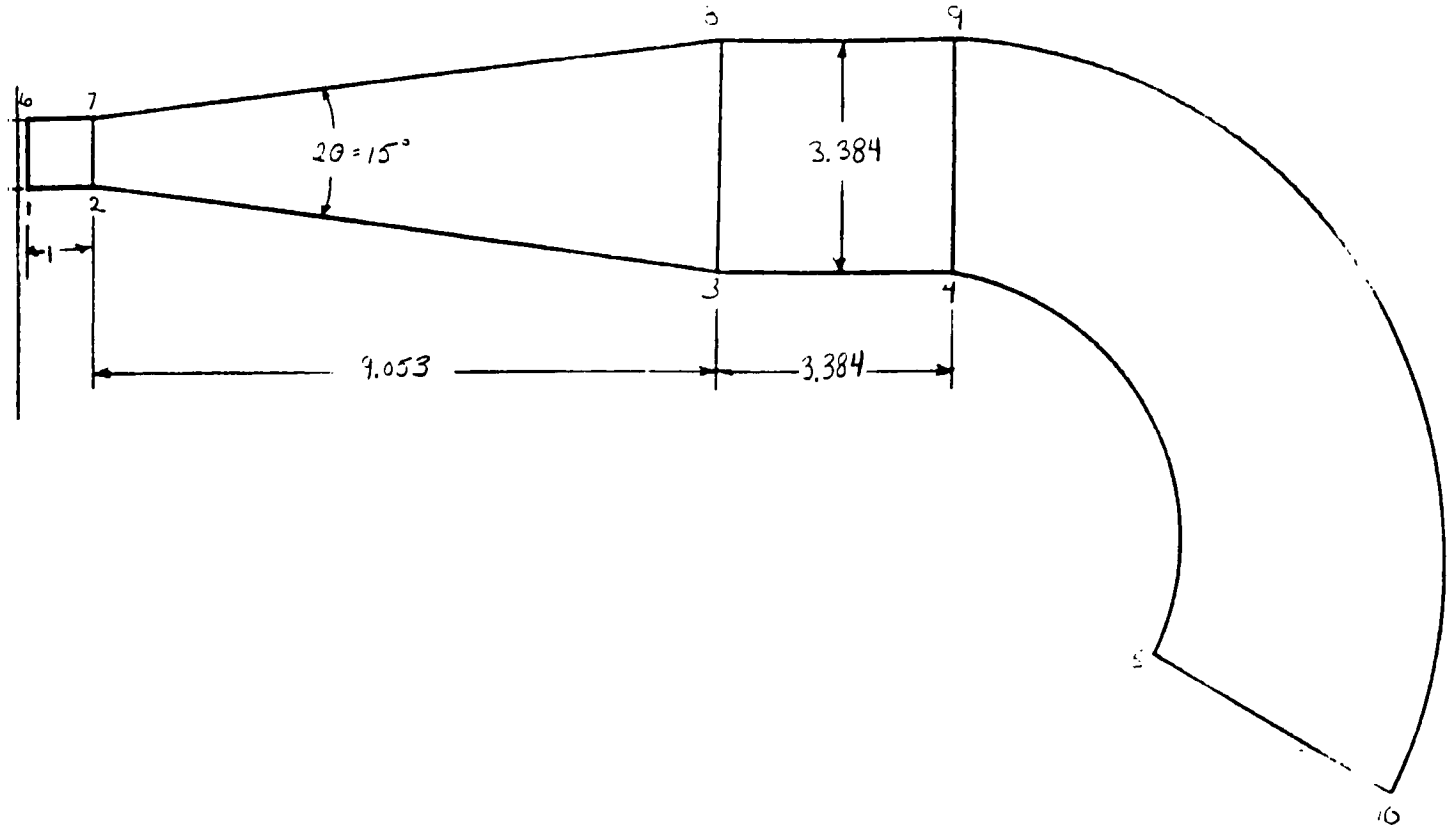

Figure 1.5 - 2-D Diffuser with Suction and Blowing Slits

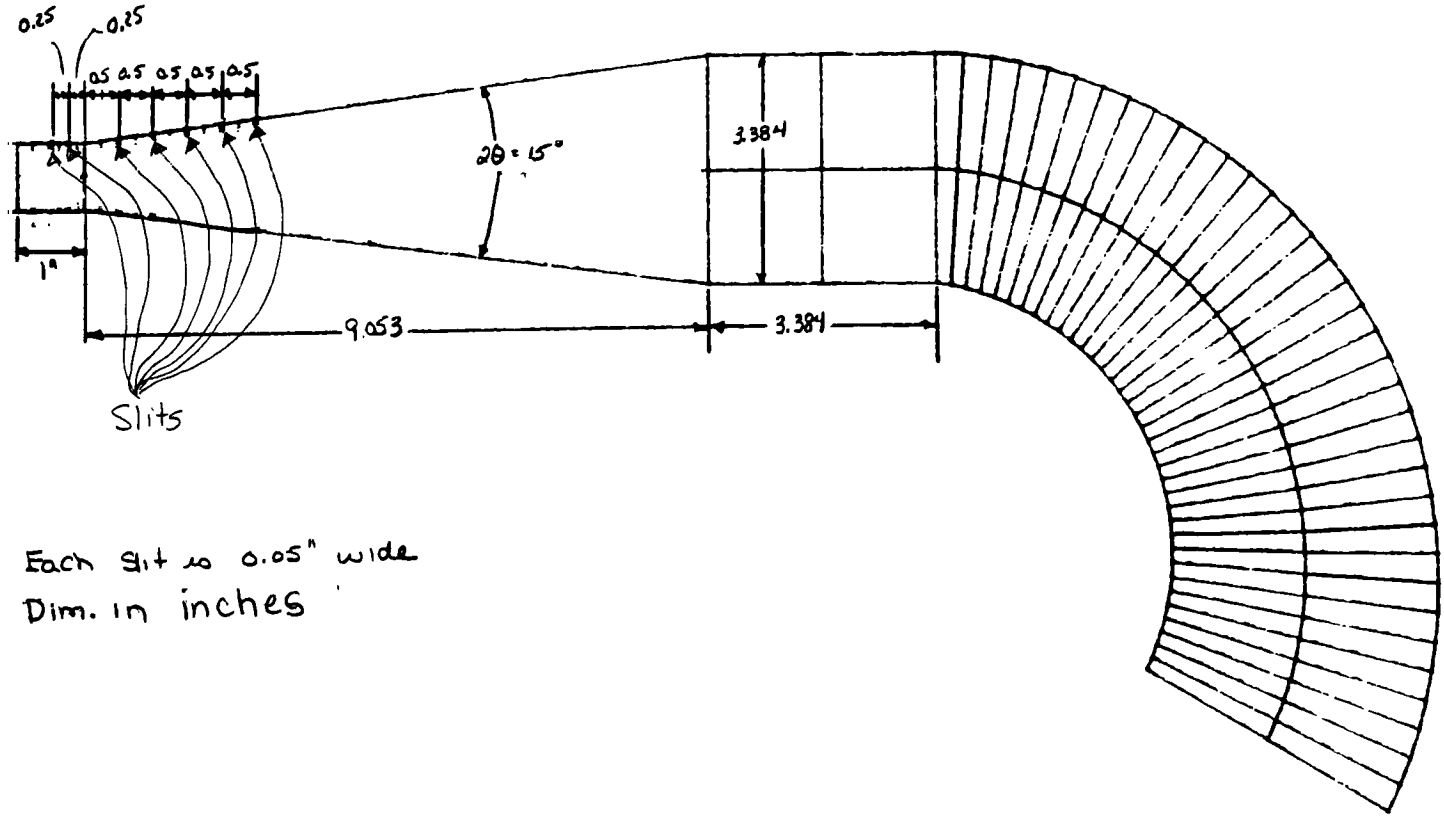

Each slit is 0.05" wide
Dim. in inches

The flow conditions at the inlet to the model remained constant throughout each test and are detailed in Table 1.2 and shown in Figure 1.6. Based on the Reynold's number of 10,000, the mass flow rate of water at the inlet was found to be 0.20887 $\frac{slug}{s\ ft}$ (see Appendix A). The kinetic energy and dissipation were found to be 0.008346 $\frac{ft^2}{s^2}$ and 0.027445 $\frac{ft^2}{s^3}$ respectively [2].

Table 1.2
Flow Conditions

$Re_i = 10{,}000$	$\Theta = -4.19^o$
$\rho = 1.94\ \frac{slug}{ft^2}$	$m_i = 0.20887\ \frac{slug}{s}$
$\mu = 2.089 \times 10^{-5} \frac{lbf\ s}{ft^2}$	$k = 0.008346\ \frac{ft^2}{s^2}$
$D_H = 0.08333$ ft	$\varepsilon = 0.027445\ \frac{ft^2}{s^3}$

Figure 1.6 - Inlet Conditions

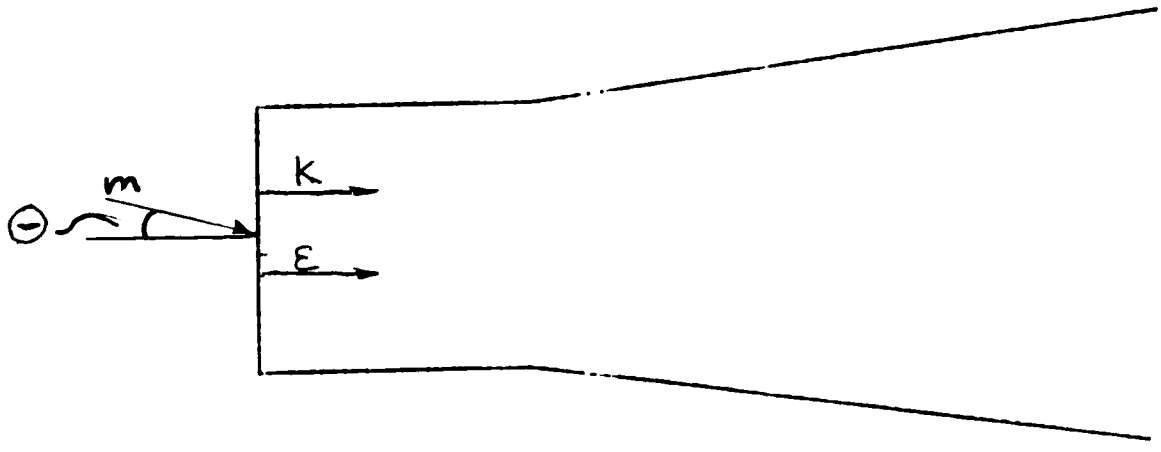

A benchmark test was run on the diffuser with no controls. This test provided the necessary description of how the diffuser worked at present. Due to the pronounced inlet incidence angles, the flow separated along the upper wall of the diffuser.

Based on these results suction and blowing was applied at the top of the diffuser in an attempt to counteract the incidence effects and energize the boundary layer. The fluid was removed from the flow at a 37.5° angle from the diffuser centerline at each of the seven slits. Fluid was injected parallel to the diffuser centerline at the five slits along the diverging wall. The slits were positioned along the wall of the diffuser such that they were shorter in the flow direction and ran the width of the diffuser. The boundary conditions at the slits are specified in Table 1.3 for each model.

Table 1.3
Slit Boundary Conditions

	Model	$m\left(\frac{slug}{ft\ s}\right)$	$u_1\left(\frac{ft}{s}\right)$	$u_2\left(\frac{ft}{s}\right)$
SUCTION				
	5%	0.001492	0.1465	0.1123
	10%	0.002984	0.2929	0.2247
	15%	0.004476	0.4393	0.3371
	20%	0.005968	0.4533	0.3479
BLOWING				
	5%	0.001492	0.1999	0.0
	10%	0.002984	0.3999	0.0
	15%	0.004476	0.5999	0.0

[See Appendix A for sample calculations]

2 EQUATIONS GOVERNING FLUID FLOW

2-1.0 General Navier-Stokes

In order to gain a better understanding of the flow field within the diffuser, we must investigate the governing flow equations paying particular attention to their application to internal flows. Flow in either a laminar or turbulent state can be described at every point in any flow regime for all time by taking into consideration the principals of conservation of mass, momentum and energy. The results are known as Navier Stokes equations and are given respectively by*

$$\rho_{,o} + (\rho u_i)_{,i} = 0 \tag{2.1}$$

$$(\rho u_i)_{,o} = -(\rho u_j u_i)_{,j} + \rho F_i - p_{,i} + \tau_{ji,j} \tag{2.2}$$

$$[\rho(e+0.5v^2)]_{,o} + \vec{\nabla}\cdot[\rho\vec{v}(e+0.5v^2)] = -\vec{\nabla}\cdot\vec{q} + \vec{\nabla}\cdot(\vec{T}\cdot\vec{v}) + \rho v\cdot F \tag{2.3}$$

These equations provide a very general description of a flow field. In many cases the complexity of the solution provided by these equations can be greatly reduced by considering the characteristics of a specific flow. Within the LH2 turbopump diffuser, the flow is steady, incompressible, isothermal and

---

* All of the equations in this thesis will employ the index notation for the equations. For a thorough review of this technique for writing equations in compact form, see [4].

Newtonian in nature. Under these conditions, the conservation of mass and momentum are reduced to

$$u_{i,j} = 0 \tag{2.4}$$

$$\rho(u_j u_i)_{,j} = \rho F_i - p_{,i} + \tau_{ij,j} \tag{2.5}$$

where u is the fluid velocity (i,j = 1,2 for a 2-D problem), ρ is the constant fluid density, F represents the body forces, p is the pressure force and τ_{ij} is the viscous stress tensor representing the normal and shear stresses on the fluid. The energy equation is neglected under the isothermal assumption.

Equations (2.4) and (2.5) form a set of three equations and three unknowns, u_1, u_2, and p, that can be solved to indicate the state of the flow at any point in the domain of interest. For the majority of laminar flows, the resulting flow field is well behaved and obtaining an exact or numerical solution in straight forward. Unfortunately, the same cannot be said for turbulent flows, ene in the simplest of domains. The complexity of this flow phenomenon causes many computational problems during the solution procedure as the next section indicates. These complexities and methods for avoiding them are important since the flows in turbopumps are turbulent.

2-2.0 Turbulent Flow

2-2.1 Definitions and Conventions Used in the Analysis of Turbulent Flows

The computational problems present in turbulent flow analysis are due in part to their nonlinear nature and in part to the wide spectrum of time and length scales that make up the flow domain. The generally accepted model of turbulence characterizes the flow by the existence of eddies within the flow field. The largest scale eddies are associated with the mean flow properties through the continued extraction of kinetic energy from hydrodynamic instabilities in the mean flow. These large eddies are unstable and eventually break down into smaller scale eddies. This process, known as the kinetic energy cascade, continues to repeat itself generating smaller and smaller eddies, each obtaining its kinetic energy from the scale above it. Finally the kinetic energy is removed from the flow by the smallest eddies through turbulent dissipation. These very small eddies are orders of magnitude smaller than the initial mean flow eddies. The existence of these time and scale differences simultaneously in the flow regime means that even the fastest computer cannot effectively solve the resulting flow field exactly. For this reason, it is necessary to approach the problem from a statistical point of view via time averaging.

Time averaging is accomplished in the following manner. If N is a generic variable representing a quantity at any instant in time,

it can be broken down into the sum of its time average quantity and fluctuation

$$N = \bar{\eta} + \eta' \tag{2.6}$$

where the time averaged quantity η is given by

$$\bar{\eta} = \frac{1}{\Delta t} \int_{t}^{t+\Delta t} N \; dt \tag{2.7}$$

(Of course, the time average of η' is equal to zero.) This approach simplifies the measurement and description of turbulent flow fields.

Incorporating the time averaging techniques into (2.4) and (2.5) gives the following results for the turbulent time averaged Navier-Stokes equations. For the rest of the thesis, when dealing with turbulent flows, the overbar indicating an average quantity will be left out for clarity. The quantities without overbars will be assumed to be time averaged in the manner of equation (2.7).

$$u_{i,j} = 0 \tag{2.10}$$

$$\rho u_j u_{i,j} = -p_{,j} + \rho F_i + [\mu(u_{i,j} + u_{j,i}) - \rho\overline{u_i' u_j'}]_{,j} \tag{2.11}$$

The addition of $-\rho\overline{u_i' u_j'}$ (known as the Reynolds stress) to the momentum equation is a result of the averaging process and renders the set of equations (2.10)-(2.11) unsolvable. In order to overcome

the closure problem, an approximation for this term must be introduced.

Before this discussion is undertaken, some definitions must be established. The time averaging technique also provides a basis for some turbulent flow definitions. The intensity of the velocity fluctuations is given by their mean square values $(\overline{u_i'})^2$. Half of this value is defined as the turbulent kinetic energy

$$k = \frac{1}{2}\left(\overline{u_i' u_i'}\right) \tag{2.8}$$

Finally, the intensity of the turbulence in the flow is defined as the ratio of the root mean square of the velocity fluctuations to the mean velocity

$$I = \frac{\left(\frac{1}{3}\overline{u_i' u_i'}\right)^2}{u_i} = \frac{k^2}{36\, u_i} \tag{2.9}$$

This dimensionless quantity is used as an indication of the turbulence level at any point in the flow based on how much the velocity fluctuations deviate from the average flow. Other relationships commonly encountered when discussing turbulent flows are as follows:

$u^+ = \frac{u}{u^*}$	Dimensionless velocity
$y^+ = \frac{\rho u^* y}{\mu}$	Dimensionless normal dist. from wall
$\tau^* = \tau_{tot}$	Shear stress at the wall

$$u^* = \sqrt{\frac{\tau^*}{\rho}}$$ Friction velocity

Based on the above definitions and characteristics of turbulent flows, the flow regime can be divided into distinct regions. The region nearest the wall within a distance of $y^+=5$ is termed the viscous sublayer. Near the centerline of the flow at a distance greater than $y^+=30\text{-}50$ exists the fully developed turbulent region. The region that exists between these two regions, $5<y^+<30\text{-}50$, is termed the buffer region. These regions are shown graphically in Figure 2.1. Each region was defined based on the different characteristics of the flow that exists within each and serves to define more explicitly the complexities of the turbulent flow. These characteristics will be developed and defined in a later section.

Figure 2.1 - Wall Layer

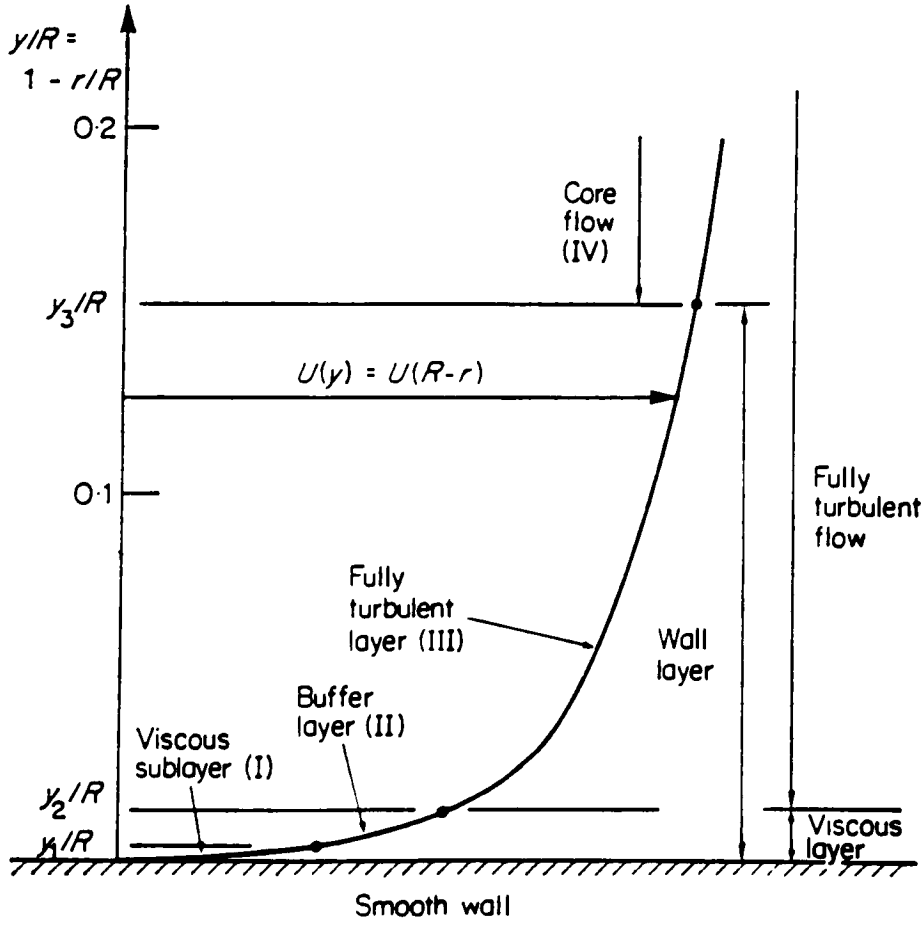

2-2.2 Turbulence Modeling

Over the years, many models have been introduced that provide approximations for the Reynolds stress term of (2.11). Broadly, they can be grouped into two categories: i) Eddy viscosity/diffusivity models and ii) Second moment closure models. The eddy viscosity/diffusivity model was employed in this work and will be discussed here. For a discussion of second moment closure models see [2].

The eddy viscosity/diffusivity model is based on the assumption that the turbulent fluxes of momentum are proportional to the gradients of the mean flow field. This is an indication that the Reynolds stress is dependent soley on the state of the turbulence at any given moment. Boussinesq introduced a term μ_t, the eddy viscosity, to describe this state of turbulence and created an eddy viscosity/diffusivity model given by

$$-\rho\overline{u_i'u_j'} = \mu_t\,(u_{i,j} + u_{j,i}) \qquad (2.12)$$

Through his analysis, Boussinesq reduced the turbulent closure problem to that of determining a single variable μ_t [2].

Since the introduction of the eddy viscosity/diffusivity model there have been many models proposed and used to determine μ_t. The three major catagories of models are termed zero equation, one equation and two equation models. The names are derrived from the number of additional partial differential equations that are solved in addition the to the Navier-Stokes equaitons. As equations are added, the models become more sophisticated and accurate as well as more

difficult to implement. The model chosen for a particular analysis depends on the flow conditions, the required accuracy of the solution and available CPU resources.

The solution used in this work employs the two equation k–ε model. This model has been shown to be more effective [2] in cases of flow separation and adverse pressure gradient flows in order to accurately capture these irregular flow conditions. The resources available to solve the problem were sufficient to allow the use of this more computationally intensive solution method.

The two equation k-ε model represents typical turbulent eddy velocity and length scales based on dimensional reasoning as

$$u_t = k^{0.5} \qquad\qquad l_t = \frac{k^{1.5}}{\varepsilon}$$

where k is the turbulent kinetic energy and ε is the turbulent dissipation. μ_t is proportional to these scales as follows

$$\mu_t \alpha \rho u_t l_t \alpha \frac{\rho k^2}{\varepsilon} \tag{2.13}$$

which leads to

$$\mu_t = c_\mu \frac{\rho k^2}{\varepsilon} \tag{2.14}$$

where c_μ is an emperical constant that has been determined to be 0.09.

Equation (2.12) can now be used along with further dimensional reasoning to obtain two additional transport equations that are solved in additon to the Navier-Stokes equations to provide the necessary solutions for k and ε

$$\rho u_j k_{,j} = \left(\frac{\mu_t}{\sigma_k} k_{,j}\right)_{,j} + \rho G - \varepsilon\rho \qquad (2.15)$$

$$\rho u_j \varepsilon_{,j} = \left(\frac{\mu_t}{\sigma_\varepsilon} \varepsilon_{,j}\right)_{,j} + c_1 \rho \frac{\varepsilon}{k} G - c_2 \rho \frac{\varepsilon^2}{k} \qquad (2.16)$$

where G is the shear generation term as is defined as

$$G = -\overline{u_i' u_j'}\, u_{i,j} = \frac{\mu_t}{\rho}\left(u_{i,j} + u_{j,i}\right) u_{i,j} \qquad (2.16a)$$

and c_1 and c_2 are empirical constants set at 1.44 and 1.92 respectively for isothermal flows. σ_k and σ_ε are the turbulent Prantl and Schmidt numbers respectively, determined to be 1.0 and 1.3 for this flow situation.

The equations (2.10), (2.11) and (2.14)-(2.16) form a set that will approximate the resulting turbulent flow in an internal passage. It must be emphasized that this set of equations is no longer exact and the results generated from it must be interpreted as approximate values.

2-2.3 Turbulent Flow Adjacent to a Solid Boundary

The results presented in section 2-2.2 were developed for high Reynolds number flows and subsequently are useful in the fully developed turbulent region where the velocity profile is rather flat. Due to the imposition of the no-slip condition at the wall, the flow quantities go through extremely sharp changes over a very short distance near the wall. The present analysis breaks down when attempting to traverse this low Reynolds number boundary layer. It is therefore necessary to develop a model that links the no-slip wall conditions with the high Reynolds number mean flow conditions. The models that have been developed are known appropriately as Law-of-the-Wall models. These models assume that the flows near the wall are all similar regardless of the model used in the mean flow approximation.

For this analysis, further assumptions must be made. The flow region under investigation is away from stagnation, reattachment and separation points and the flow is parallel to the wall, there are no strong body forces to contend with, and the pressure gradients are weak. These assumptions do not necessarily hold for diffuser geometries, but this analysis does provide useful insight as to the general nature of flows adjacent to a wall and will be modified to relax the above restrictions.

Employing the above assumptions and a coordinate system with the first (1) axis tangent and the second (2) axis normal to the wall, the tangential momentum equation (2.11) reduces to

$$(\tau_{tot})_{,2} = 0 \qquad (2.17)$$

where τ_{tot} is the sum of the laminar and turbulent shear stress across the flow regime given as

$$\tau_{tot} = \mu u_{1,2} - \rho\overline{u_1'u_2'} \qquad (2.18)$$

where $\mu u_{1,2}$ is the laminar shear stress and $-\rho\overline{u_1'u_2'}$ is the turbulent shear stress. From (2.17) it is seen that τ_{tot} is constant in the near wall region ($y^+<50$). The resulting experimentally determined profiles for each stress is shown in Figure 2.2.

Figure 2.2 - Stress Profiles in the Near Wall Region

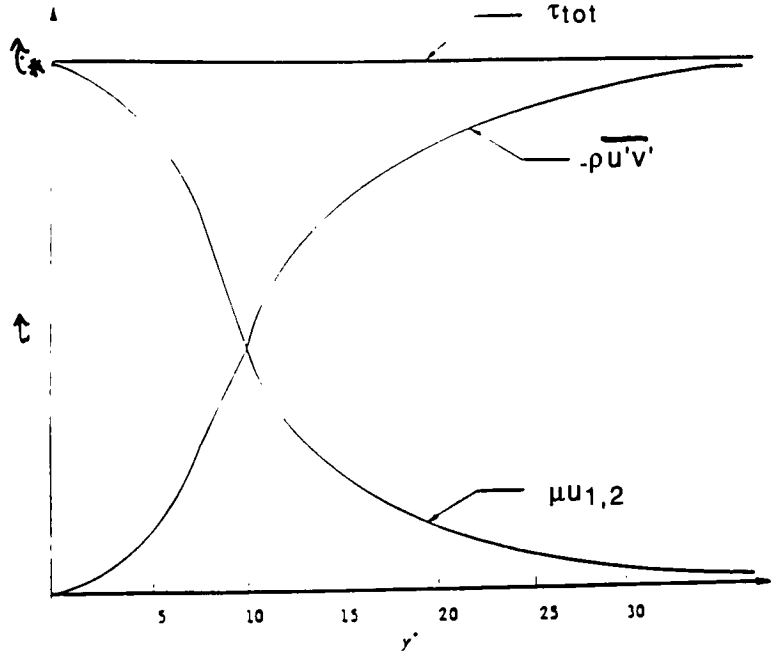

Within the viscous sublayer, the laminar shear dominates the flow conditions. As the flow progresses through the buffer layer, a great deal of turbulence is generated by the increase in the turbulent shear and a corresponding decrease of laminar shear. In the fully

turbulent region, the situation has reversed and the turbulent shear dominates the flow properties. This analysis is in agreement with boundary layer theory that indicates that the fluid viscosity is only accountable within a very narrow region close to the wall.

Using the dominant shear analysis, the velocity profiles in each region can be determined which will allow a Law of the Wall model to be developed. As was indicated in the viscous sublayer ($y^+<5$)

$$\tau_{tot} = \mu u_{1,2} \tag{2.19}$$

By appropriate substitutions and rearrangement, (2.19) leads to

$$\frac{u}{u^*} = \frac{\rho u^* y}{\mu}$$

which by definition is the linear velocity profile

$$u^+ = y^+ \tag{2.20}$$

Beyond $y^+=30$, the viscosity of the fluid does not influence the total shear, so

$$\tau^* = -\rho u_1' u_2' = \rho u^{*2} \tag{2.21}$$

Through dimensional reasoning (2.21) leads to the classical logarithmic velocity profile [2]

$$\frac{u}{u^*} = \frac{1}{\kappa} \ln \frac{E\rho u^* y}{\mu} \qquad (2.22)$$

where κ = 0.41 and is known as the von Karman constant and E is an imperical constant found to be 9.0 for smooth walls. Equations (2.20) and (2.22) are plotted in Figure 2.3 along with a typically employed velocity profile for the entire near wall region.

Figure 2.3 - Universal Velocity Profiles

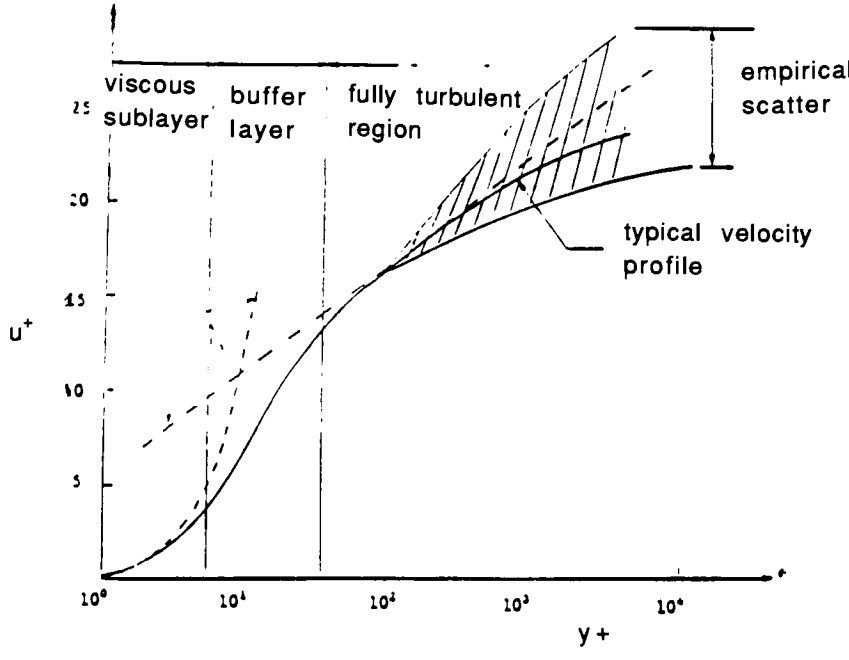

Similarly, the profiles for k and ε in the near wall region exhibit universal characteristics. From dimensional analysis, the equations for k and ε in this region are given by [2]

$$k = c_\mu^{-0.5} u^{*2} \qquad (2.23)$$

$$\varepsilon = \frac{u_*^3}{\kappa y} \qquad (2.24)$$

The profiles for k and ε are shown in figure 2.4 and 2.5.

Equations (2.20), (2.22)-(2.24) are the basis of the Law-of-the-Wall models. These equations will be employed in the solution of the diffuser flow with modifications to account for flow separation and reversal that occurs in adverse pressure gradient flows.

Figure 2.4 - Kinetic Energy in Near Wall Region

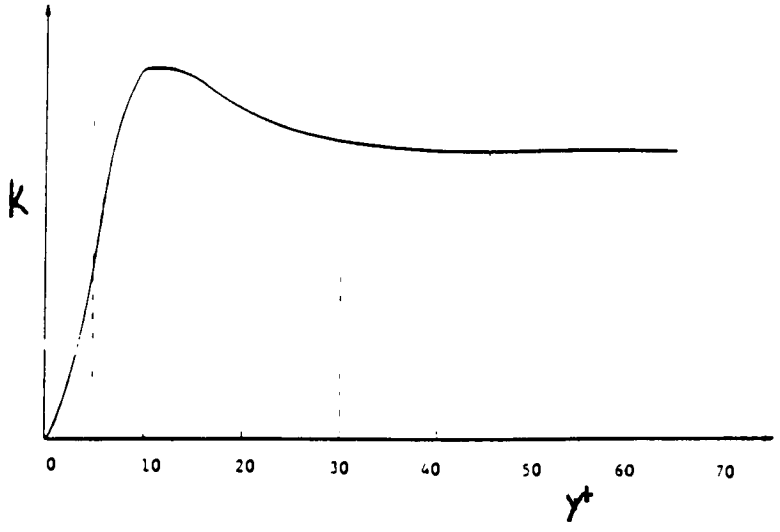

Figure 2.5 - Dissipation in Near Wall Region

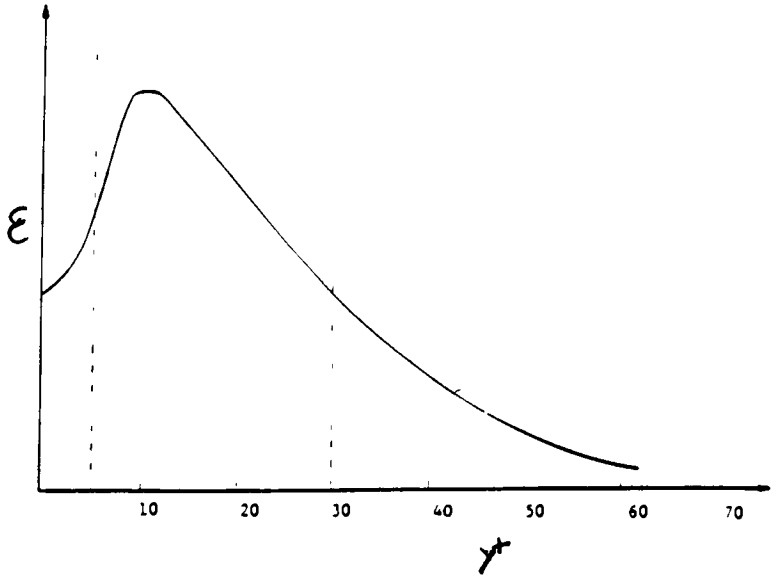

3 DIFFUSERS

3-1.0 Principles of Diffusion

A typical diffuser is shown in Figure 3.1. In order to better analyze the performance of a diffuser, some quantities need to be defined based on the flow in the diffuser and its geometry. The geometry of a diffuser is fully specified by the aspect ratio $\frac{b}{W_1}$ and any two of the following parameters 2θ, $\frac{L}{W_1}$, $\frac{N}{W_1}$, and the area ratio $\frac{W_2}{W_1}$. The performance of a diffuser is specified by the pressure recovery coefficient

$$c_p = \frac{P_2 - P_1}{\frac{1}{2}\rho v_t^2} \tag{3.1}$$

where P is the pressure and v_t is the mean throat velocity. The efficiency η is defined by

$$\eta = \frac{c_p}{c_{p\ ideal}} \tag{3.2}$$

$c_{p\ ideal}$ is a function soley of the area ratio and is given as

$$c_{p\ ideal} = 1 - \frac{1}{AR^2} \tag{3.3}$$

where AR is the area ratio.

Figure 3.1 - Geometry for a 2-D, Straight Walled Diffuser

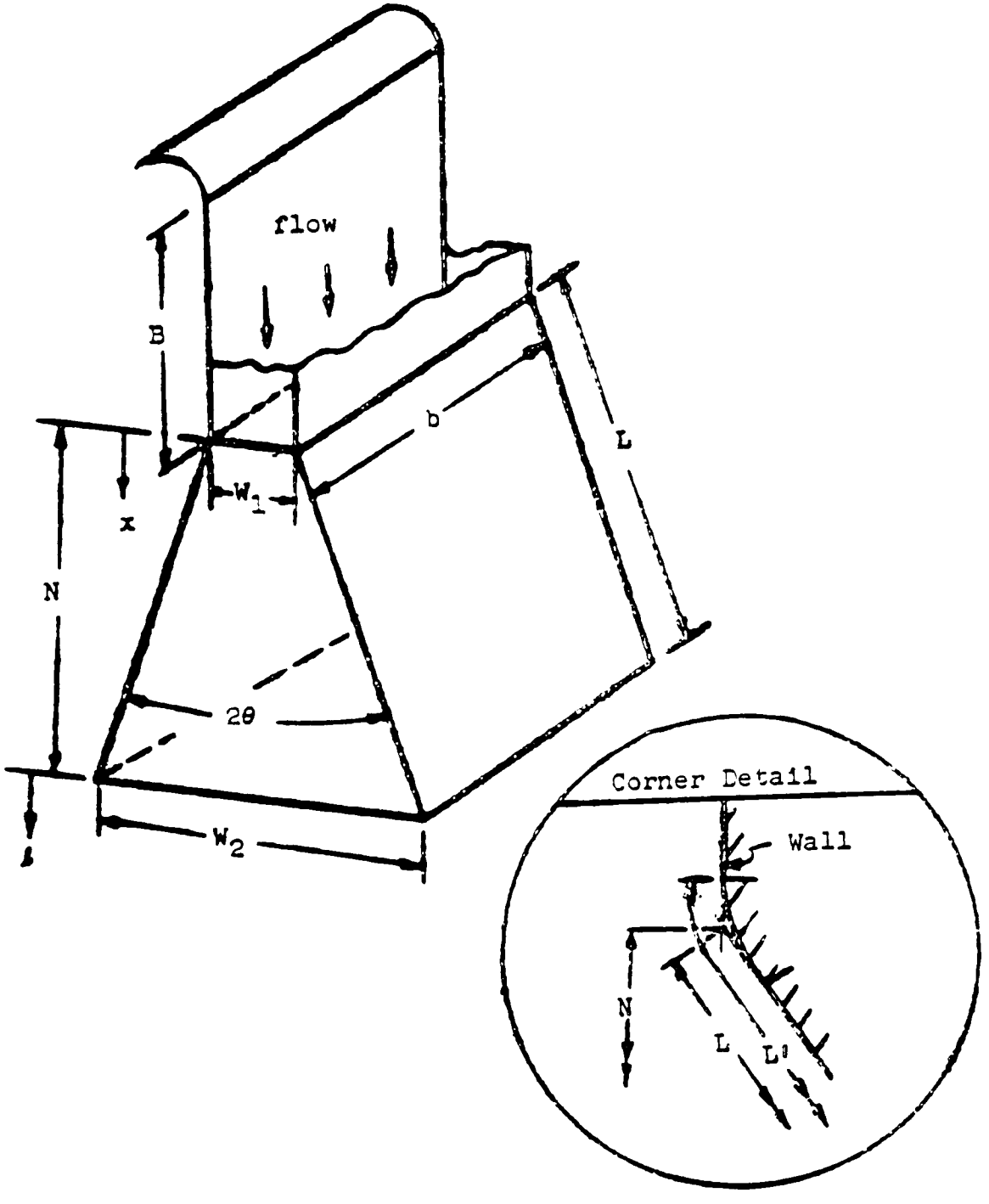

The diffuser flow characteristics are given by three parameters, the throat mach number, the throat Reynolds number and the throat blockage. Their definitions are given respectively as

$$M_t = \frac{v_t}{c} \tag{3.4}$$

$$Re_t = \frac{\rho v_t A}{\nu} \tag{3.5}$$

$$B_t = \frac{2\delta^*}{W} \tag{3.6}$$

where c is the speed of sound in air, W is the width of the throat and δ^* is the displacement boundary layer thickness calculated from the velocity profile

$$\delta^* = \int_0^{\delta} \left(1 - \frac{u}{v_t}\right) dy \tag{3.7}$$

These definitions and concepts will be used in the analysis of the diffuser performance to determine the type of flow that exists within the diffuser and as a gauge as to how well it performs its desired function.

3-2.0 Diffuser Stall

The nature of the boundary layer at the inlet to a diffuser has a significant impact on the diffuser performance characteristics. If

the flow has a thick turbulent boundary layer and a correspondingly large throat blockage, separation often occurs near the throat at the diverging section. Near the wall region of the diffuser fluid particles continue to decelerate in the presence of increasing pressure gradient and reduced transverse momentum transfer as they progress through the diffuser causing excessive blockage at the outlet. This excessive blockage is the main cause of the reduced efficiency of the diffuser. Turbopumps operating at off-design flow rates create conditions for separation in the diffuser through lack of turbulence and increased frictional drag.

The underlying concept of stall stems from Prantl's boundary layer theory [8]. Sketches of the transition to stall and flow reversal are shown in Figure 3.2. If the flow is considered a steady, two-dimensional flow pattern then Prantl's theory predicts that the point of separation will occur in an adverse pressure gradient region when the velocity gradient at the wall is zero, $\left(\frac{du}{dy}\right)_{y=0}$. Since the viscosity of the fluid is finite, this implies zero shear stress at the wall

Figure 3.2 - Prantl's Boundary Layer Concept

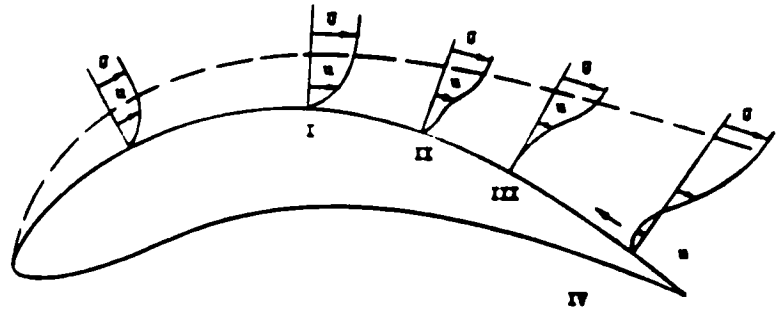

$$\tau = \mu \left(\frac{du}{dy}\right)_{y=0} = 0 \qquad (3.8)$$

Unfortunately, the boundary layer concept has not been successfully employed as a prediction method for the location of the onset of stall and so other methods must be employed.

The difficulty in employing and designing diffusers is that the maximum pressure recovery and peak efficiency of most diffusers occurs when the adverse pressure gradient is greatest or near the so called stall line. This can be seen by examining a sketch that indicates the pressure recovery as a function of area ratio for a constant aspect ratio (Figure 3.3). The peek pressure recovery is in an area dominated by 'large transitory stall.' which indicates that to get the highest efficiency, the diffuser must work very close to failure.

Figure 3.3 - Peak Pressure Recovery

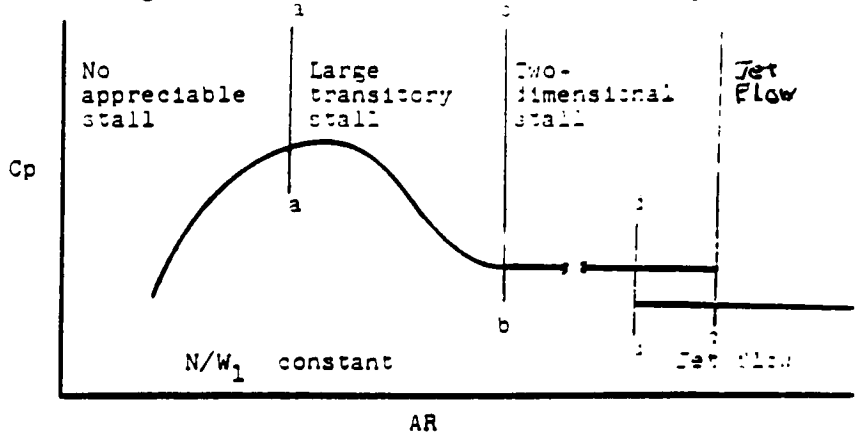

Many researchers have investigated this flow paradox and attempted to provide design criteria for engineers that find it necessary to employ diffusers based on test data. A summary is given by Reneau, Johnston and Kline in [9] as well as by Runstadler, Dolan and Dean [10]. Both of the papers attempt to correlate diffuser data into useful tables and charts to aid in designing effective diffusers. The standard chart for predicting stall was

established by Fox and Kline [1962] and has become known as the 'Flow Regime Chart' (Figure 3.4). It defines the areas of stall based on $\frac{N}{W_1}$ and 2θ and groups them into four major regions known as no appreciable stall, large transitory stall, fully developed two-dimensional stall, and jet flow.

Figure 3.4 - Flow Regime Chart

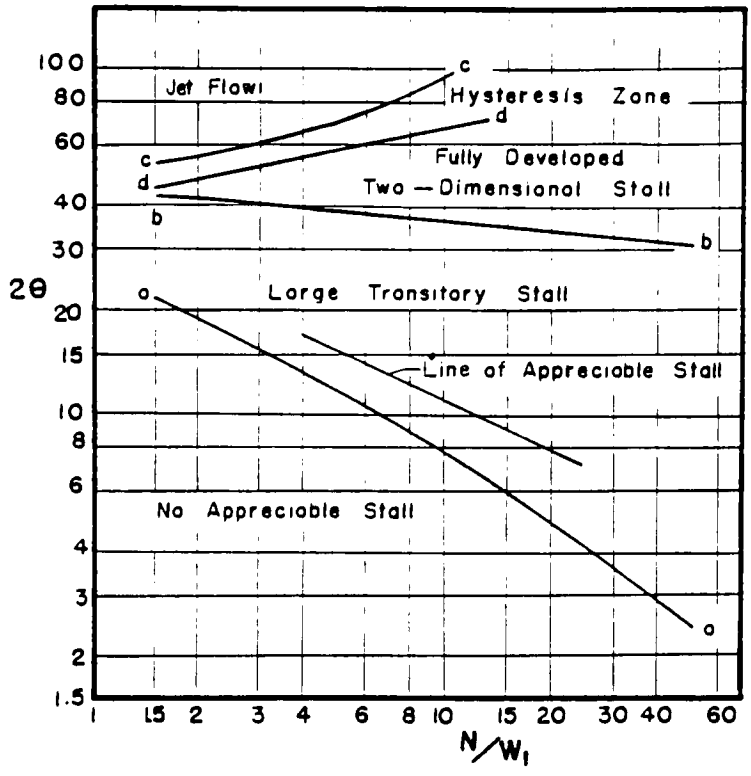

The area of no appreciable stall is characterized by small angles and area ratios shown as the area below line a-a. The flow has very small stall bubbles that are repeatedly created and destroyed on the diverging walls. For the most part, the flow field is steady and symmetric with no apparent disturbances.

The area of large transitory stall is defined in the region between lin a-a and b-b. This region is characterized by the formation of large stall regions that are constantly formed and washed away causing very large fluctuations in the resulting pressure field. Near the line b-b the stall regions form near the throat of the diffuser and exist for a longer period of time approaching the fixed stall regime.

Two dimensional stall is observed in the region between the lines b-b and c-c. This type of stall is characterized by a large stationary stall bubble that begins at the throat of the diffuser and continues along the wall typically causing some blockage of the diffuser exit. The flow adheres to the wall opposite the stall. The pressure in the diffuser generally remains constant throughout the stall region with a small amount of diffusion occuring before the onset of stall.

The region of the chart above line c-c is considered the jet flow region. This flow resembles the two-dimension stall in that stall regions form on the wall near the diffuser inlet. The difference being that stall regions form on both walls and the flow continues between them along the center of the flow resembling a jet flow. This type of flow is very steady.

The diffuser under investigation falls into the large transitory stall region based on its geometry. It must be noted, the criteria presented is for zero incidence angle effects at the inlet. Within the turbopump, the flow regime chart may not be able to predict the stall accurately due to the incidence effects introduced by the flow entering the diffuser from an impeller. As the results will indicate,

it seems that the diffuser under investigation actually operates in the fully developed stall region.

4 STALL REDUCTION IN DIFFUSERS

The reduction or elimination of stall within diffusers has been investigated as an alternative to changing the diffuser geometry. One approach that has been widely used for correcting flow separation is boundary layer control by suction and blowing.

The boundary-layer control by suction or blowing has been studied theoretically and experimentally in flows over flat plates and through pipes. These techniques are an attempt to control the excessive growth of the boundary layer which leads to stall. Several of these studies have shown that these techniques can be used effectively to improve diffuser performance.

4-1.0 Suction

The effects of suction consists of the removal of decelerating fluid particles from the boundary layer before they cause stall or separation. Ball [11] studied the effects of wall suction and blowing on the performance of 2- and 3-D diffusers. He showed that small amounts of wall suction or blowing upstream of the separation point can improve the diffuser performance. Nelson and Hudson [12] provided guidelines for the design of low suction axially symmetrical contoured wall diffusers. Stepanenko [13] experimentally demonstrated best performance effects with suction through a slot located near the inlet cross section of the diffuser. Fujimoto et.al. [14] also investigated the performance of two-dimensional diffusers with suction at the entrance. Yang et.al. [15] investigated the feasibility of designing separation-free axially

symmetrical short curved wall subsonic diffusers utilizing suction through slots. They showed that with suction rates of 6 to 12 percent of inlet flow, separation can be prevented.

4-2.0 Blowing

It has also been shown that flow separation can be prevented by supplying additional energy to the fluid particles which are being decelerated near the wall by blowing into the boundary layer. Fiedler and Gassner [16] investigated the influence of tangential fluid injection on the performance of two-dimensional diffusers. They reported that significant increases in diffuser performance can occur with jet blowing through slots along the diverging walls in inherently stalled diffusers.

5 FINITE ELEMENT METHOD

5-1.0 Finite Element Analysis

5-1.1 General Concepts

The Navier-Stokes equations presented in Chapter 2 serve to describe the flow field at every point in the domain of interest. For all but the simplest of flows, obtaining the exact solution in this manner is cost prohibitive, if possible at all. The nonlinearities present in equations (2.10), (2.11) and (2.14)-(2.15) as well as the scale ranges in turbulent flows means that even the fastest computers are unable to obtain a solution in a reasonable period of time. An alternate approximate approach to solving the flow field must be undertaken.

In the early 1950's, the refinement of matrix computation and the introduction of the computer spurred on the development and implementation of an approximation method used for solving complex stress analysis problems known as the finite element analysis (FEA) method. This approach is useful in that it breaks the particular region of interest into small geometric regions called finite elements and replaces the partial differential equations which govern the entire region with ordinary differential equations or algebraic equations within these regions. All of the regions are then linked together via common boundary conditions and solved as a large system of equations using matrix algebra. Since its inception, FEA has been successfully applied to a wide variety of engineering problems including fluid flow.

FEA and the conversion of the partial differential continuum equations to the ordinary differential equations is accomplished through a sequence of well defined steps which make it simple to implement on a computer:

(1) Discretization of the domain of interest
(2) Derivation of the element equations
(3) Assembly of the element equations to obtain global equations
(4) Imposition of boundary conditions
(5) Solution of assembled equations

The above steps will be detailed in subsequent sections.

In order to develop the steps involved, a one-dimensional boundary value problem will serve as an example. The extraction to higher dimensions is a straight forward extension of this 1-D concept. For an arbitrarily shaped domain Ω with boundary conditions specified on $d\Omega^1$ and $d\Omega^2$ (Figure 5.1), the governing differential equations are given as

Figure 5.1 - Boundary Value Problem

$$A\,u = F \quad \text{on } \Omega \qquad (5.1a)$$

$$B_i u = g_i \quad \text{on } d\Omega^i \qquad (5.1b)$$

where A is a differential operator of order 2m and B_i is a boundary operator of order n. The boundary conditions can be classified as either essential (EBC) or natural (NBC) (commonly known as Dirichlet and Nueman respectively) depending on the relationship of

m to n. For $0<n<m-1$, the boundary conditions are considered essential. For $m<n<2m-1$ they are termed natural. The notation in the following sections will have $d\Omega^1$ as an EBC and $d\Omega^2$ as an NBC. Once the domain has been specified and the boundary conditions identified, the analysis can proceed.

5-1.2 Weak Form

The basis of FEA is the development of the weak form of the governing partial differential equations that will be transformed into ordinary differential equations. Let v be a function such that $v=0$ on all $d\Omega^1$. Assuming v has sufficient smoothness over the domain, v is considered a test function. Multiplying (5.1) by v and integrating over the domain yields the so called weak form

$$\int_{\Omega}(Au-F)v\, d\Omega = 0 \qquad (5.2)$$

To equate the smoothness requirements on u and v, (5.2) is integrated by parts to obtain

$$\int_{\Omega}[f(u^i,v^i)]\, d\Omega + \int_{d\Omega^1}( ) + \int_{d\Omega^2}( ) = 0 \qquad (5.3)$$

where $f(u^i,v^i)$ is a function of u and v and its derivatives. The resulting integral is represented by $\beta(u,v)$. Over $d\Omega^1$, set $v=0$ and on $d\Omega^2$, set $B_j u=g_j$ to determine the boundary terms, l(v). Rewriting (5.3) in a more familiar manner yields

$$\beta(u,v) = l(v) \tag{5.3a}$$

By introducing the weak form, the continuum problem of (5.1) has be reduced to determining u such than (5.3a) holds for all admissible v.

The most common method for solving (5.3a) is known as the Galerkin method which uses the following approximation for u and v

$$u = u_i = \Phi_o + \sum_{j=1}^{n} \alpha_j \Phi_j \tag{5.4a}$$

$$v = \Phi_i \tag{5.4b}$$

where Φ_ι is a known function called a basis function. Substituting (5.4) into (5.3a) and expanding yields

$$\beta(\Phi_o + \sum_{j=1}^{n} \alpha_j \beta(\Phi_j,\Phi_\iota),\Phi_i) = l(\Phi_i) \tag{5.5}$$

For linear differential equations, the principle of linearity is imposed with further rearrangement and (5.5) becomes

$$\sum_{j=1}^{n} \alpha_j \beta(\Phi_j,\Phi_i) = l(\Phi_i) - \beta(\Phi_o,\Phi_i) \tag{5.6}$$

The right hand side of (5.6) acts as a forcing term and can be rewritten as F_i. Further, $\beta(\Phi_j,\Phi_i)$ is known and can be written as B_{ij}. In matrix notation, (5.6) is expressed as

$$[B_{ij}]\ [\alpha_i] = [F_i] \tag{5.7}$$

which is a linear set of equations where α_i are the unknowns. B_{ij} is formally known as the element stiffness matrix and is dependent on the selection of Φ_i, the basis functions.

Equation (5.7) is valid over the entire domain Ω and can be solved by imposing appropriate boundary conditions on $d\Omega^i$. We must now examine the extrapolation of (5.7) to each element in the domain.

5-1.3 Discretization

The domain of interest must be partitioned into finite elements (Figure 5.2). The selection of type and size of these elements is dependent on the accuracy requirement of the solution. In order to obtain the optimal mesh density many parameters of the region must be taken into consideration, including making the mesh fine in regions where the properties of interest are changing rapidly and coarser in regions of lesser interest and more well behaved responses. The selection of a discretization scheme is expounded upon in Chapter 6.

Figure 5.2 - Mesh Discretization

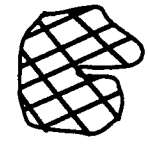

5-1.4 Element Types and Basis Functions

FEA attributes its flexibility and wide applicability to the large number of available element types and the varying accuracy of each. Typical element types in two-dimensions are triangular and

rectangular employing linear and quadratic interpolation functions. The shape of the element chosen should best fit the shape of the domain of interest. The basis functions should be chosen depending on the accuracy requirement of the solution.

The basis function provides an approximation of the solution across an element. A general approximation for u was given by the Galerkin Method in (5.4a) which depends on the selection of Φ_j, the basis function. Within the constraints of the variational formulation a basis function on an element must be chosen such that outside of the element, $\Phi_i^e=0$. For demonstration purposes a linear interpolation function will be considered across a 1-D element.

Figure 5.3 shows a 1-D element Ω_e with endpoints x_e and x_{e+1}. The basis functions Φ_1 and Φ_2 are shown in Figure 5.4. The function is one and zero at x_e or x_{e+1} respectively. Across the element, Φ_i are given by

Figure 5.3 - 1-D Element

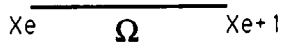

Figure 5.4 - Basis Functions

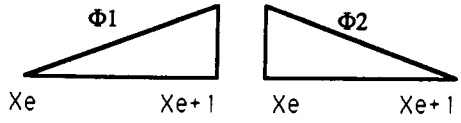

$$\Phi_1 = \frac{x_{e+1} - x}{x_{e+1} - x_e} \qquad (5.8a)$$

$$\Phi_2 = \frac{x - x_e}{x_{e+1} - x_e} \qquad (5.8b)$$

Φ_1 and Φ_2 will serve to scale α_j at each endpoint. These functions will in turn match up to give a piecwise linear global basis function ψ_i. In order to tie together local and global basis functions,

continuity of solutions is imposed at each of the nodes as in Figure 5.5. So, globally, the solution at each node is given as

$$u_a = \quad U_i \, \psi_i(x) \tag{5.9}$$

Higher order elements in 2- and 3-dimensions can be constructed in a similar manner depending on the selection of the form of Φ.

Figure 5.5 - Continuity of Solutions

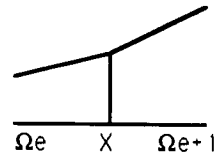

5-1.5 Element and Global Formulation

Applying (5.7) across each element gives the element equations. Unfortunately, the solution U_i at each node is not known. Based on the continuity of solutions, the displacement at the x_{e+1} node of the Ω_e element is the same as at the x_e node of the Ω_{e+1} element. This situation allows the element equations to be linked throughout the domain to obtain a global set of equations of the form

$$[K_{ij}] \, [U_i] = [F_i] \tag{5.10}$$

where $[K_{ij}]$ is the global stiffness matrix made up a combination of the element stiffness matrices. $[U_i]$ are the unknowns. With the imposition of boundary conditions, (5.10) can be solved using an

appropriate numerical solver (see 6-4.0) to yield a solution to the problem at hand.

5-2.0 Application of Finite Element Method to the Navier-Stokes Equations

In the manner outlined in sections 5-1.0, the Navier-Stokes equations can be generated in finite element form. The derivation and manipulation of the equations is quite extensive and only a summary is presented here. It is therefore left for the reader to review [18] chapters 3-6 for the full analysis.

The velocity, pressure and temperature fields across each element are approximated by

$$u_i = \Phi^T U_i \tag{5.11a}$$

$$P = \psi^T P \tag{5.11b}$$

$$T = \vartheta^T T \tag{5.11c}$$

where U_i, P and T are column vectors of the unknowns at each nodal point and Φ, ψ and ϑ are column vectors of the interpolation functions.

Employing the Galerkin method of solution, (5.11) can be manipulated and expressed by the matrix equations representing conservation of mass, momentum and temperature respectively as

$$C^T U = 0 \tag{5.12a}$$

$$MU + A(U)U + K(T\cdot U)U - CP + B(T)T = F(T) \qquad (5.12b)$$

$$NT + D(U)T + L(T)T = G(U\cdot T) \qquad (5.12c)$$

where $(a\cdot b)$ denotes the inner product defined as

$$(a\cdot b) = \int_v a\ b\ \ dv \qquad (5.13)$$

where v is the volume of the element. The quantities in (5.12) are defined as follows

$$C_i = (\Phi_{,i}\cdot\psi^T)$$

$$M = (\rho\Phi\cdot\Phi^T)$$

$$A_i(U_j) = (\rho\Phi u_j\cdot\Phi_{,i}^T)$$

$$K_{ij} = (\mu\Phi_{,j}\cdot\Phi_{,i}^T)$$

$$B_i = (\rho c_p\vartheta u_j\cdot\vartheta_{,i}^T)$$

$$F_i = \int_s t_i\Phi\ dS\ \ + (\rho f_i\cdot\Phi) + (\rho g_i B T_o\cdot\Phi)$$

$$N = (\rho c_p\vartheta\cdot\vartheta^T)$$

$$D_i(U_j) = (\rho c_p \vartheta u_j \cdot \vartheta_{,i} T)$$

$$L_{ij} = (k \vartheta_{,i} \cdot \vartheta_{,j} T)$$

$$G = -\int_S (q_s + q_c + q_x)\vartheta \, dS + (q_s \cdot \vartheta) + (\mu \Phi \cdot \vartheta)$$

Setting $U = (U_1\ U_2\ U_3)^T$ and $V = (U_1\ U_2\ U_3\ T\ P)^T$ a single matrix equation results from (5.12)

$$\begin{bmatrix} M & 0 & 0 \\ 0 & N & 0 \\ 0 & 0 & 0 \end{bmatrix} \begin{bmatrix} U \\ T \\ P \end{bmatrix} = \begin{bmatrix} A(U)+K(U\cdot T) & B(L) & -C \\ 0 & D(U)+L(T) & 0 \\ -C^T & 0 & 0 \end{bmatrix} \begin{bmatrix} U \\ T \\ P \end{bmatrix} = \begin{bmatrix} F(T) \\ G(U\cdot T) \\ 0 \end{bmatrix}$$

or in a more compact form

$$MV + K(U\cdot T)V = F(U\cdot T) \qquad (5.16)$$

Equation (5.16) is the Navier Stokes representation in discrete form.

For solving this system, the pressure can be eliminated from (5.12b) by employing a penalty formulation of the form

$$C^T U = -\varepsilon M_p P \qquad (5.17)$$

where ε is the penalty parameter. Through substitution and rearrangement, (5.16) becomes

$$\begin{bmatrix} M & 0 \\ 0 & N \end{bmatrix} \begin{bmatrix} U \\ T \end{bmatrix} + \begin{bmatrix} A(U)+K(U\cdot T)+\frac{1}{\varepsilon}CM_P^{-1} & B(T) \\ 0 & D(U)+L(T) \end{bmatrix} \begin{bmatrix} U \\ T \end{bmatrix} = \begin{bmatrix} F(T) \\ G(U\cdot T) \end{bmatrix}$$

where M_p^{-1} is given as

$$M_p^{-1} = (\psi \cdot \psi^T)$$

Equation (5.18) is the generalized Navier-Stokes equation in discrete form. Obviously, under the assumption for the model under investigation, it will be reduced significantly during the solution process.

6 FINITE ELEMENT IMPLEMENTATION - FIDAP

Chapter 5 indicated that it is necessary to use advanced computational fluid dynamics techniques in order to gain better insight into the complex flow patterns within the turbopump sub-components. FIDAP is a finite element based code that is capable of modeling incompressible, 3-D, viscous flows that result in the diffuser section of the LH2 turbopump. FIDAP has many options for solving the Reynolds averaged Navier-Stokes equations for turbulent flow that were developed in chapters 2 and 5. In this study, the solution is made possible by employing the two equation k-ε turbulence model. In order to use finite element analysis effectively choices of grid density, inlet and boundary conditions, solution technique and the implementation of the k-ε and near wall model for turbulent flow are critical in ensuring a solution that converges as well as gives meaningful results.

6-1.0 Mesh

The mesh density as discused in section 5-1.3 is critical in ensuring a reasonable solution. The mesh must be fine where specific flow properties are of interest and coarser where the flow properties are not critical. It is important to note that the transition between these two zones must be smooth so that the solution is not compromised. The mesh for the suction and blowing models is shown in Figure 6.1.

Figure 6.1a - Mesh with Suction and Blowing Slits

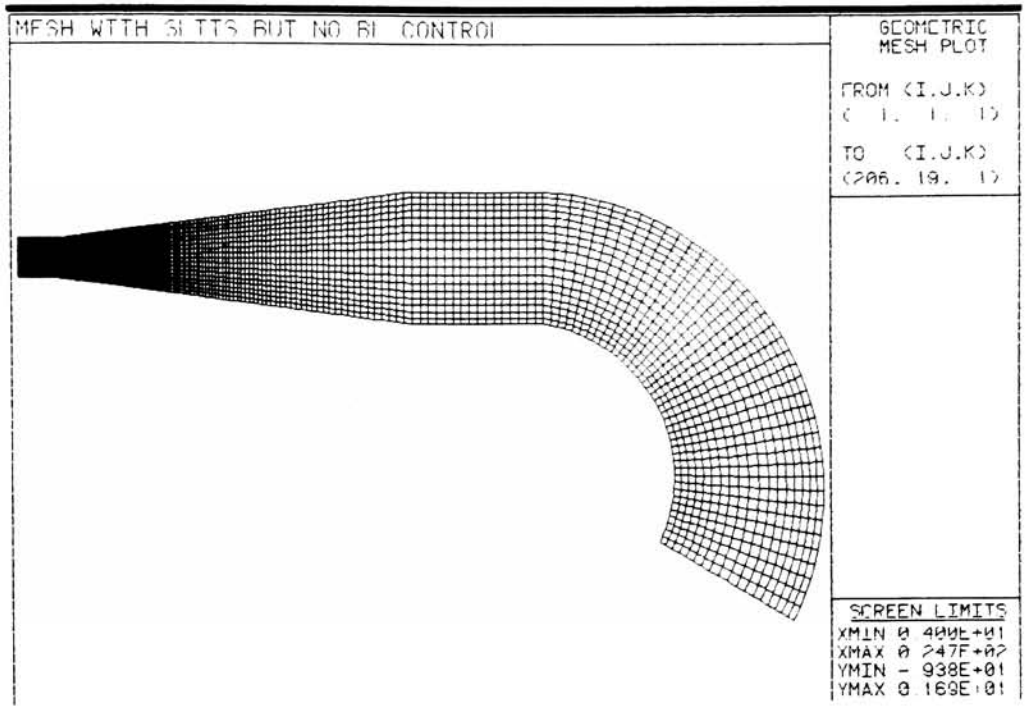

Figure 6.1b - Enlargement of Inlet Region

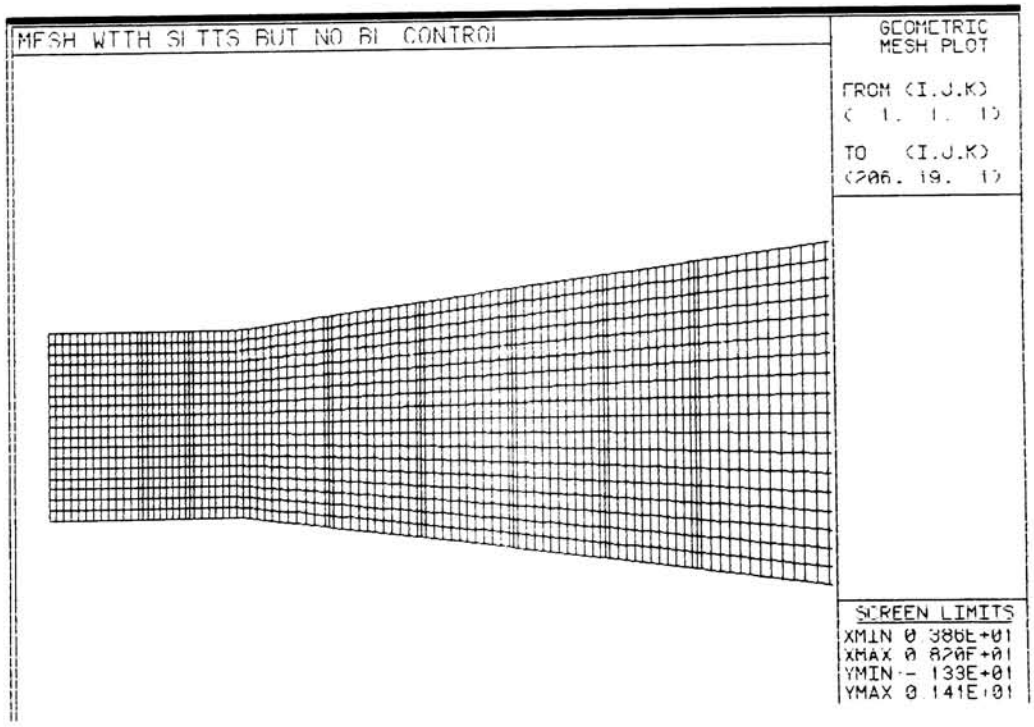

6-2.0 Non-dimensionalization

Obtaining numerical solutions to flow problems is often difficult due to the limited space available within computers to represent numbers internally. The smaller numbers present in an analysis are often "lost" through truncation rendering accurate solutions unattainable. To overcome this problem and force the numbers involved in the solution to be on the same order of magnitude, the variables are non-dimensionalized with respect to characteristic values. These characteristic values are arbitrary but should be representative of the problem at hand.

The variables of interest for the diffuser are the dimension of the diffuser, the velocities, pressure, kinetic energy and dissipation. The characteristic values were chosen to be at the inlet to the diffuser. The characteristic length, l_c, was chosen to be one inch and the characteristic velocity, u_c, to be 1.292 ft/s.

Based on these characteristic values, the non-dimensional variables of interest are defined as follows

$$x_i^* = \frac{x_i}{l_c} \qquad \text{length} \qquad (6.1a)$$

$$u_i^* = \frac{u_i}{u_c} \qquad \text{velocity} \qquad (6.1b)$$

$$p^* = \frac{p}{\rho u_c^2} \qquad \text{pressure} \qquad (6.1c)$$

$$k^* = \frac{k}{u_c^2} \qquad \text{kinetic energy} \qquad (6.1d)$$

$$\varepsilon^* = \frac{l_c}{u_c{}^3}\varepsilon \qquad \text{dissipation} \qquad (6.1e)$$

FIDAP has the capability of solving problems in either non-dimensional or dimensional form. To specify a non-dimensional model, the input file must set the density of the fluid to one and the viscosity to a value equal to $\frac{1}{Re}$. This invokes the non-dimensional Navier-Stokes equations for solving the problem. The non-dimensional parameters are determined and tabulated in Appendix A.

6-3.0 Element Selection

The elements chosen for the solution were four-noded quadrilateral with the necessary corresponding two-noded wall elements. Although nine-noded quadrilateral elements were available for the solution, the four-noded elements were adequate to solve the flow. These types of elements allowed a quicker solution to be obtained which is particularly advantageous when solving for five unknowns at every node for a turbulent problem.

6-4.0 Solution Technique

The most common method of solving the resulting systems of equations (Eq 5.10) for the finite element method is a Newton type solver. Unfortunately, these solvers have rather large storage requirements due to the formation of the large global system matrix. For large 2-D and most 3-D problems, the peripheral storage requirements are such that the available computer resources are

often exceeded. To try and reduce this burden on disk storage, FIDAP provides a solver known as the ***segregated solver*** that solves the Navier-Stokes equations for each degree of freedom successively instead of simultaneously. This approach substantially reduces the required storage requirements, but there is a trade off. The convergence of this solution technique is slower and may require many more iterations than a Newton type solver. In most turbulence modeling, this method still results in a savings.

The only shortcoming of the segregated solver approach is that the decoupled Navier-Stokes equations do not have an explicit matrix equation for the pressure degree of freedom. This is addressed by replacing the continuity equation that implicitly governs the pressure degree of freedom with a Poison type matrix equation that explicitly governs the pressure distribution. FIDAP provides three options for this replacement: pressure projection, pressure correction and pressure update versions. The pressure projection version was employed in this thesis.

The pressure projection approach to the segregated solver uses the current field variables at the beginning of each iteration to solve the Poison type matrix equation for the pressure. The other variables in the flow are then sequentially solved for using the most recent variables. Finally, the velocity field is forced to meet the incompressibility constraint by a method that involves the solution to an additional Poisson type matrix equation for a pressure correction vector.

The segregated solver technique was used with the pressure projection approach for all of the models under consideration.

6-4.0 FIDAP Near Wall Model

The particular difficulty in solving turbulent flows is the steep gradients in the velocities that occur near the wall. This concept was discussed in section 2-2.3 and near wall equations developed for flow parallel to the wall. Unfortunately, the model developed is not well suited in areas of flow separation and reversal. The models that are effective in solving these types of flow are cost prohibitive due to the disproportionate number of elements required in the near wall region. For the above reasons, FIDAP employs special near-wall elements which provide the best of both solution techniques.

These elements account for the steep gradients provided that the viscous sublayer is wholly enclosed in the element nearest the wall by employing specialized shape functions that accurately capture the steep gradients present. These shape functions are based on the characteristic turbulent Reynolds number and automatically adjust during the solution procedure to reflect the variable profiles.

It is important to note that ***the near-wall region must be wholly enclosed within these special elements in order for the model to work correctly.*** To ensure this compliance, a y^+ value is written to an output file. If this value is above 30, the mesh is satisfactory and the solution should be accurate.

Finally, these near wall elements must be chosen such that the number of nodes present match with the corresponding side of the continuum elements in the center of the flow.

6-5.0 Initial and Boundary Conditions

The inlet and boundary conditions for velocity, turbulent kinetic energy and turbulent dissipation are dictated by the model being considered. These values were presented in section 1-3.0. The velocity at the inlet was obtained from the mass flow rate at the inlet

$$m = \rho u A \tag{6.2}$$

Similarly, the velocities for suction and blowing at each slit were obtained by using the appropriate reduction in mass flow rate and area [See Appendix A for the calculations for each model.].

The values for kinetic energy and dissipation were found using equations provided by Pourahmadi and Humphrey [18] for internal flow in tubes

$$k = 0.005\ u_c^2 \tag{6.3}$$

$$\varepsilon = \frac{c_\mu\ k^2}{0.03\ l_c} \tag{6.4}$$

The values obtained were in agreement with the values by Veres and Chang [20] for a similar FIDAP model. For simplicity, the initial guesses for the solution were specified to be the same as the inlet boundary conditions.

The input files that were used for each model are given in Appendix C.

7 RESULTS AND DISCUSSION

The results presented in this thesis are for a 2-dimensional finite element model of a liquid hydrogen turbopump diffuser design based on the Space Transfer Vehicle Diffuser design. The first portion of the project was to establish design flow conditions and then verify that diffuser stall did occur at the studied, off-design flow rate. Subsequently, modifications were made to the diffuser to implement suction and blowing boundary layer control at various rates.

7-1 Design Flow Conditions

In order to gain insight into the effectiveness of boundary layer control devices, it is necessary to establish the design flow conditions for comparison. The streamline contour plot (Figure 7.1) and the velocity vector plot at the diffuser outlet (Figure 7.2) indicate that there is flow separation in this particular configuration. Considering the low incidence angle and recalling the Flow Regime Chart (Figure 3.4), it appears that this separation may be directly caused by the diffuser geometry. The speed contour plot (Figure 7.3) shows a rather uniform inlet speed through the throat and does not indicate a severe jet flow along the bottom wall of the diffuser.

The pressure contour plot (Figure 7.4a) and the pressure line plot at the diffuser centerline (Figure 7.4b) indicate a relatively uniform conversion of dynamic head to static pressure as the diffuser is traversed. A high pressure along the outer diameter of

the turning channel seems to help generate the small amount of flow separation that is present. The overall pressure recovery of the diffuser was determined to be 0.7343 (Table 7.2) which is rather favorable in comparison with the ideal recovery of 0.9127.

The kinetic energy (Figure 7.5), dissipation (Figure 7.6) and the vorticity (Figure 7.7) contour plots are included for flow verification. The majority of the kinetic energy generation occurs at the diffuser throat with a corresponding amount of dissipation in the same location. It appears to occur around the inactive suction and blowing holes. This is entirely reasonable due to the lack of smoothness around these holes even though they are not in operation. Some energy is generated as the flow goes through the turning channel but it seems to be washed out of the model instead of being dissipated.

The vorticity of the fluid is an indication of the viscosity present in the fluid at a particular location. Boundary layer theory indicates that the viscosity of a fluid should only be considered in a small region near a solid wall known as the boundary layer. From Figure 7.7, it can be seen that a small boundary layer exists at the bottom wall of the diffuser. The distancing of vorticity from the upper wall is an indication of separation along that region. When the flow reattaches in the turning channel, the boundary layer is again formed.

The flow profiles at the inlet and the outlet of the diffuser are of particular interest in determining the operating characteristics of the diffuser. For this reason, velocity plots are provided that traverse these regions, specifically in the locations specified by

Figure 7.8. The inlet velocity profiles (Figure 7.9) indicate a well developed and slightly skewed turbulent velocity profile. The outlet profiles (Figure 7.10) indicate the flow separation that exists on the upper wall of the diffuser as well as the significant reduction in flow speed. The profiles resemble skewed laminar profiles. Table 7.3 provides further verification of the flow conditions at the inlet and outlet by tabulating the Reynolds numbers at locations 3 (inlet) and 7 (outlet).

Figure 7.1 - Streamline Contour Plot, 100% Flow

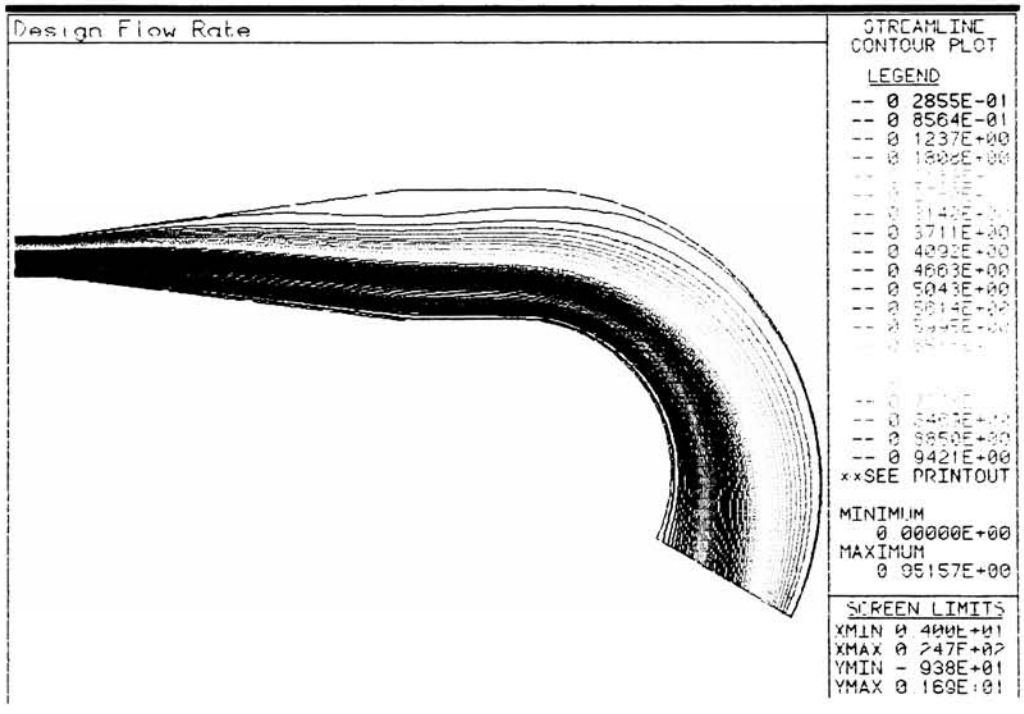

Figure 7.2 - Velocity Vector Plot at Outlet, 100% Flow

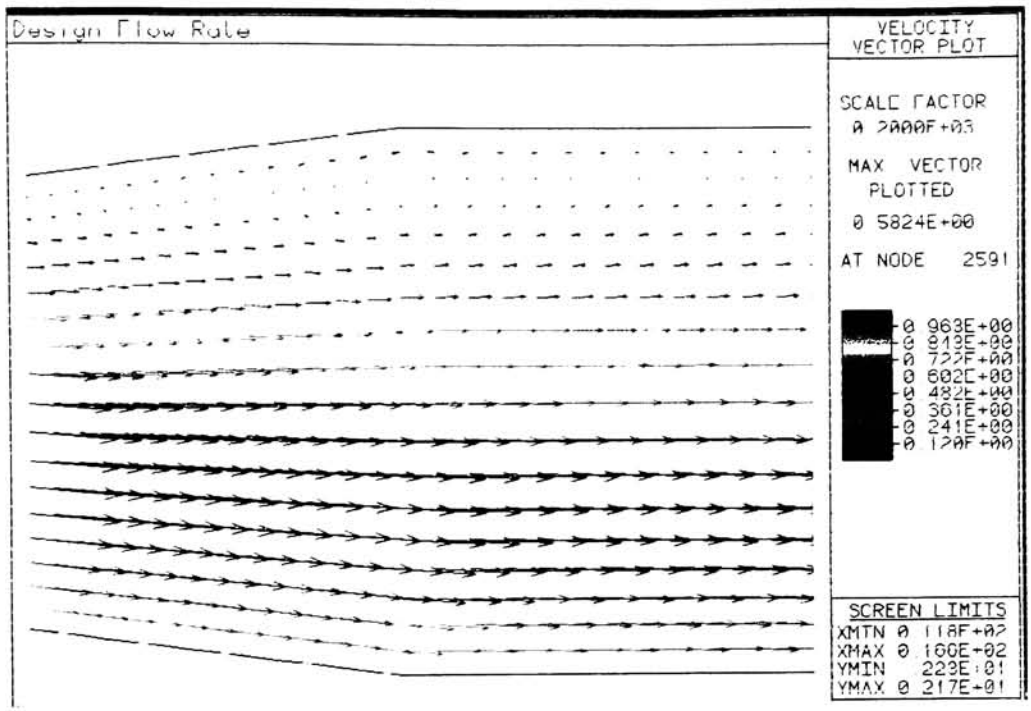

Figure 7.3 - Speed Contour Plot, 100% Flow

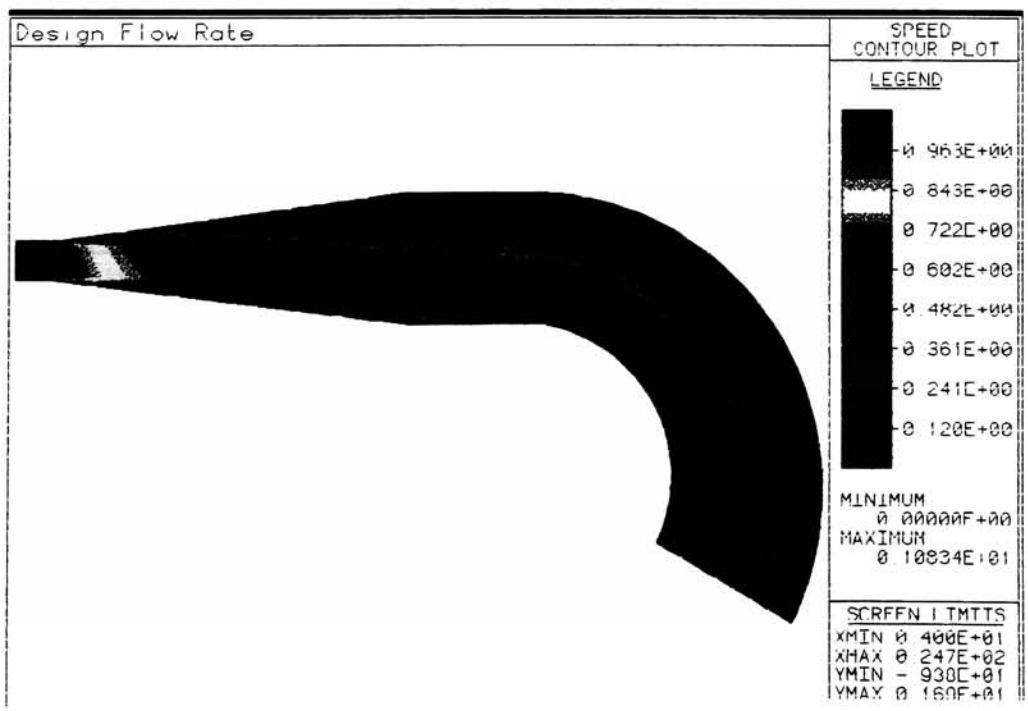

Figure 7.4a - Pressure Contour Plot, 100% Flow

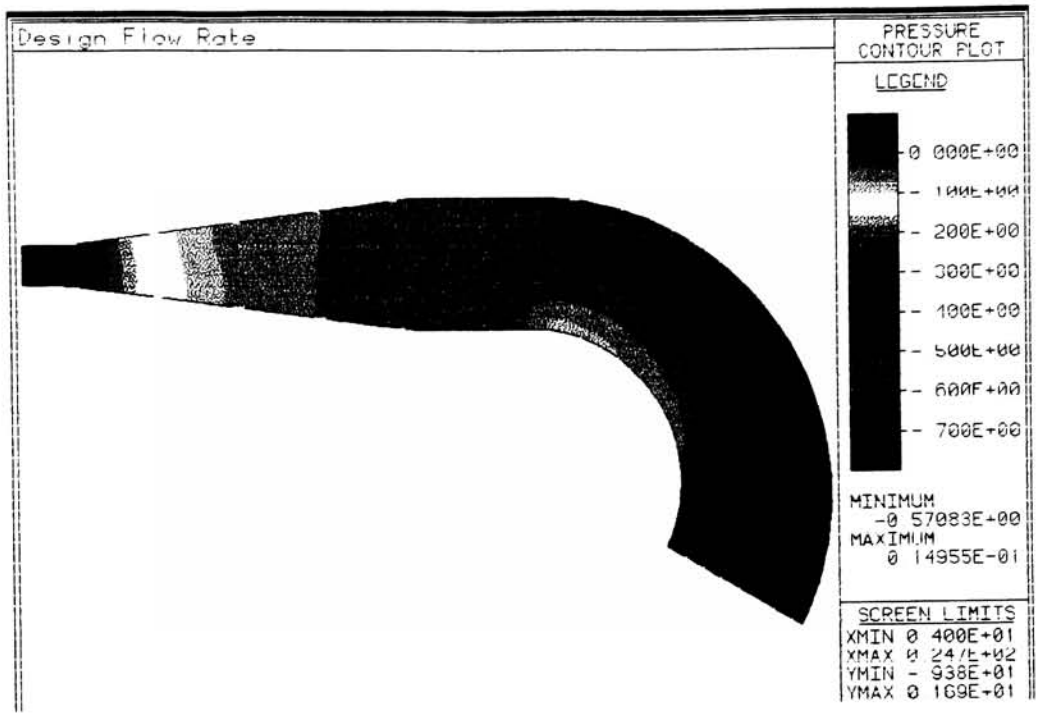

Figure 7.4b - Pressure Along the Diffuser Centerline, 100% Flow

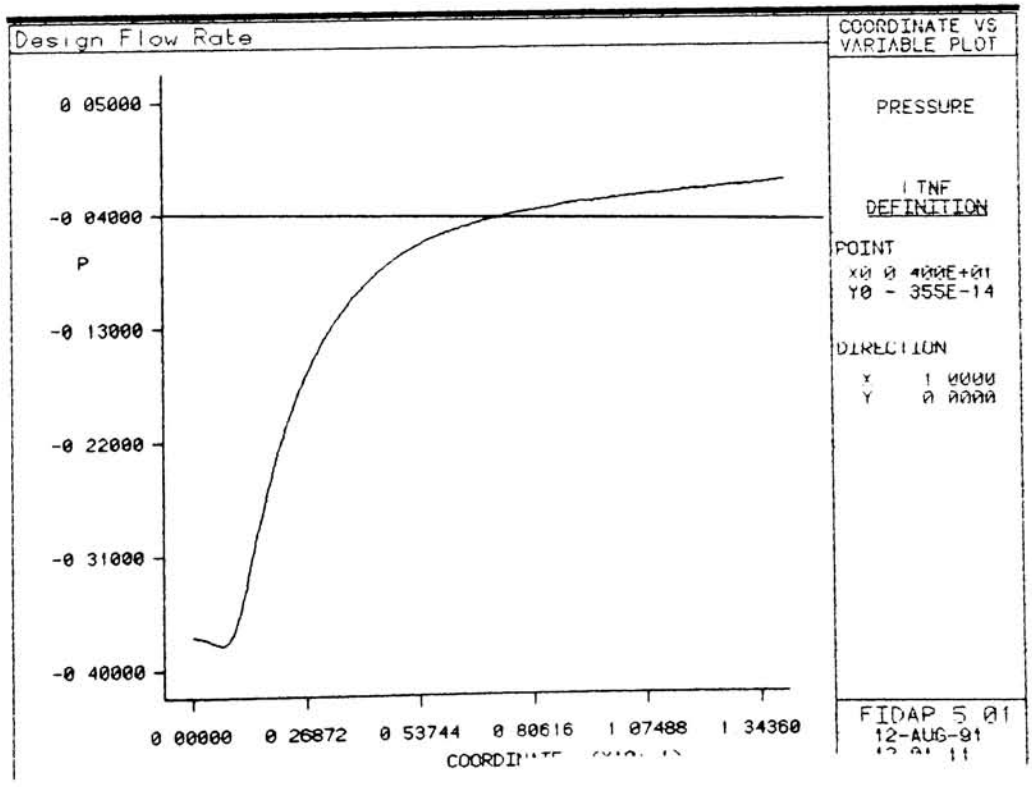

Figure 7.5 - Kinetic Energy Contour Plot, 100% Flow

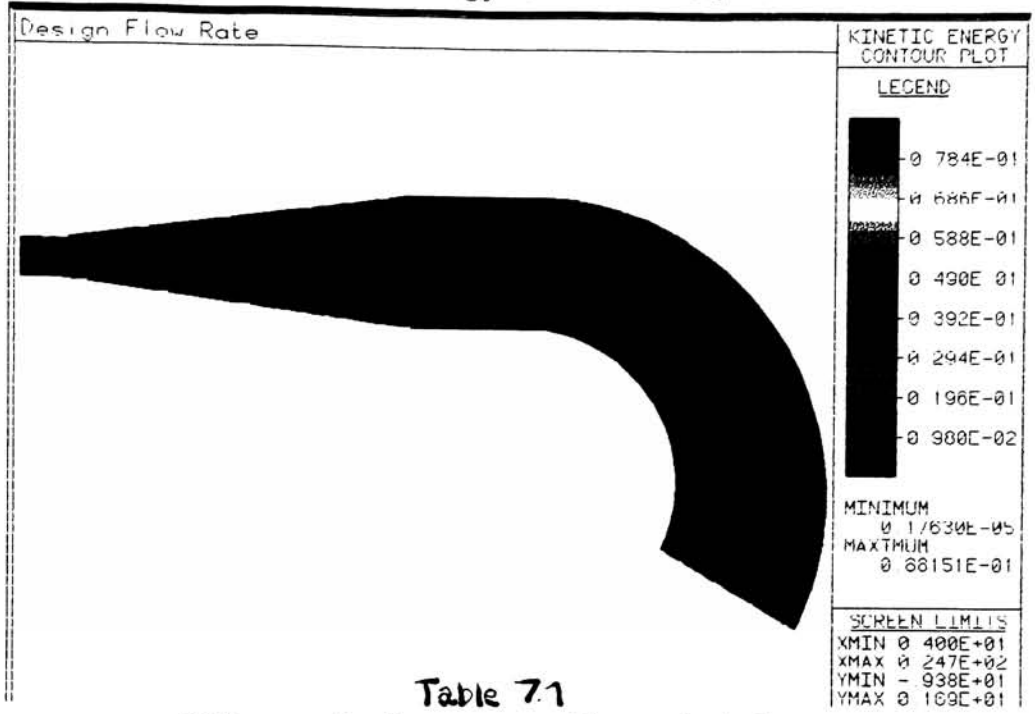

Table 7.1

Diffuser Performance Characteristics

Model	M_t	B_t (%)
Ideal Flow	-	-
100% Flow	0.00119	66
60% Flow	0.00119	28
5% Suction	0.00117	41
10% Suction	0.00115	48
15% Suction	0.00117	46
20% Suction	0.00116	41
5% Blowing	0.00119	43
10% Blowing	0.00122	29
15% Blowing	0.00151	0.2

[See Appendix D for calculation of B_t]

Table 7.2
Pressure Recovery Characteristics

Model	P_i^*	P_o^*	C_p	η
Ideal Flow			0.9127	1.0000
100% Flow	-0.3924	-2.5296e-2	0.7343	0.8045
60% Flow	-0.3575	-3.6261e-2	0.6424	0.7048
5% Suction	-0.3752	-1.8349e-2	0.7138	0.7821
10% Suction	-0.3680	-6.3551e-3	0.7232	0.7923
15% Suction	-0.3739	-8.5118e-3	0.7648	0.8379
20% Suction	-0.3525	-1.9793e-2	0.7461	0.8175
5% Blowing	-0.3143	-2.6825e-2	0.5749	0.6299
10% Blowing	-0.4041	-2.2376e-2	0.8529	0.9345
15% Blowing	-0.7987	7.6942e-2	1.7514	1.9189

[See Appendix B for Calculation of c_p]

Figure 7.6 - Dissipation Contour Plot, 100% Flow

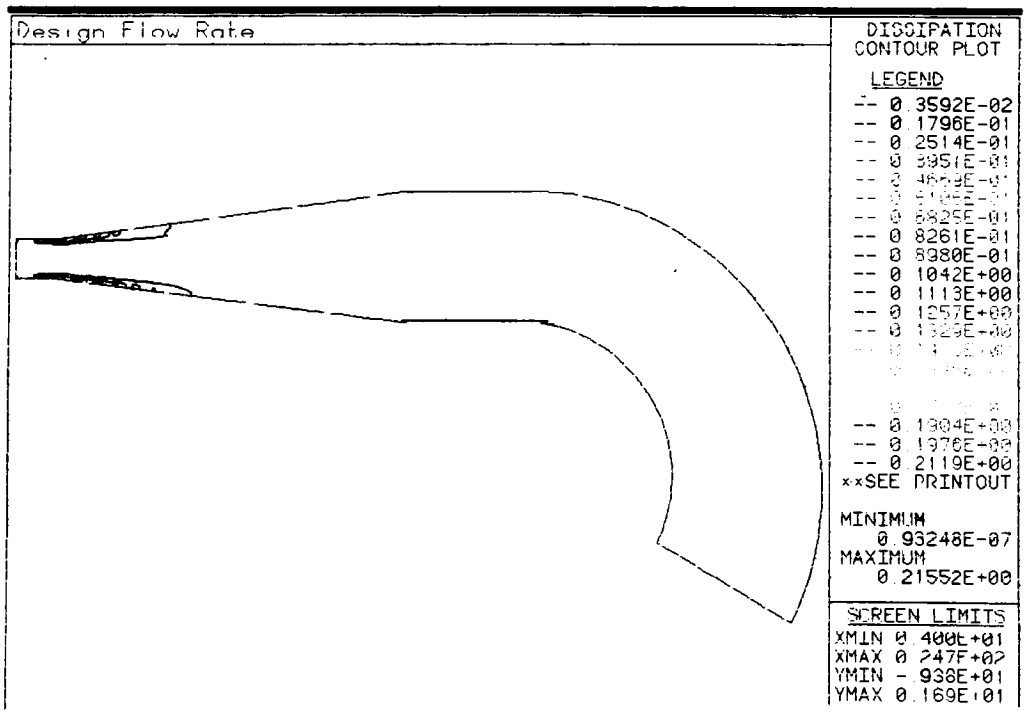

Figure 7.7 - Vorticity Contour Plot, 100% Flow

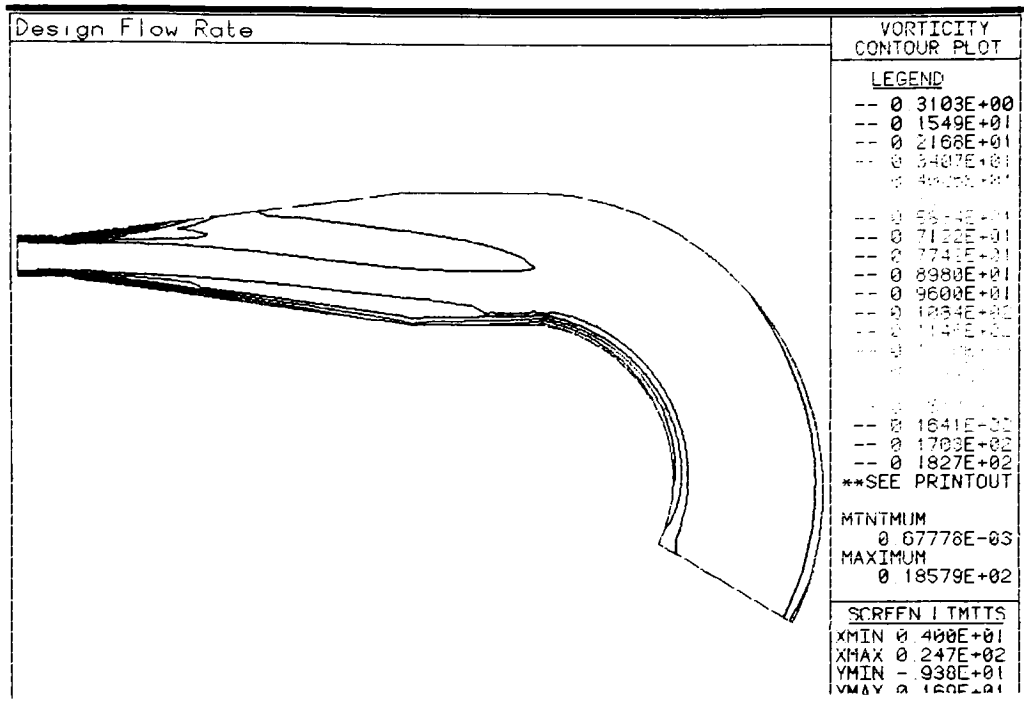

Figure 7.8 - Location of Velocity Profiles, 100% Flow

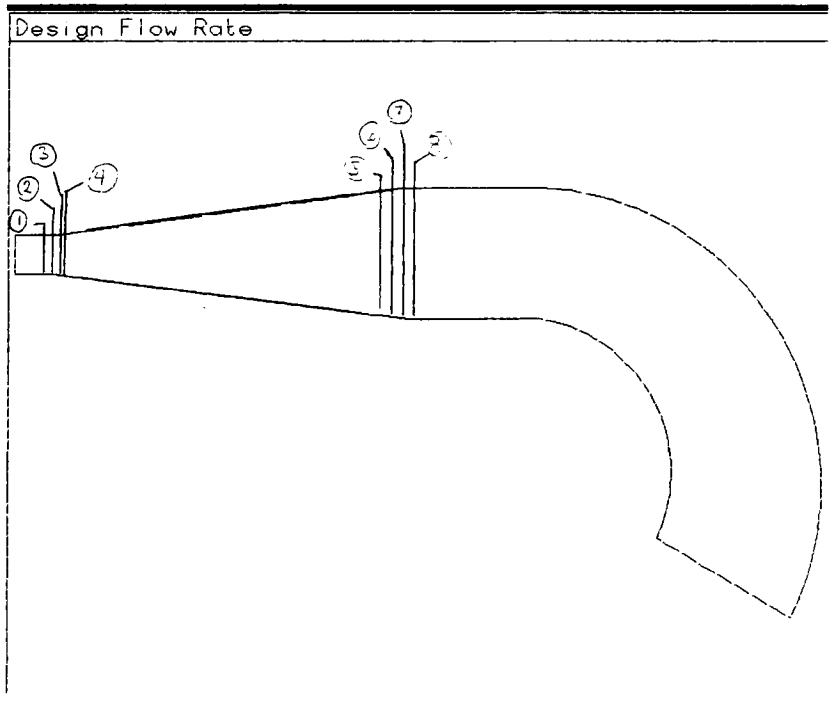

Figure 7.9 - Velocity Profiles at Inlet, 100% Flow

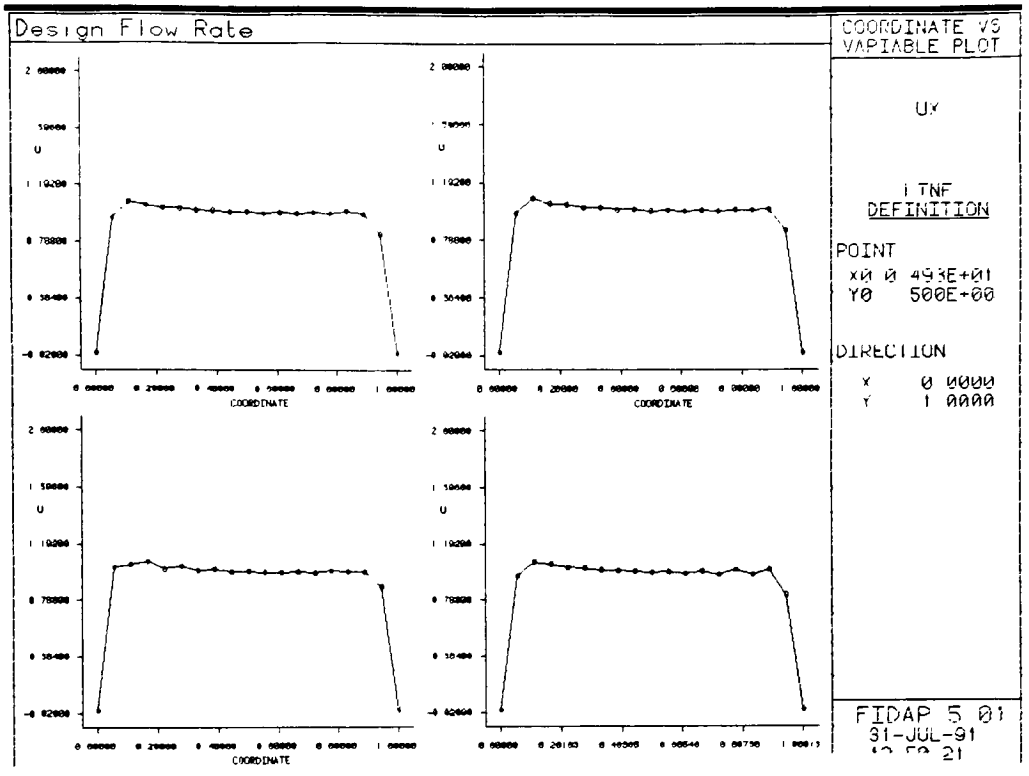

Figure 7.10 - Velocity Profiles at Outlet, 100% Flow

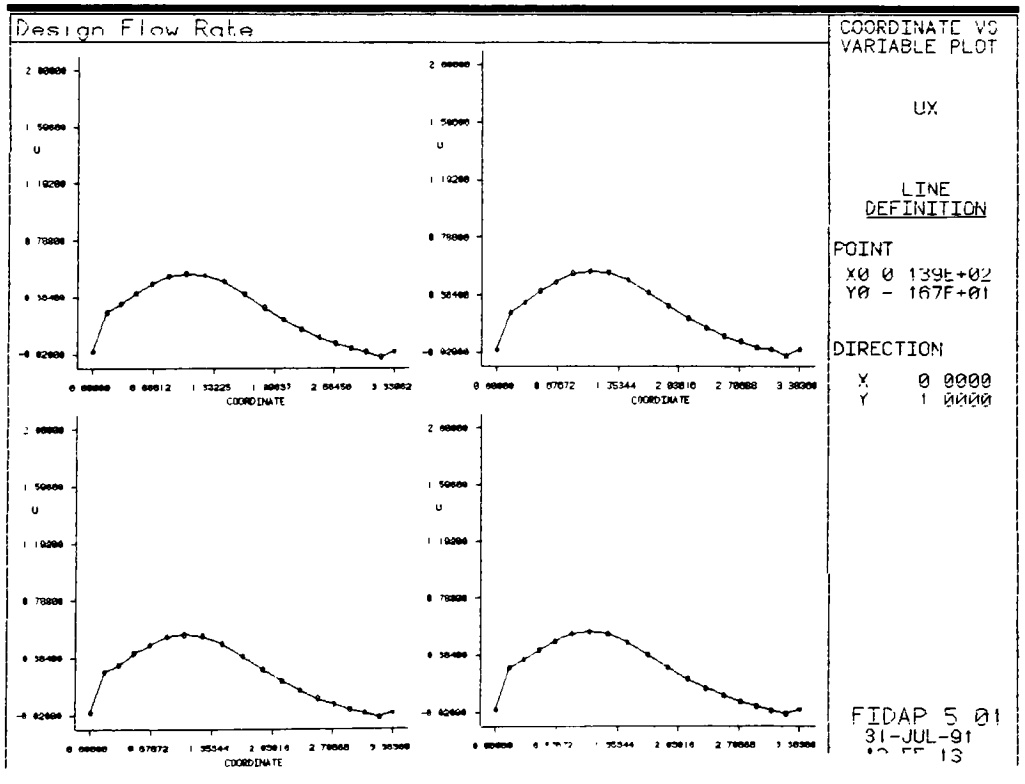

Table 7.3
Diffuser Reynolds Numbers

Model	Inlet Re	Outlet Re
100% Flow	14902	4418
60% Flow	8922	2781
5% Suction	8783	2630
10% Suction	8650	2451
15% Suction	8740	2468
20% Suction	8704	2398
5% Blowing	8941	3017
10% Blowing	9148	3134
15% Blowing	11281	3389

[See Appendix B for calculation of Re]

7-2 Off-Design Flow Conditions (60% Design Flow Rate)

Rocketdyne reported diffuser stall in the single stage water tester at off design flow rates of 76% of design. In order to investigate this reported stall in the diffuser, it was necessary to choose a flow rate that would ensure a stalled condition existed within the diffuser. The flow rate for the tests was chosen to be 60% of the design flow rate. As illustrated in the streamline contour plot (Figure 7.11) and the velocity vector plot at the outlet of the diffuser (Figure 7.12), this model resulted in a large region of separated flow at the upper surface of the diffuser. Consequently, a high speed jet like flow is observed (Figure 7.13) to exist at the lower wall, indicating that the diffuser is experiencing fully developed stall. The data presented in Figure 3.4 predicted stall in the large transition stall region based on the geometry of the diffuser, but it appears that the incidence angle plays a large role as well.

Inspection of the pressure contour plot (Figure 7.14a) shows that a uniform pressure distribution at the diffuser inlet section is followed by a large variation (pressure gradient) across the diffuser outlet and turning channel. At the outer wall of the turning channel or wall farther from the center or curvature, the pressure is greatest and least at the inner wall, or wall near the center of curvature in correlation with the design flow rate results. Intuitively, it is not obvious why flow around a bend adheres to the inner wall, but many examples indicate this counter-intuitive result [2]. The pressure recovery along the centerline (Figure 7.14b) shows a gradual approach to the total recovery obtained by the diffuser.

This flow separation and diffuser stall is an indication that the static pressure recovery of the diffuser will not be as high as desired. From Table 7.2, it is obvious that the pressure recovery attained in a throttling thrust situation will not provide acceptable performance when compared with the design flow model and the ideal pressure recovery coefficient.

The kinetic energy (Figure 7.15), dissipation (Figure 7.16) and vorticity (Figure 7.17) contour plots as well as the velocity profile plots near the inlet (Figure 7.18) and outlet (Figure 7.19) are included to verify the flow field. The dissipation of turbulent energy is concentrated near the inlet of the diffuser in regions of higher turbulence and kinetic energy generation around the suction and blowing holes. The kinetic energy generated in the turning channel appears to be carried out of the model.

The vorticity of the fluid is an indication of the shear rate between the layers of fluid. Figure 7.17 shows a region of high vorticity along the lower diffuser wall indicating the presence of a shear boundary layer. The absence of vorticity near the top of the diffuser is an indication of the slowing, laminarized fluid with a small boundary layer formed by the reversed flow.

The velocity profiles at the inlet resemble typical turbulent profiles that are skewed to reflect the incidence effects. A slight disturbance in the velocity flow field is introduced at the throat due to the change in flow area. At the outlet, the flow resembles a skewed laminar profile, with flow reversal at the upper wall. The Reynolds numbers indicated on Table 7.2 serve to reinforce these observations.

Figure 7.11 - Streamline Contour Plot

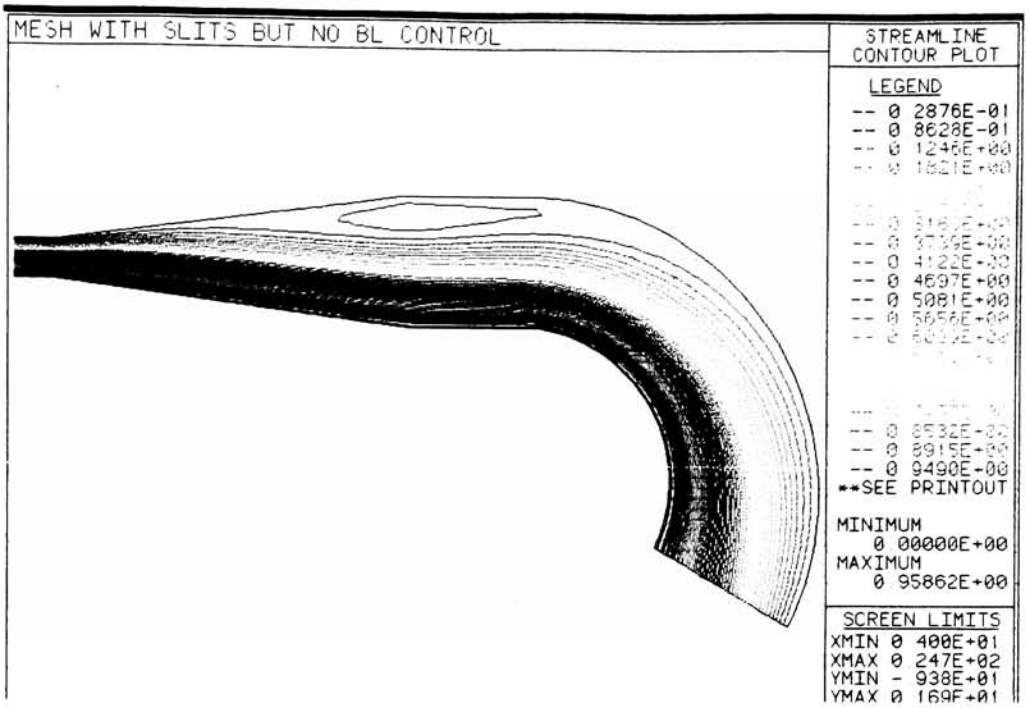

Figure 7.12 - Velocity Vector Plot at Outlet

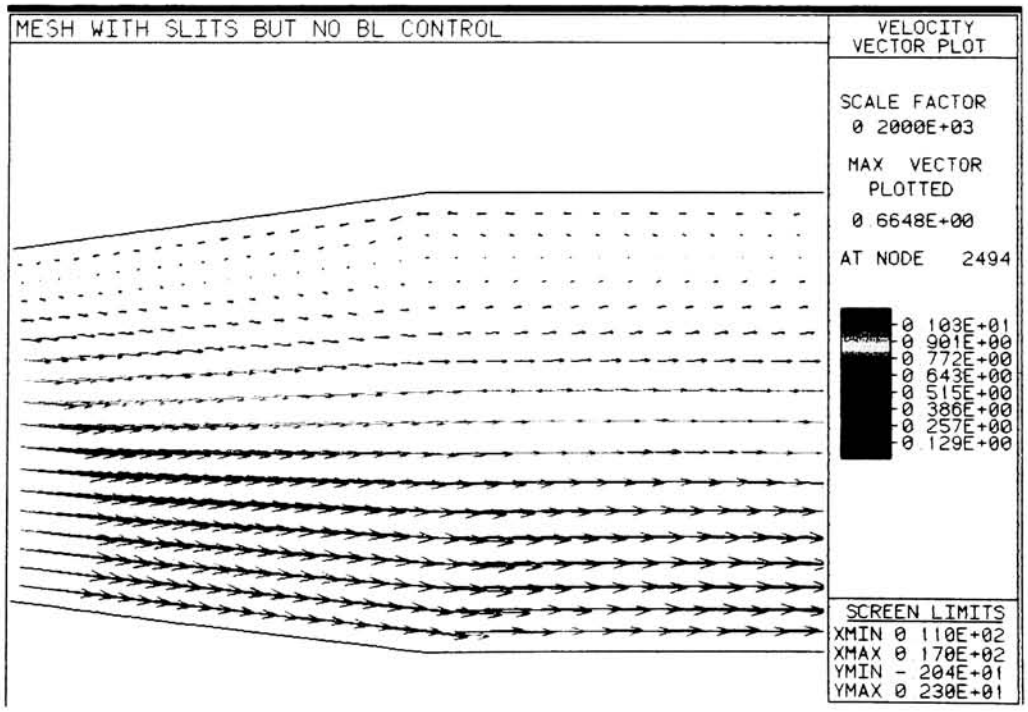

Figure 7.13 - Speed Contour Plot, 60% Design

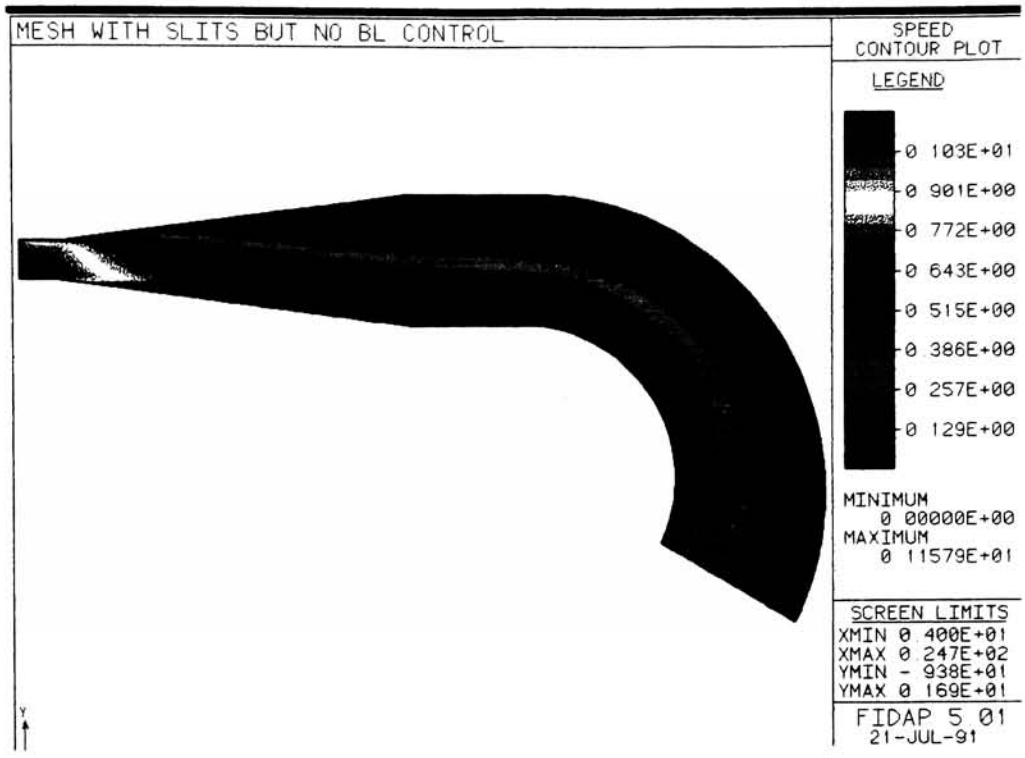

Figure 7.14a - Pressure Contour Plot, 60% Design

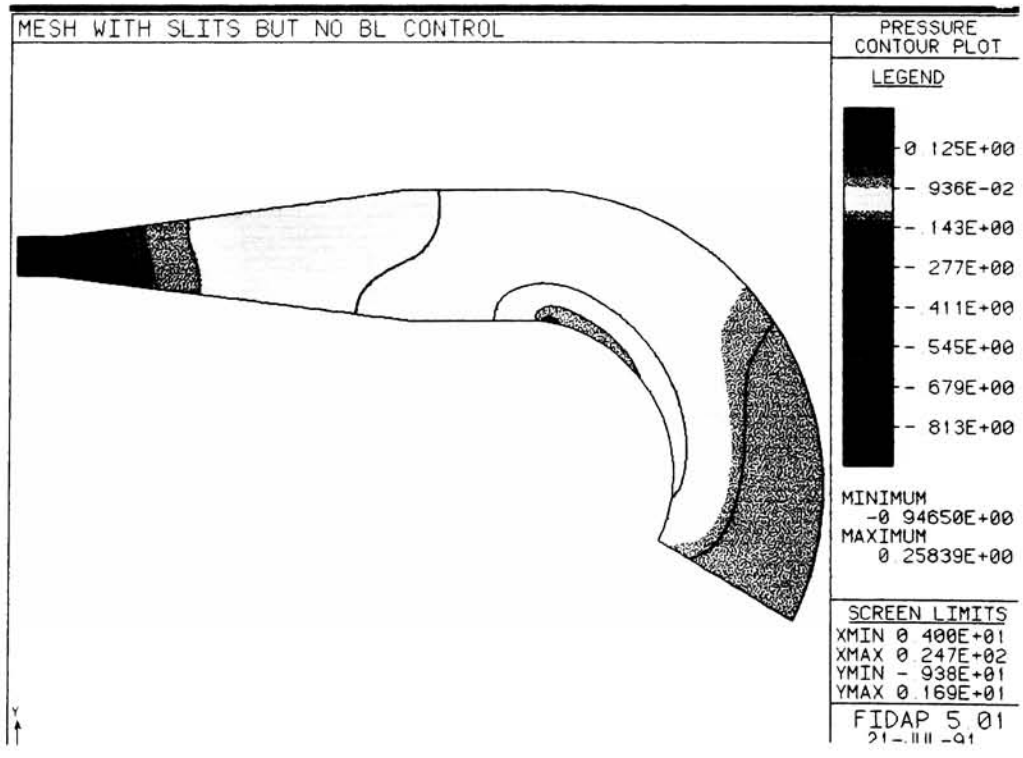

Figure 7.14b - Pressure Along the Diffuser Centerline, 60% Design

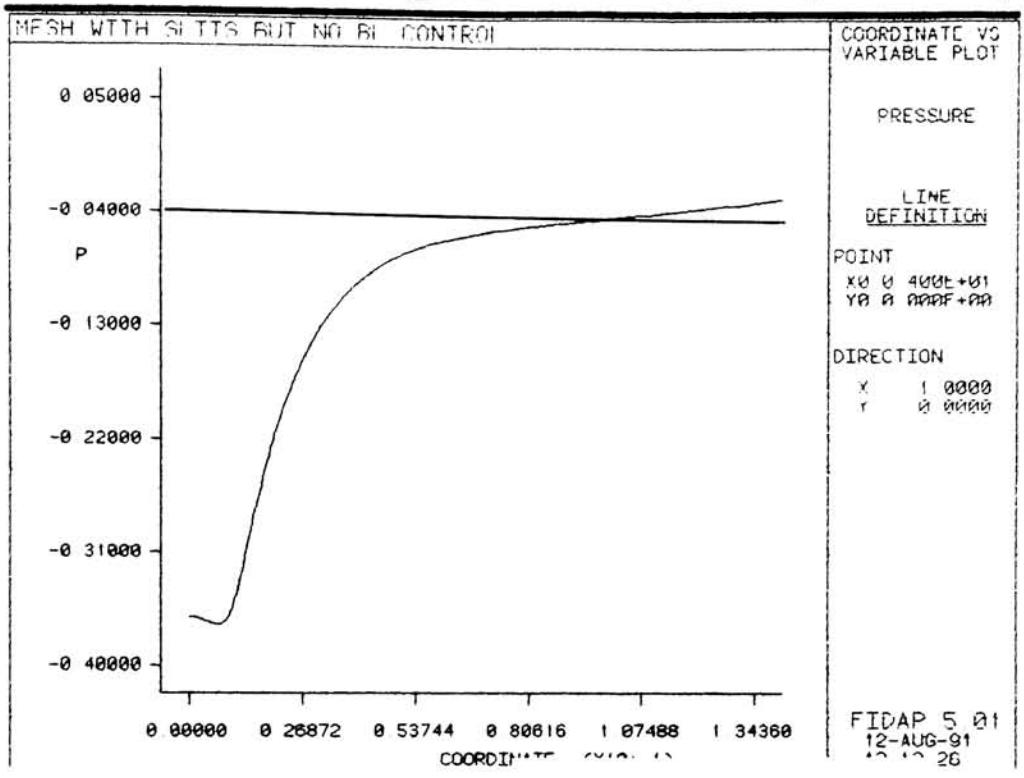

Figure 7.15 - Kinetic Energy Contour Plot, 60% Design

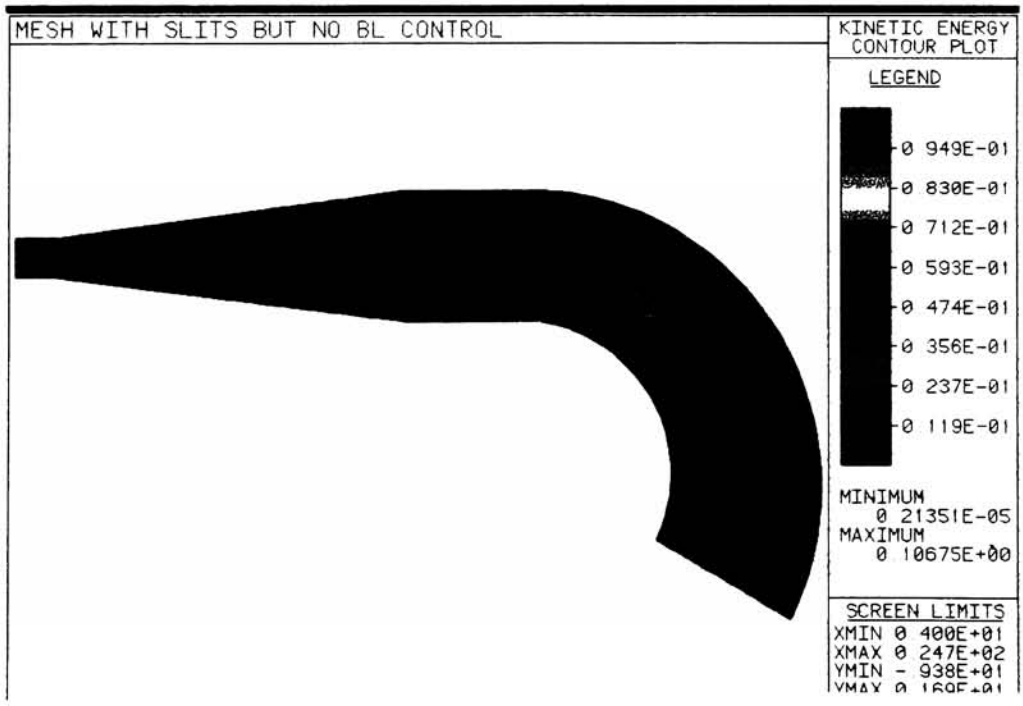

Figure 7.16 - Dissipation Contour Plot, 60% Design

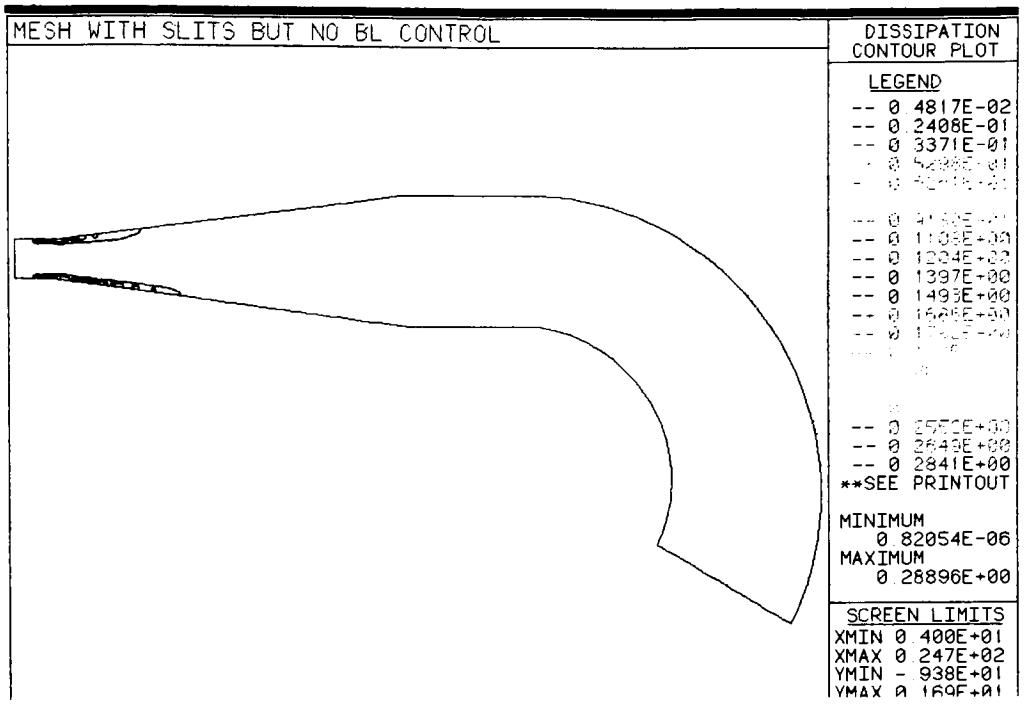

Figure 7.17 - Vorticity Contour Plot, 60% Design

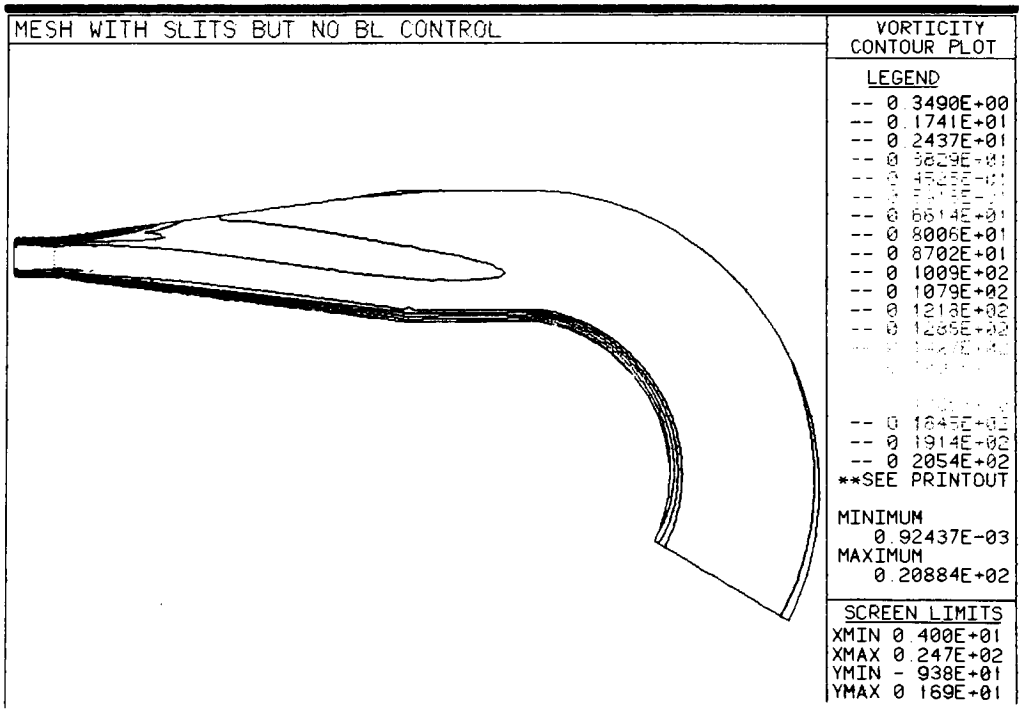

Figure 7.18 - Velocity Profiles at Inlet, 60% Design

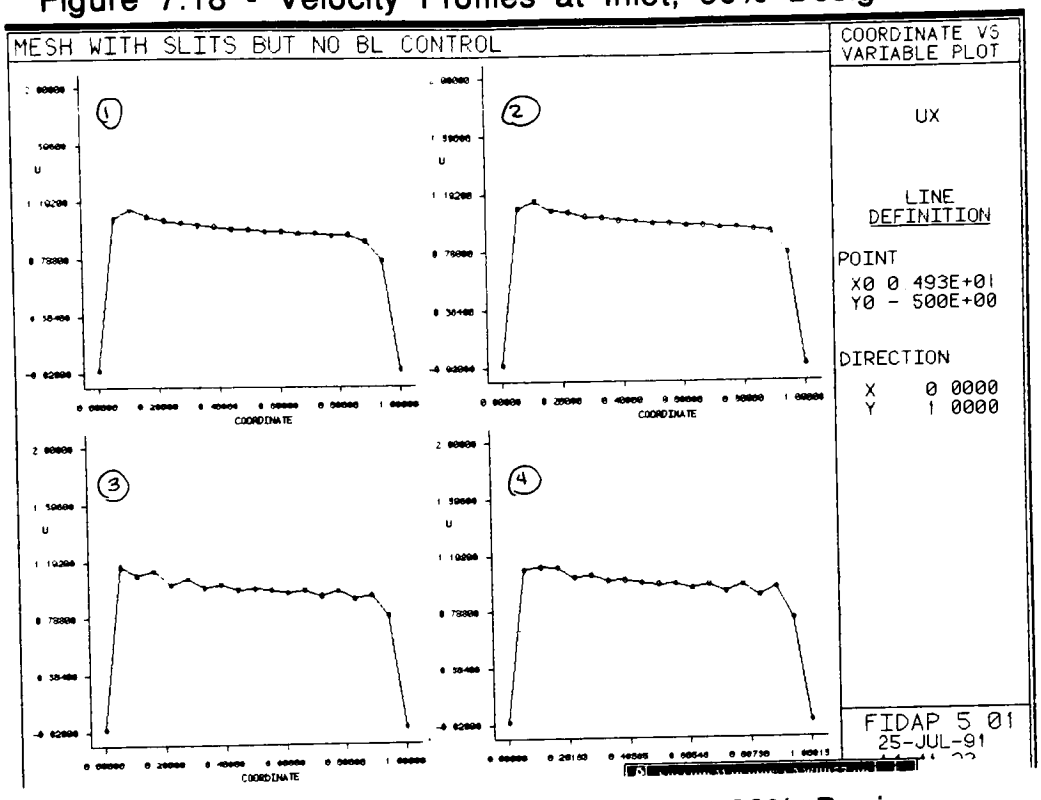

Figure 7.19 - Velocity Profiles at Outlet, 60% Design

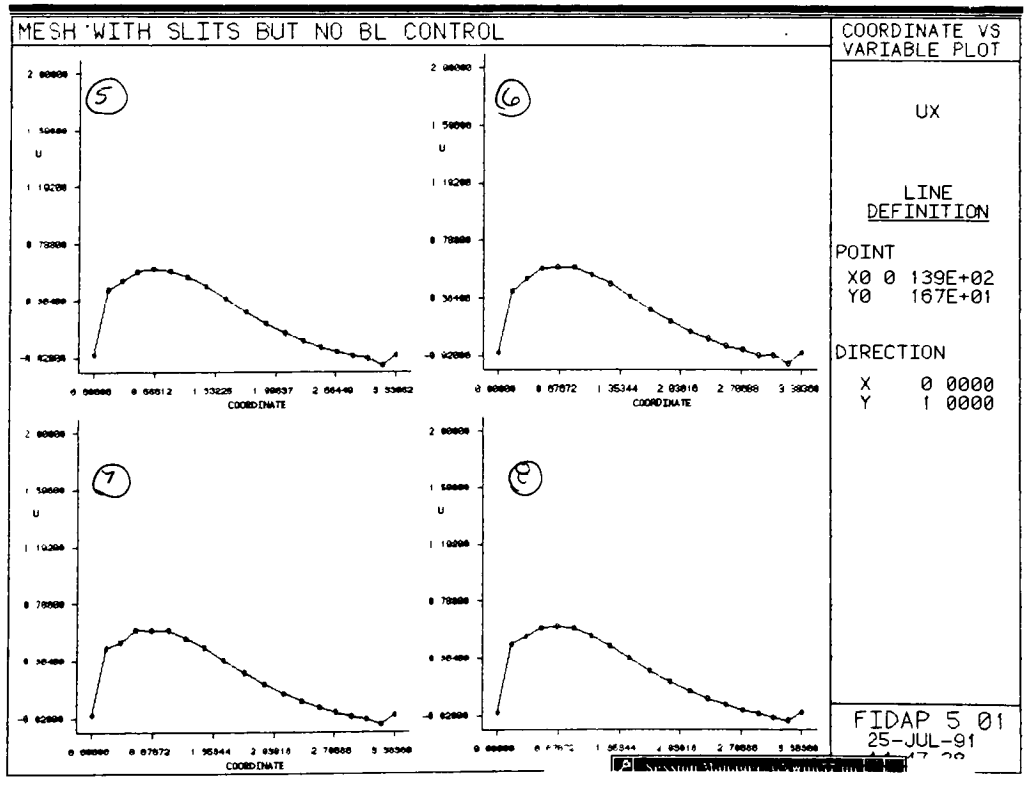

7-3 Suction

Suction was applied to the off-design flow model to test its effectiveness in reducing or preventing stall. Various rates of suction were tested in order to determine a level that would produce the best results. The literature search indicated that suction between the rates of 6 and 18 percent of the inlet mass flow rate were most effective, (Note: Suction and blowing rates will always be given as a percentage of the inlet mass flow rate.) so the results presented here are for suction rates of 5, 10,15 and 20 percent.

Results from preliminary tests indicated that the best configuration to counteract the incidence effects introduced at the lower flow rate was to apply suction through the top wall of the diffuser. The total suction rate was distributed equally across the seven available slits with the velocity of the fluid at each slit being equal. The results presented here indicate that a suction rate of 15% of the inlet mass flow rate provides a significantly higher pressure recovery than that obtained in the diffuser with no controls. The resulting flow field in this configuration is more uniform and well behaved in accordance with this higher pressure recovery.

7-3.1 5% Suction

The implementation of 5% suction significantly reduced the flow separation that was experienced in the uncontrolled diffuser. The streamline contour plot (Figure 7.20) and the velocity vector plot at the diffuser outlet (Figure 7.21) show a marked decrease in the area of flow reversal as well as a delay in the actual separation

point resulting in a more uniform pressure recovery. The velocity vector plot at the outlet indicate a more uniform velocity profile across the outlet region and especially within the region encompassed by the flow reversal. The speed contour plot (Figure 7.22) provides further verification of a relatively more uniform outlet velocity.

The pressure contour plot (Figure 7.23a) and the pressure line plot at the diffuser centerline (Figure 7.23b) indicate that the majority of the pressure recovery appears to take place in a more uniform fashion prior to the separation point, indicating that the remaining flow separation should have little effect on the diffuser performance. The pressure field that exists in the turning channel is more uniform in nature, indicating a more well behaved flow in this region as well. The pressure recovery of this configuration is increased above the uncontrolled flow situation indicating that even slight suction does provide an improved diffuser performance.

The kinetic energy generation (Figure 7.24) and the dissipation (Figure 7.25) within the diffuser are in agreement with the governing equations providing most of the dissipation at the location of the generation. The majority of the turbulent kinetic energy generation occurs at the throat and in the turning channel, both regions of apparently high turbulence. The laminarized flow at the outlet does not provide much energy except in the flow reversal region where the vorticity (Figure 7.26) of the flow indicates a region of higher shear stress.

The velocity profiles across the inlet region (Figure 7.27) resemble the typical, skewed turbulent profiles of the uncontrolled

diffuser until the diffuser throat is traversed. At the throat, the flow seems to have become unstable due to the implementation of suction. Beyond the suction slits, the flow settles down into a more uniform profile. The flow has a slight bit of oscillation at the diffuser exit (Figure 7.28) possible due to the abrupt change in geometry, but it quickly dies out. It resembles the expected skewed laminar profiles of the previous models.

Figure 7.20 - Streamline Contour Plot, 5% Suction

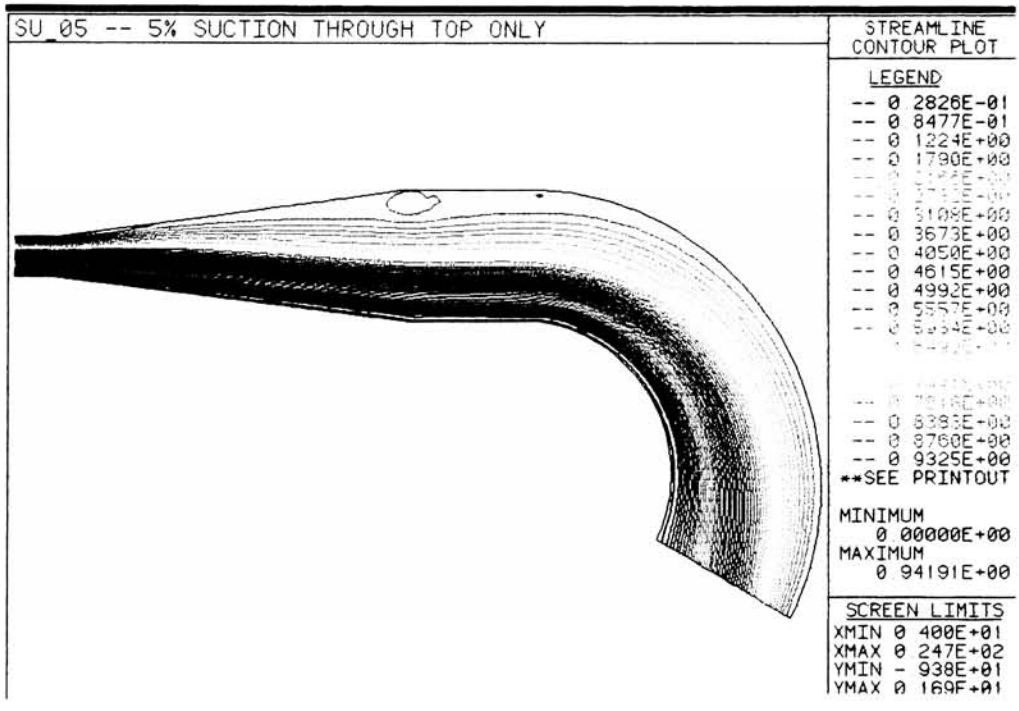

Figure 7.21 - Velocity Vector Plot at the Outlet, 5% Suction

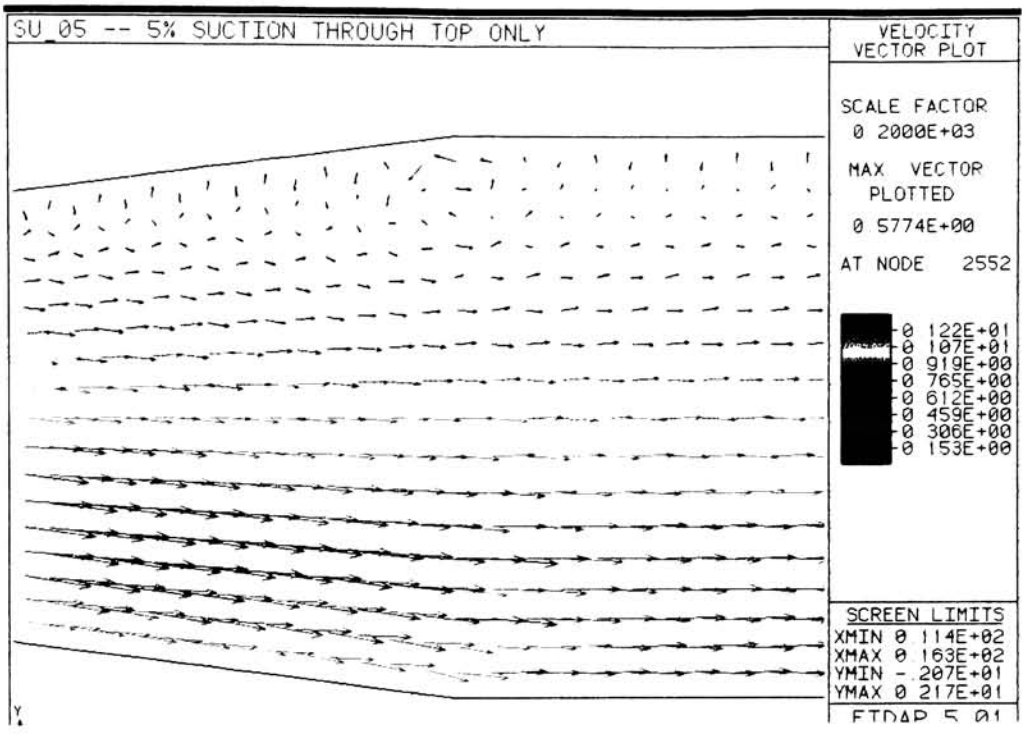

Figure 7.22 - Speed Contour Plot, 5% Suction

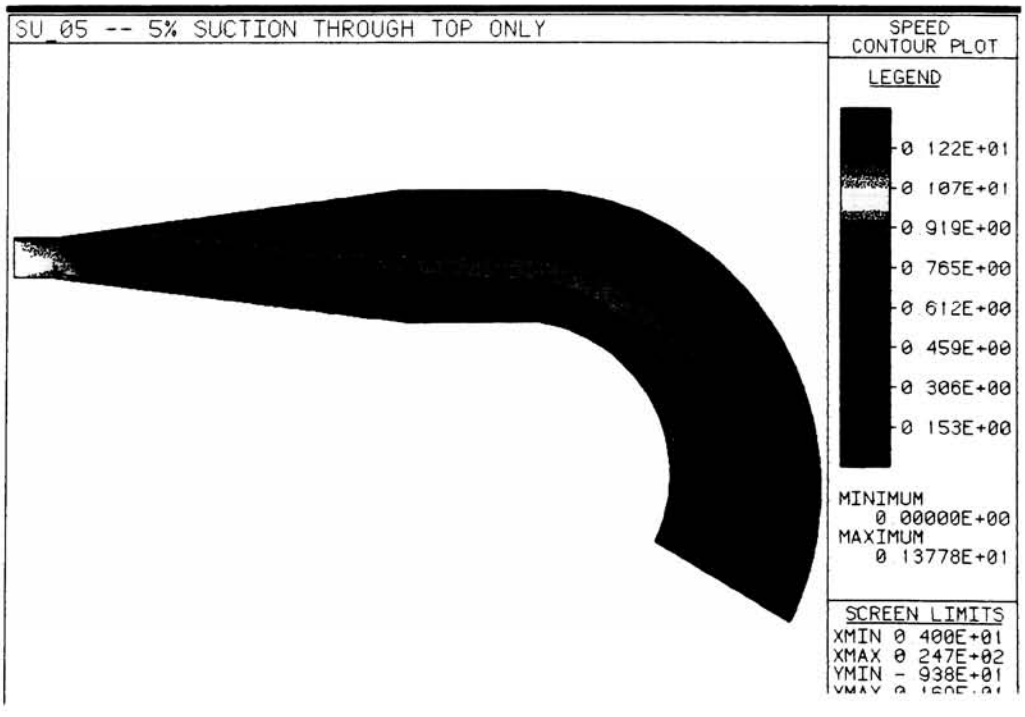

Figure 7.23a - Pressure Contour Plot, 5% Suction

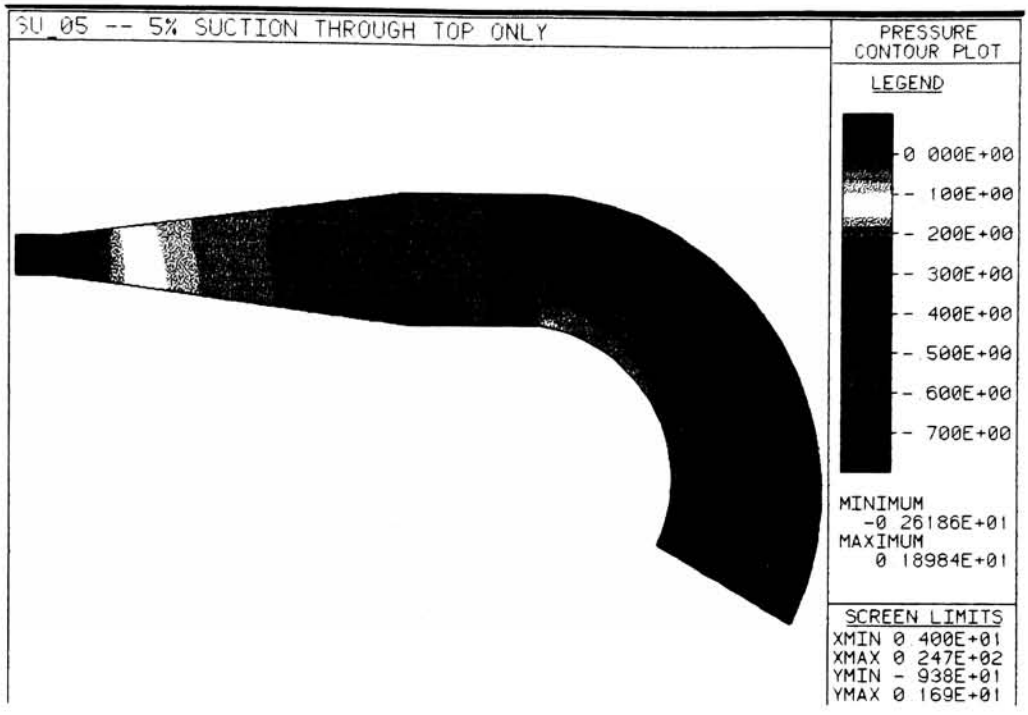

Figure 7.24b - Pressure Along the Diffuser Centerline, 5% Suction

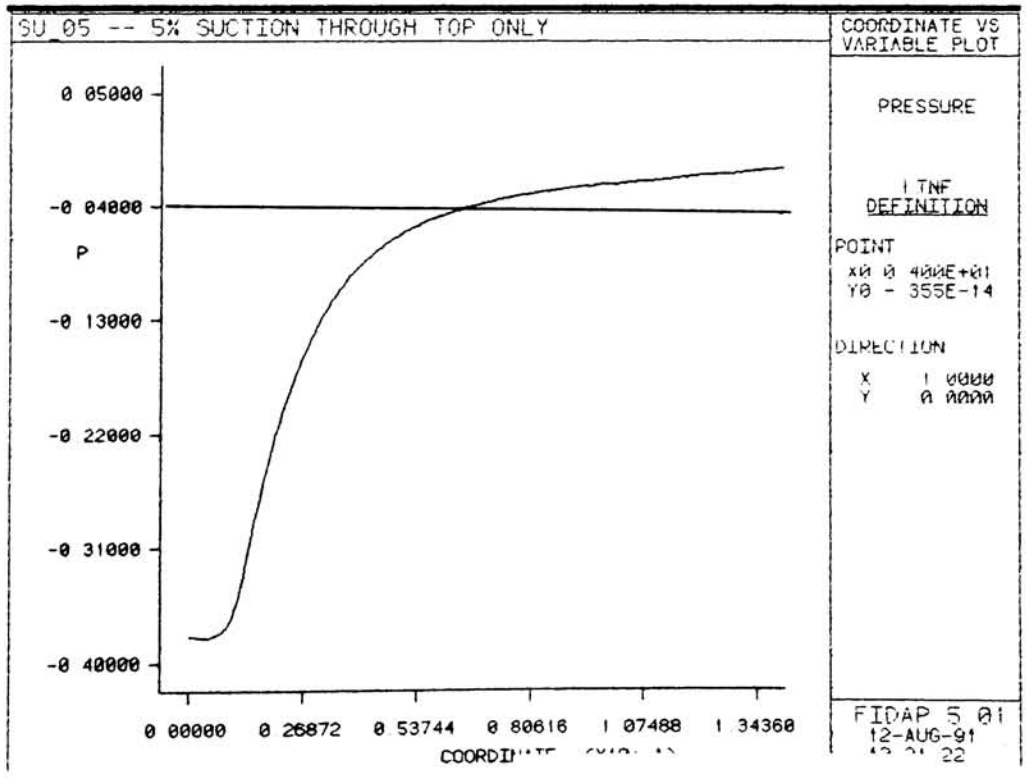

Figure 7.24 - Vorticity Contour Plot, 5% Suction

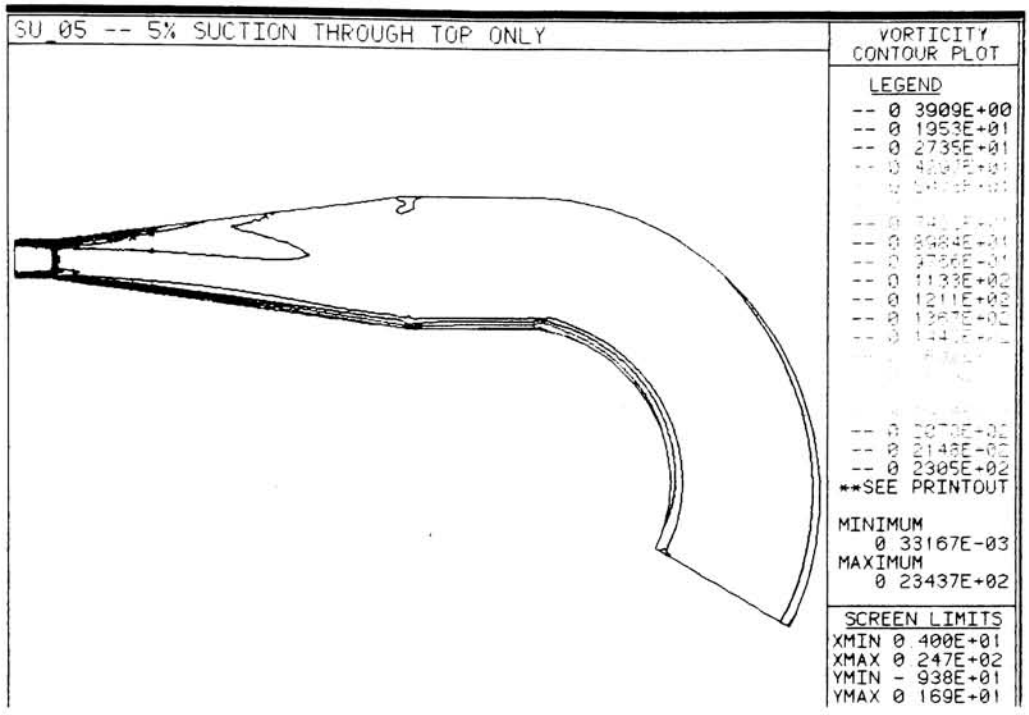

Figure 7.25 - Kinetic Energy Contour Plot, 5% Suction

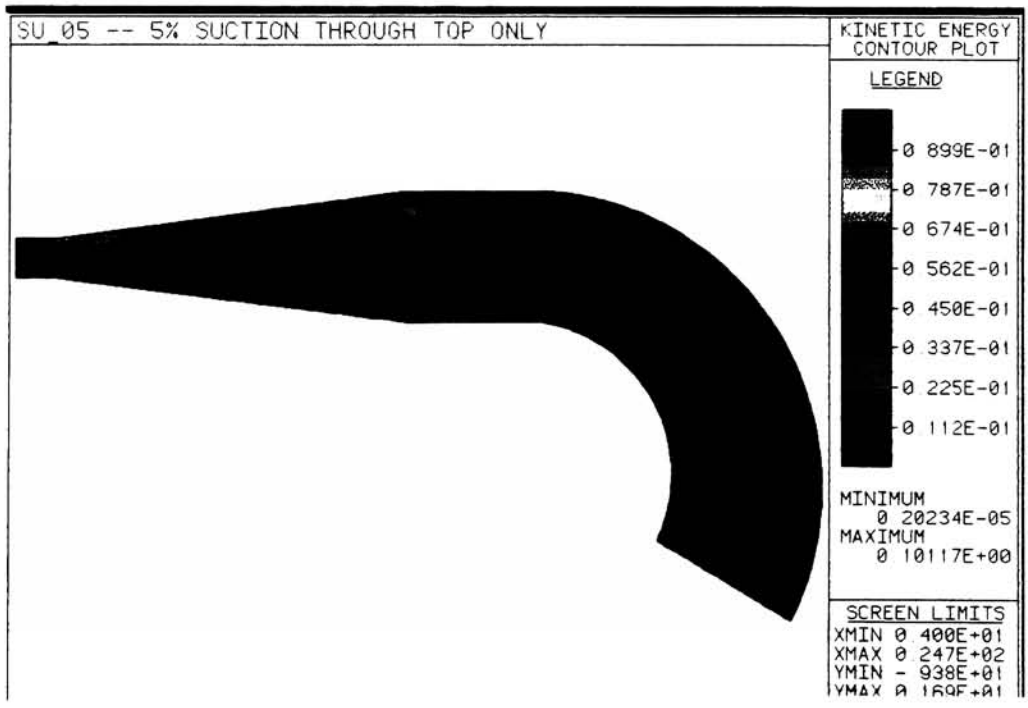

Figure 7.26 - Dissipation Contour Plot, 5% Suction

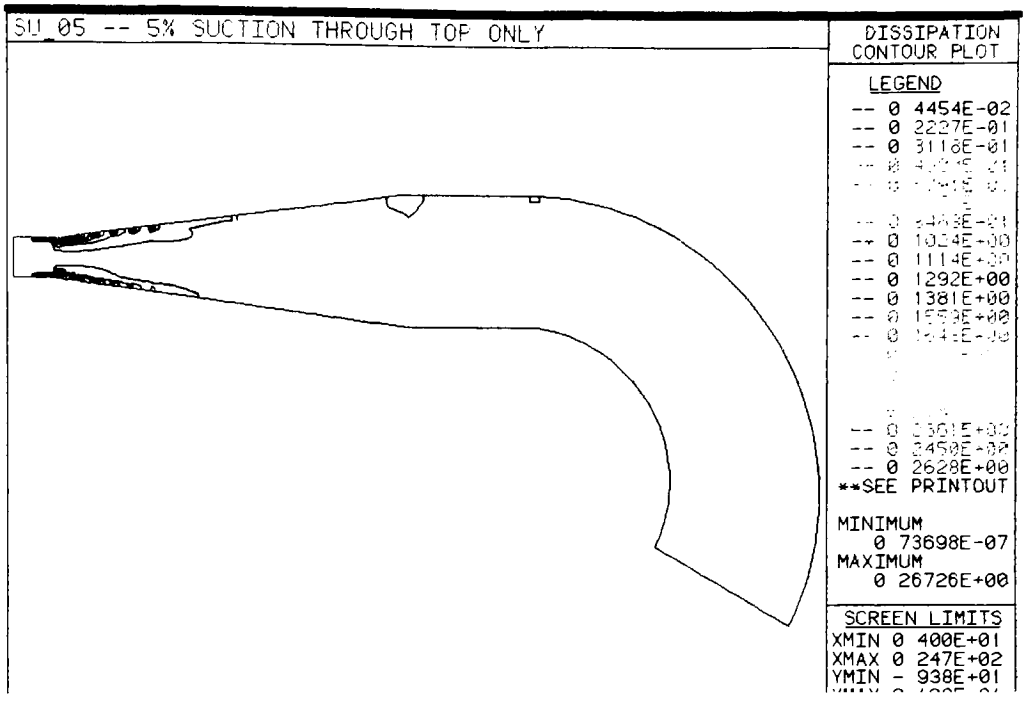

Figure 7.27 - Inlet Velocity Profiles, 5% Suction

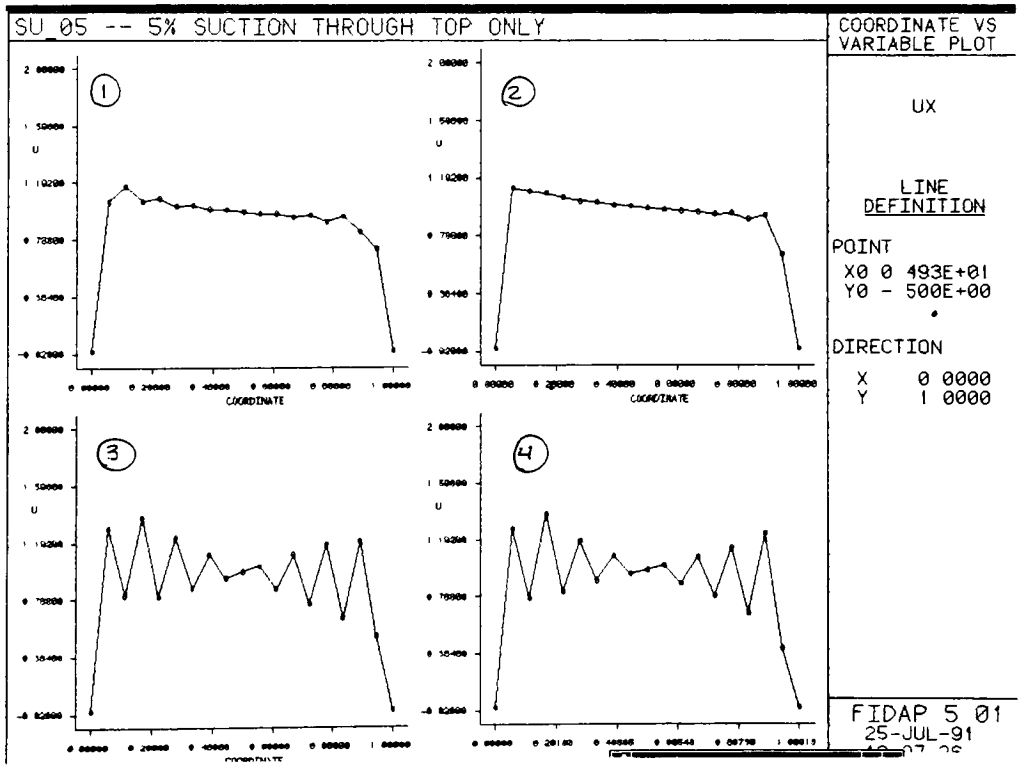

Figure 7.28 - Outlet Velocity Profiles, 5% Suction

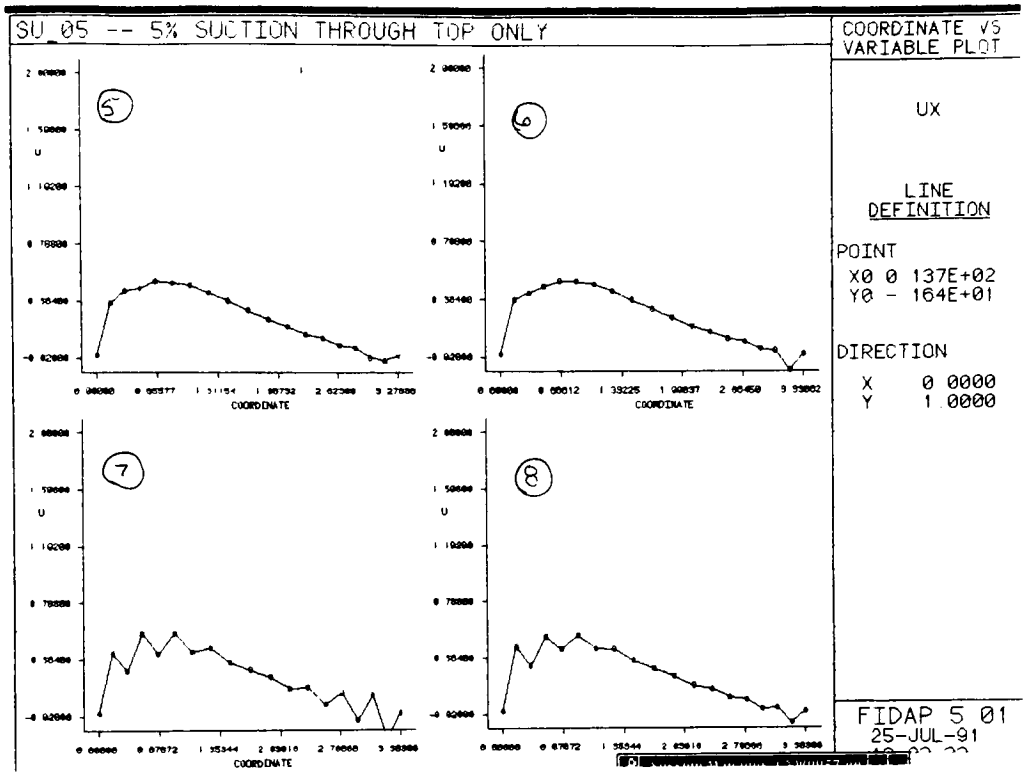

7-3.2 10% Suction

With the application of 10% suction, the separation point on the wall moved further along the diffuser wall towards the diffuser exit. This can be seen by examining the streamline contour plot (Figure 7.29) as well as the velocity vector plot at the outlet (Figure 7.30). The speed contour plot (Figure 7.31) indicates a reduced jet flow situation along the lower wall and consequently a more uniform flow field throughout the diffuser.

The pressure contour plot (Figure 7.32a) and the pressure at the diffuser centerline (Figure 7.32b) indicate a uniform pressure recovery throughout the diffuser with the majority of the pressure being recovered before the separation point. The higher pressure recovery coefficient (Table 7.2) and more uniform conversion of kinetic energy indicates that the remaining flow separation has little effect on the diffuser performance.

The vorticity of the flow field (Figure 7.33) at the inlet seems to have been reduced as a consequence of the suction allowing a more uniform flow field to develop, helping to increase the pressure recover. The kinetic energy generation (Figure 7.34) and the dissipation (Figure 7.35) appear to have decreased in response to the uniformity of the flow field in the main section of the diffuser.

The previously observed local instabilities at the throat of the diffuser (Figure 7.36) seem to have increased in intensity with the increased suction rate. The outlet velocity (Figure 7.37) decreased as expected due to the increase in suction rate. Again instabilities at the outlet can be attributed to the change in geometry.

Figure 7.29 - Streamline Contour Plot, 10% Suction

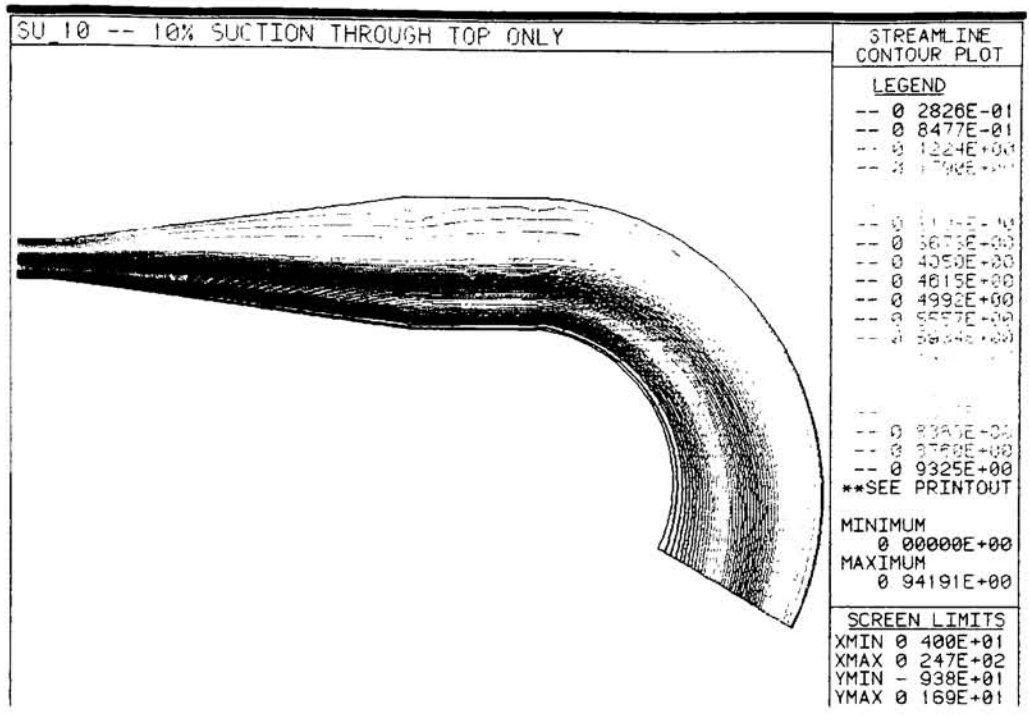

Figure 7.30 - Velocity Vector Plot at the Outlet, 10% Suction

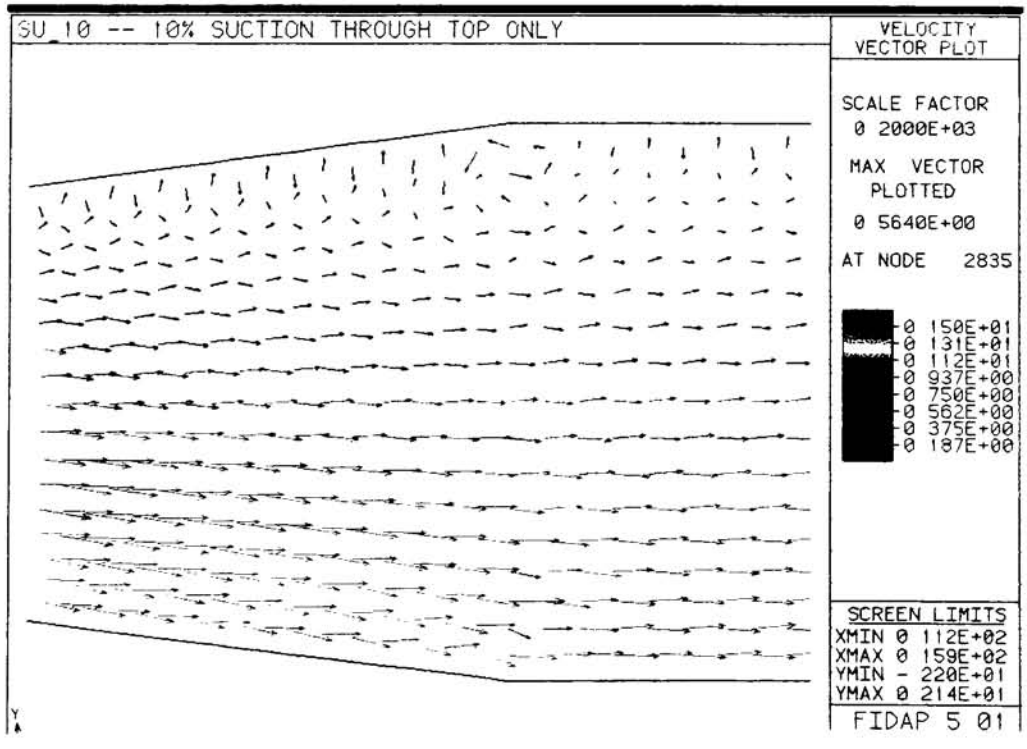

Figure 7.31 - Speed Contour Plot, 10% Suction

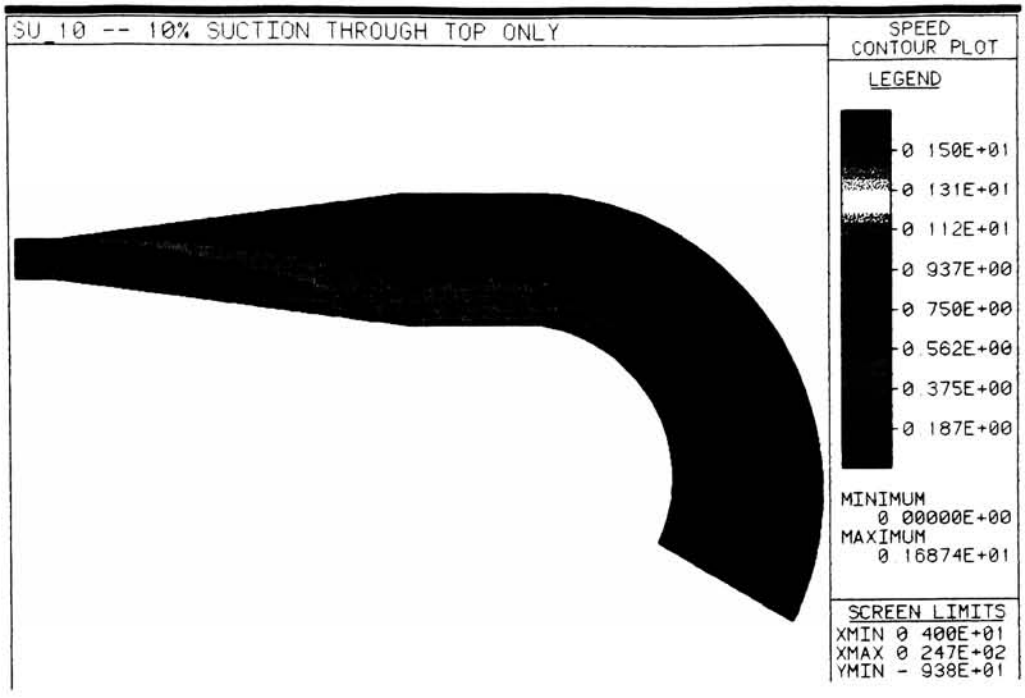

Figure 7.32a - Pressure Contour Plot, 10% Suction

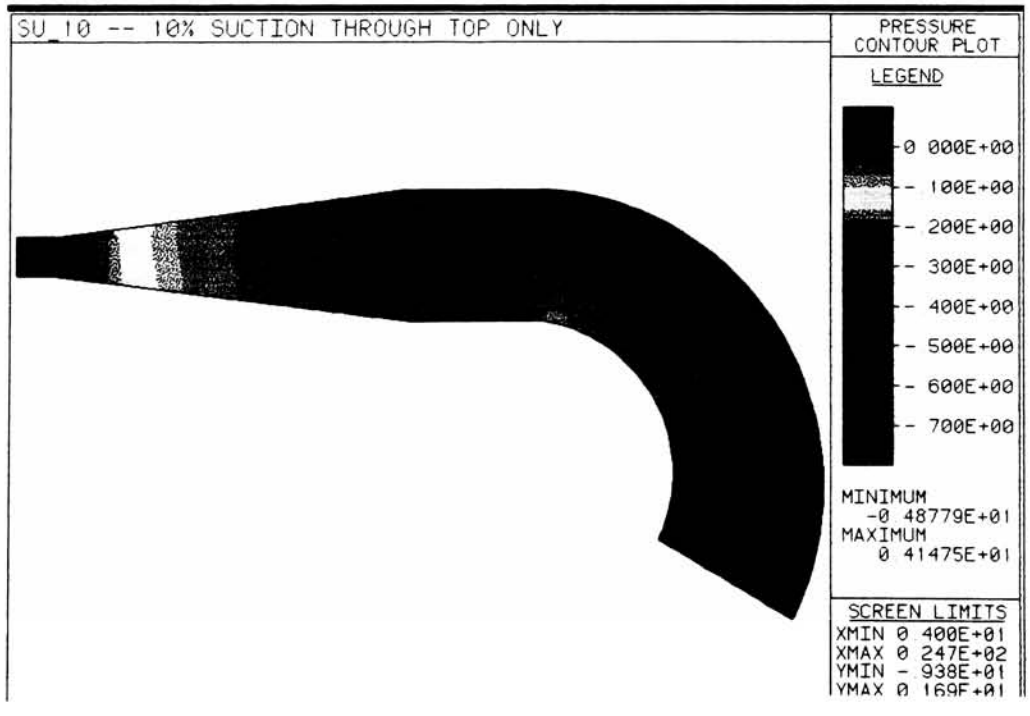

Figure 7.32b - Pressure Along the Diffuser Centerline, 10% Suction

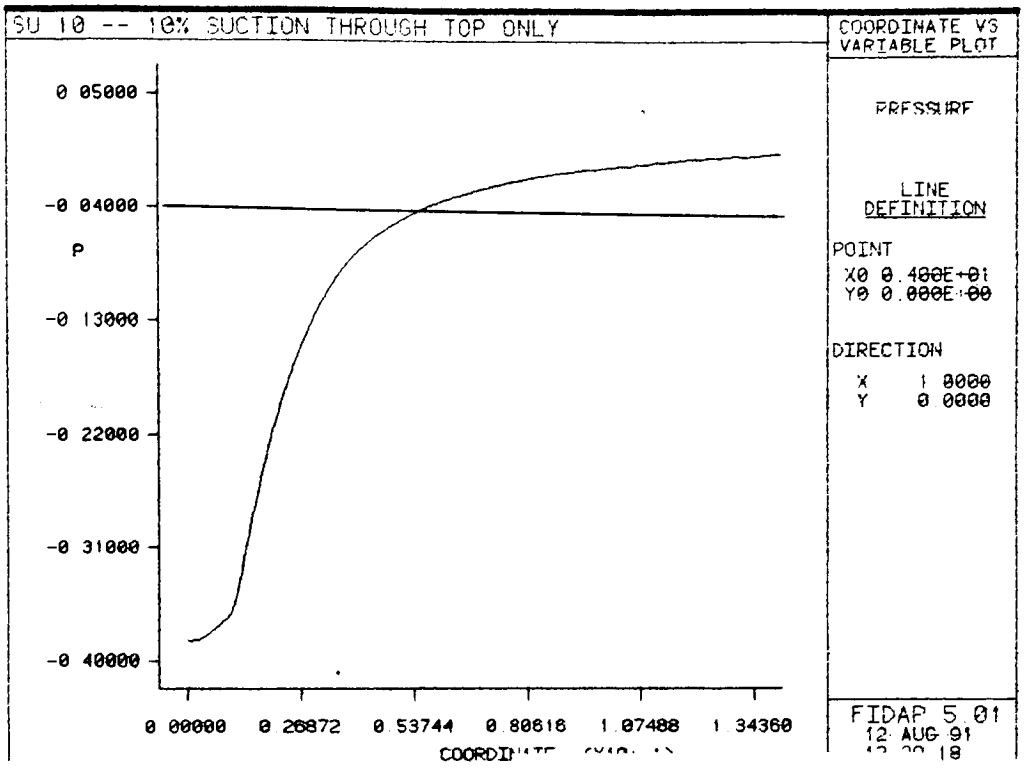

Figure 7.33 - Vorticity Contour Plot, 10% Suction

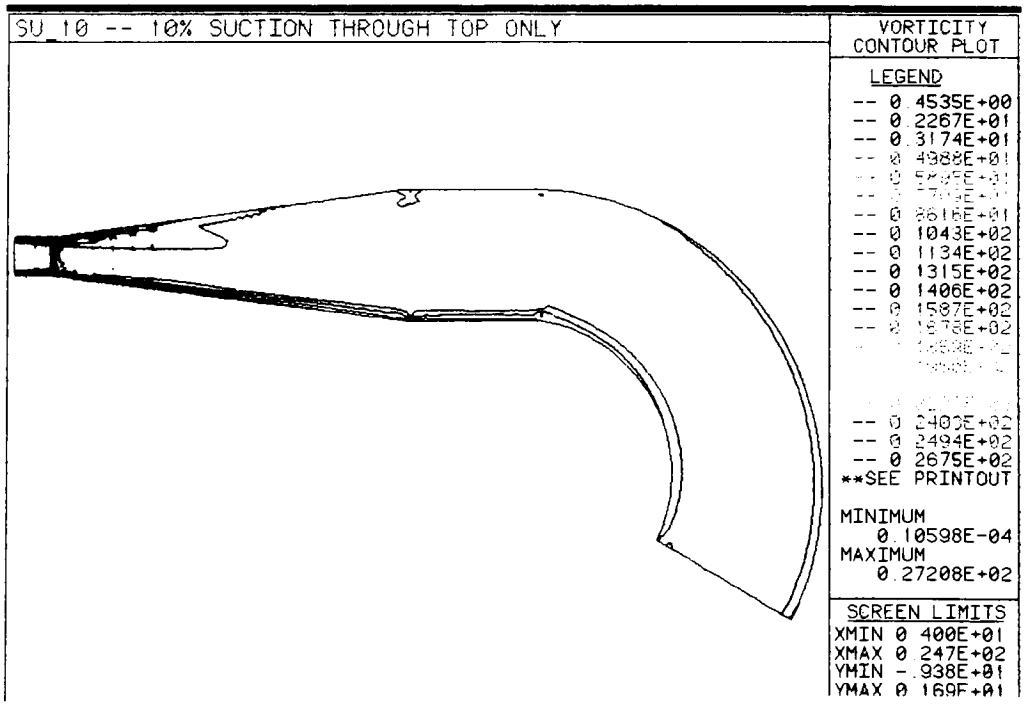

Figure 7.34 - Kinetic Energy Contour Plot, 10% Suction

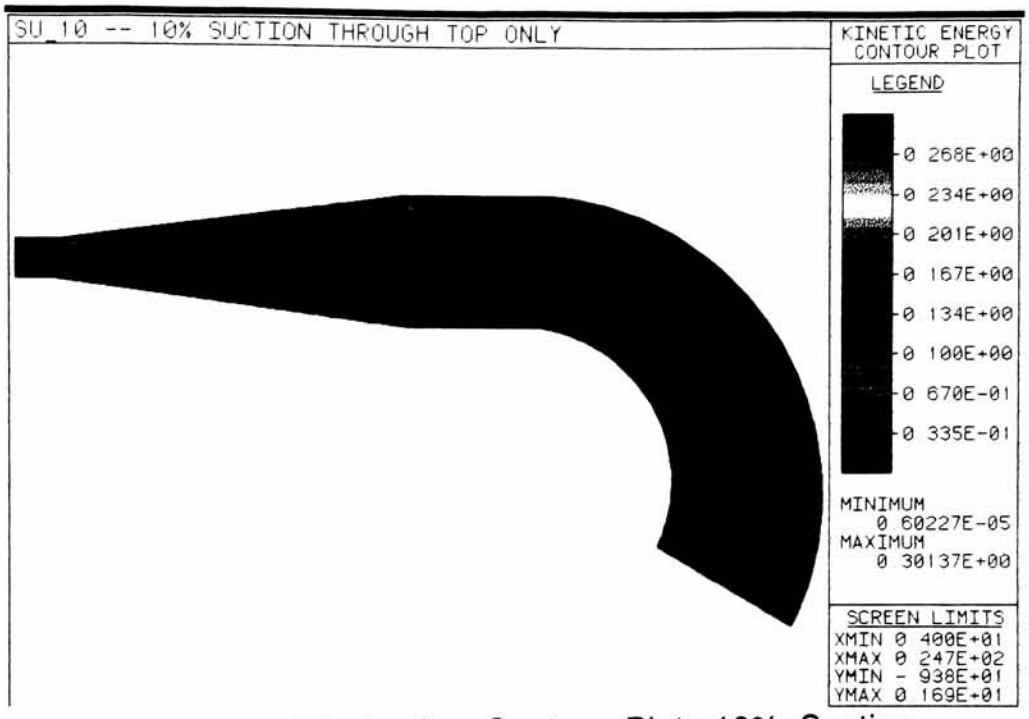

Figure 7.35 - Dissipation Contour Plot, 10% Suction

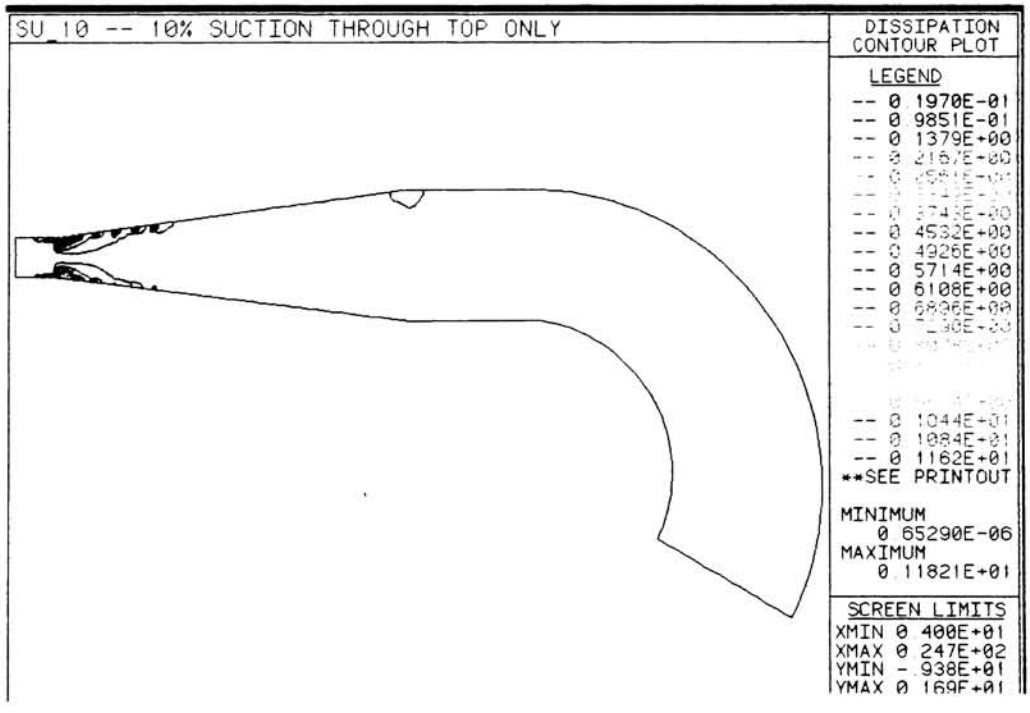

Figure 7.36 - Inlet Velocity Profiles, 10% Suction

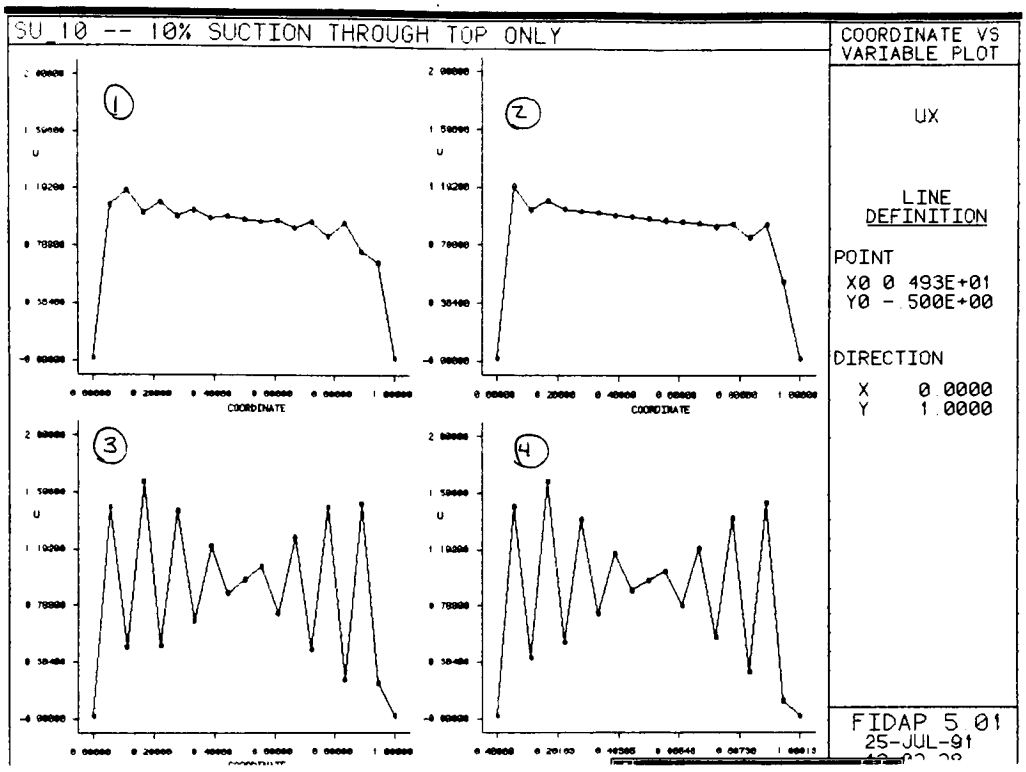

Figure 7.37 - Outlet Velocity Profiles, 10% Suction

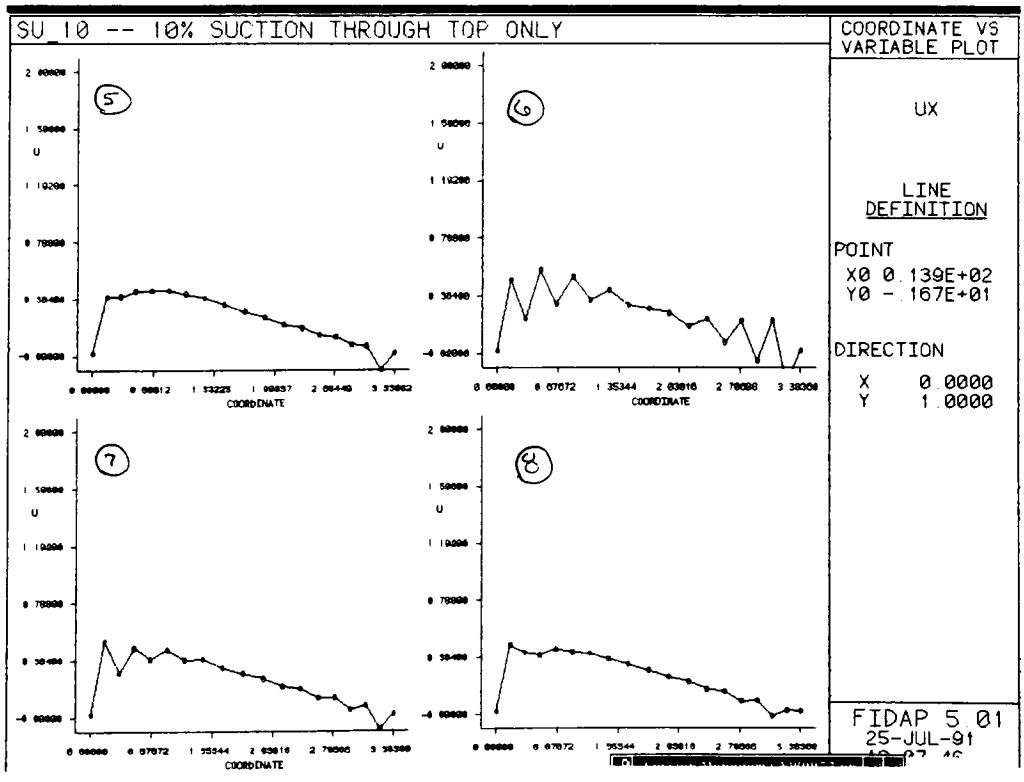

7-3.3 15% Suction

The implementation of 15% suction provides the best pressure recovery of the three suction rates tested. The streamline contour plot (Figure 7.38) and velocity vector plot of the outlet (Figure 7.39) indicate a larger flow reversal area at the diffuser outlet which would tend to indicate a reduced performance for this configuration. The speed contour plot (Figure 7.40) and Table 7.2 indicate that the throat Reynolds number has reached a maximum which, in turn, provides a lower inlet pressure, thereby increasing the overall pressure recovery. This increase in speed can be attributed to the higher suction rate pulling the fluid through the throat very efficiently. The pressure contour plot (Figure 7.41a) and the pressure at the diffuser centerline (Figure 7.41b) indicate a uniform pressure recovery along the diffuser that occurs well before the separation point, implying that the separation that does occur once again is not significant.

The vorticity (Figure 7.42), kinetic energy generation (Figure 7.43) and the dissipation (Figure 7.44) are in accordance with the previous models. It should be noted that the vorticity along the outer radius of the turning channel has been increasing as the suction increases. This is an indication of a growing viscous boundary layer along this wall.

The flow field at the inlet (Figure 7.45) again exhibits some instabilities that are more pronounced that the previous models. It seems that the stability of this inlet region depends on the suction rate in some fashion. The characteristics of the velocity at the

outlet (Figure 7.46) resembles that observed in previous models with a minor instability caused by the change in geometry.

Figure 7.38 - Streamline Contour Plot, 15% Suction

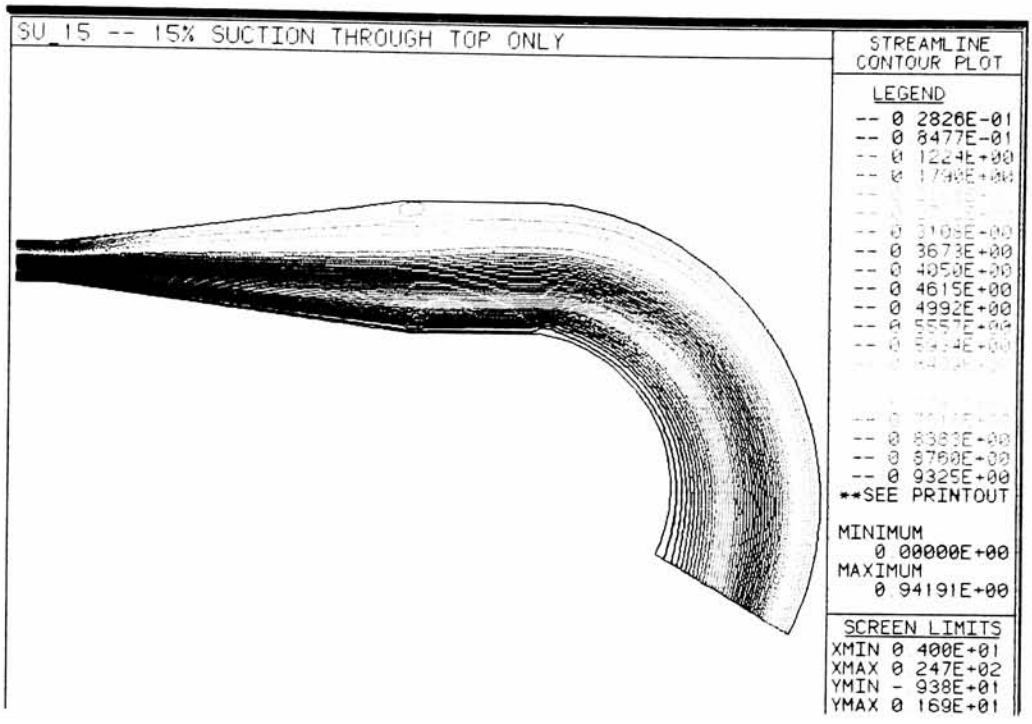

Figure 7.39 - Velocity Vector Plot at the Outlet, 15% Suction

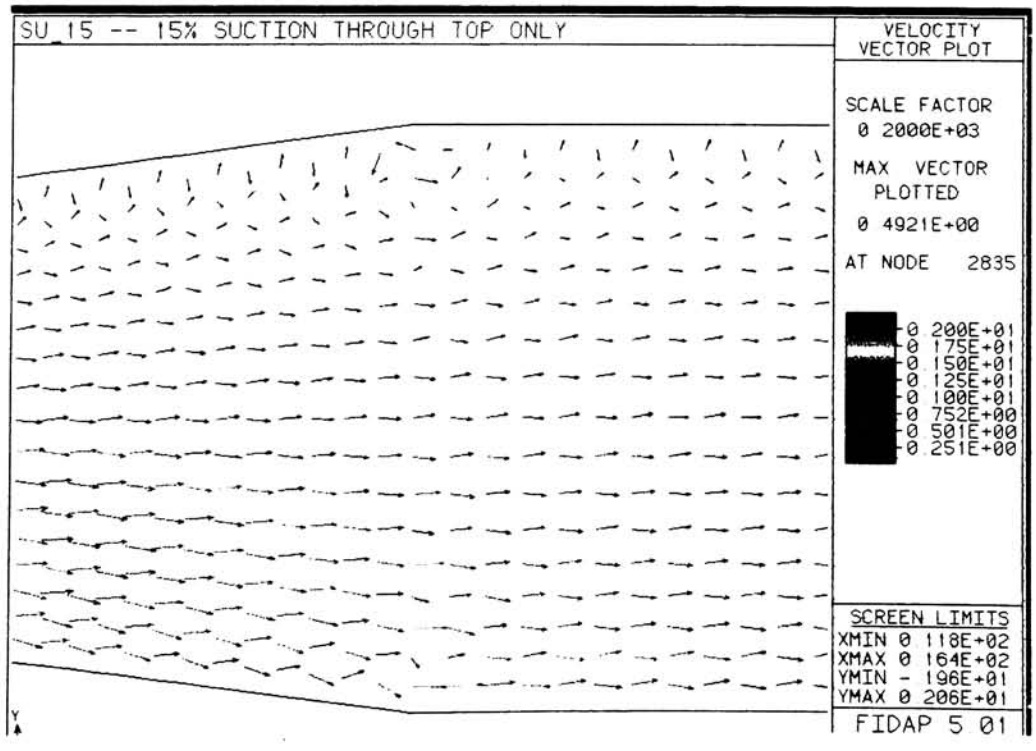

Figure 7.40 - Speed Contour Plot, 15% Suction

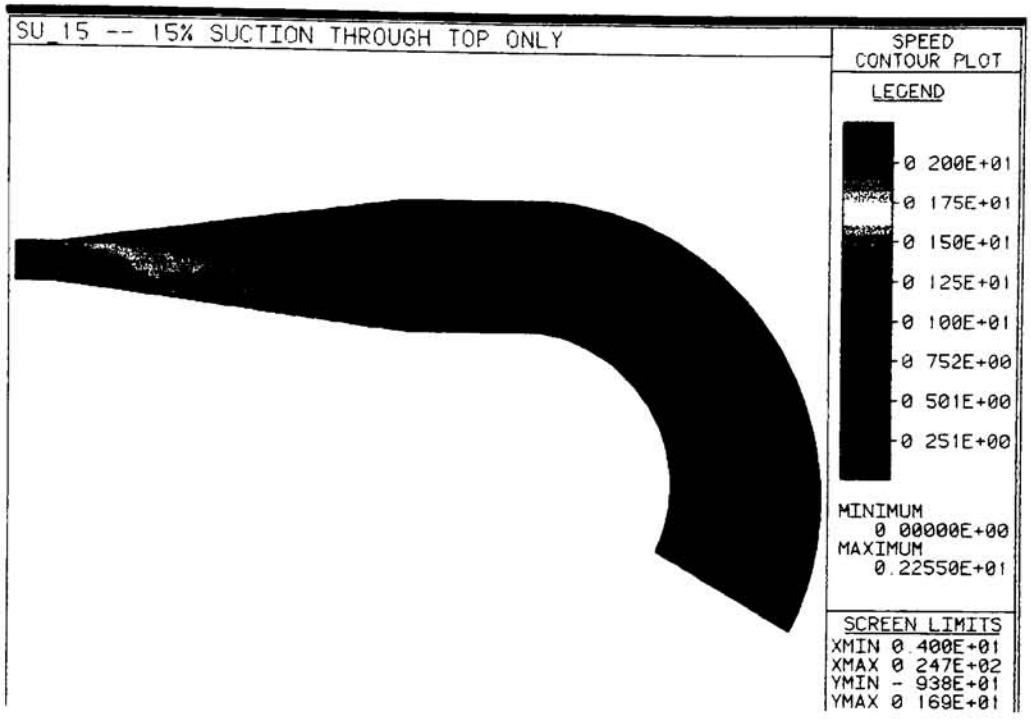

Figure 7.41 - Pressure Contour Plot, 15% Suction

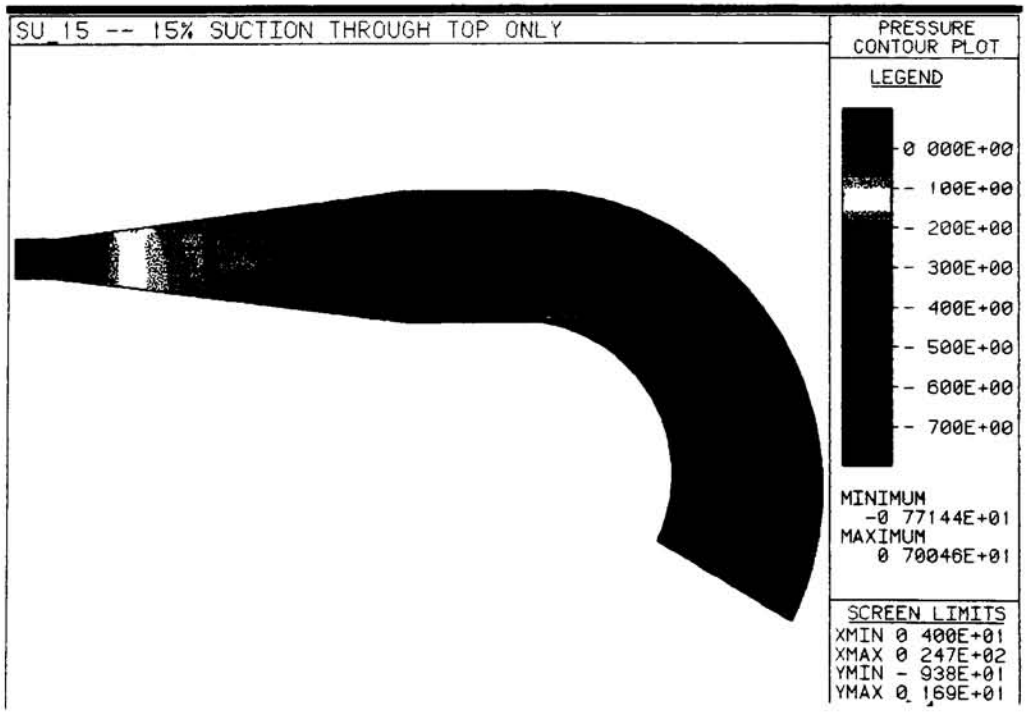

Figure 7.41b - Pressure Along the Diffuser Centerline, 15% Suction

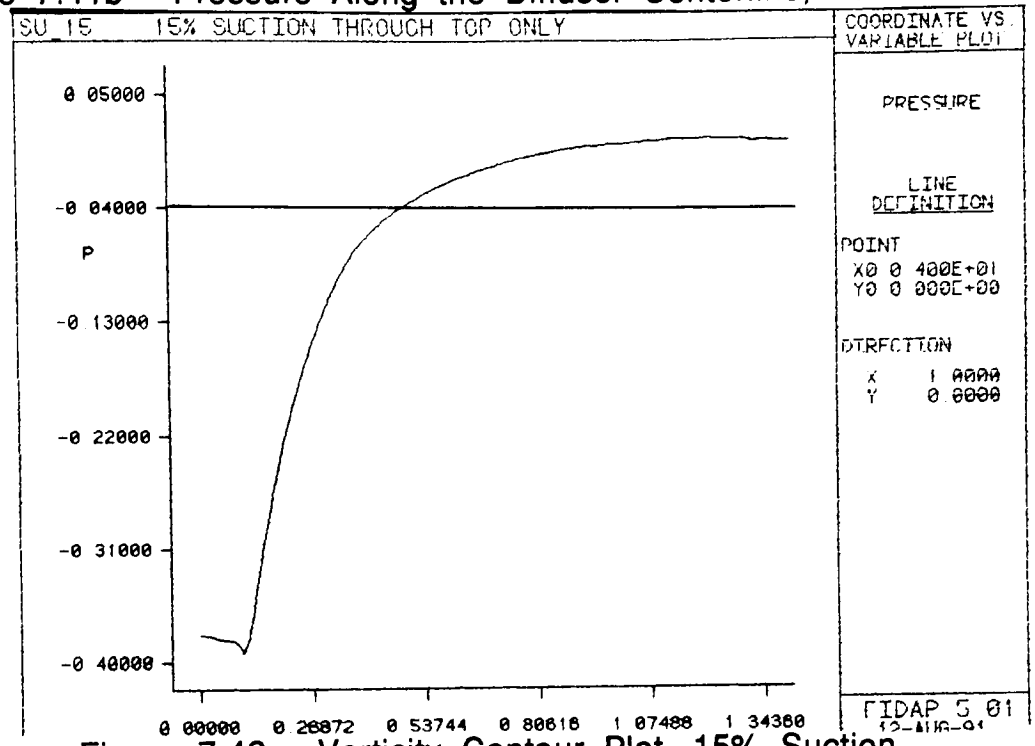

Figure 7.42 - Vorticity Contour Plot, 15% Suction

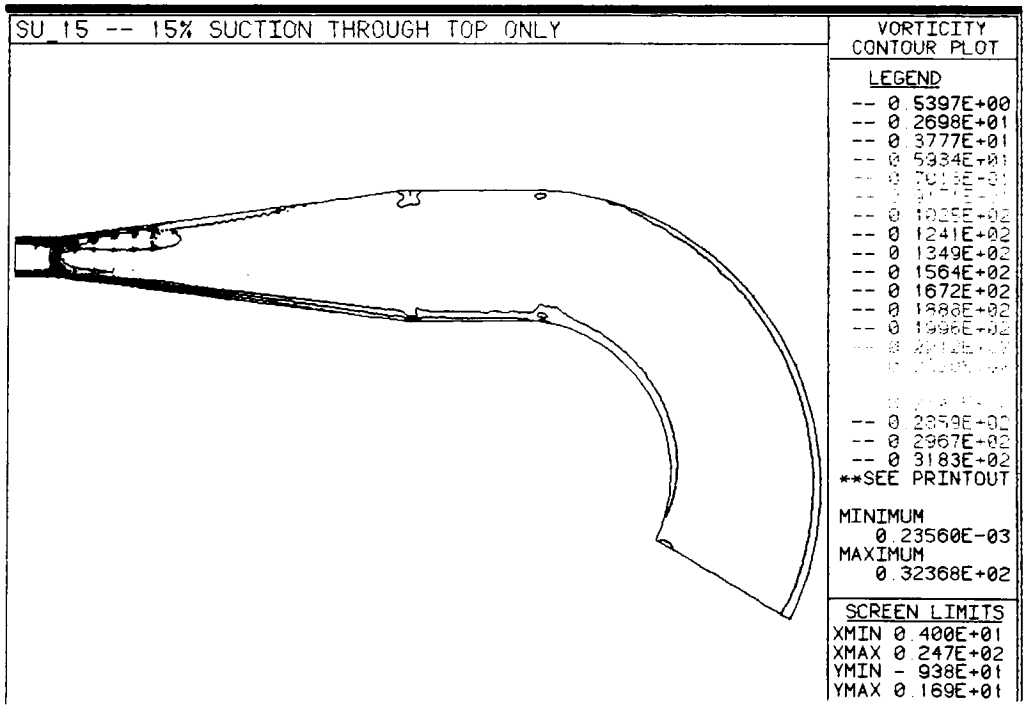

Figure 7.43 - Kinetic Energy Contour Plot, 15% Suction

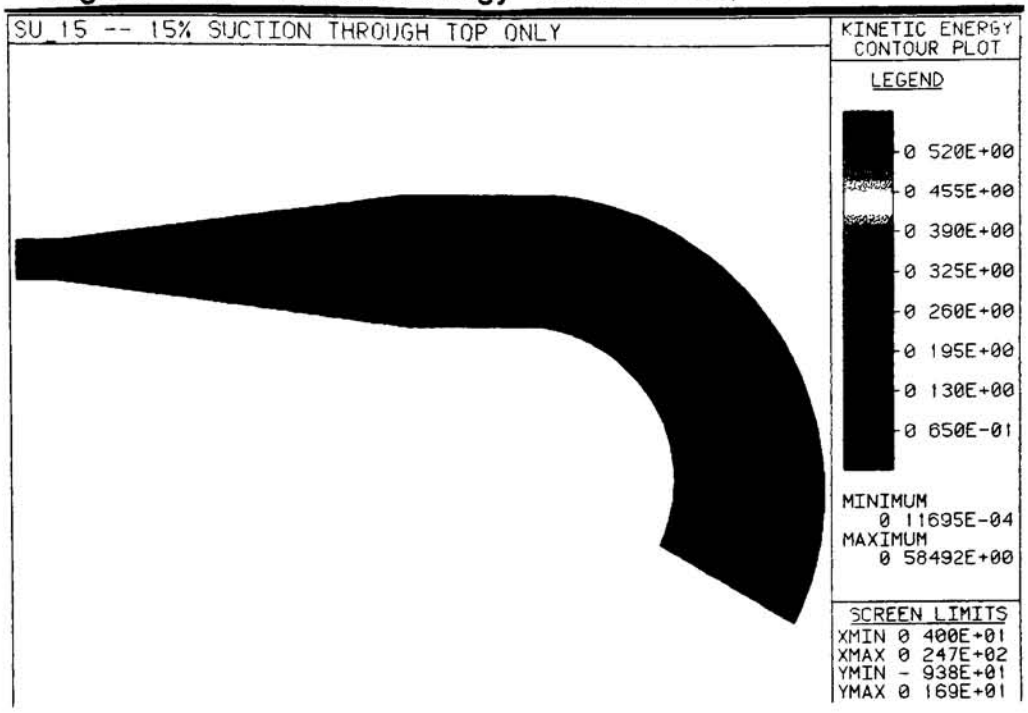

Figure 7.44 - Dissipation Contour Plot, 15% Suction

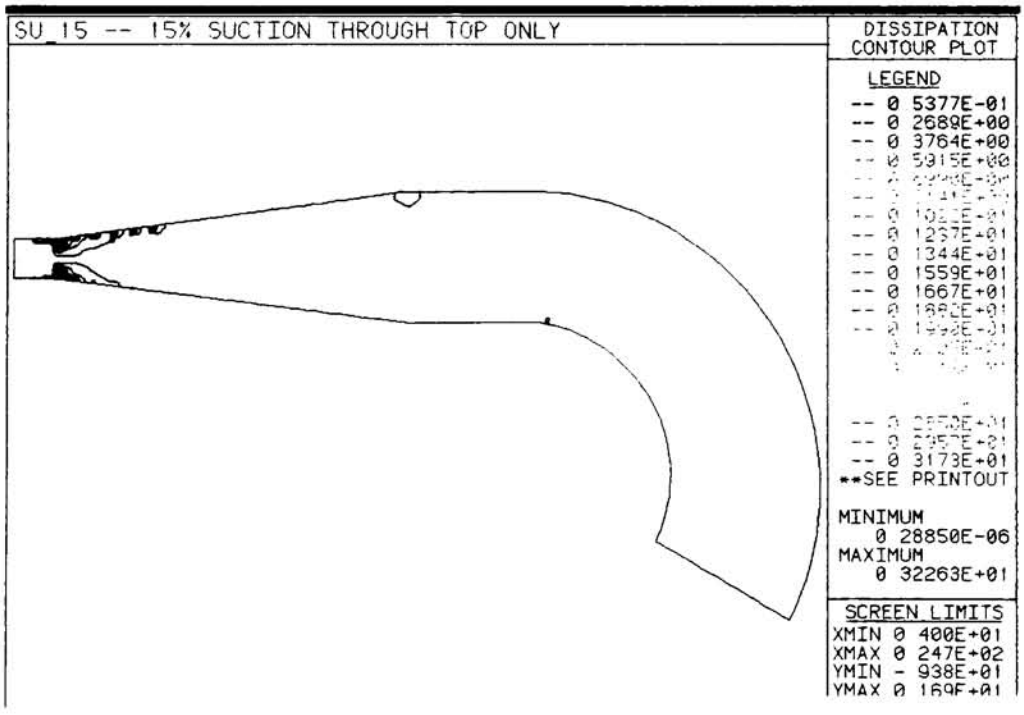

Figure 7.45 - Inlet Velocity Profiles, 15% Suction

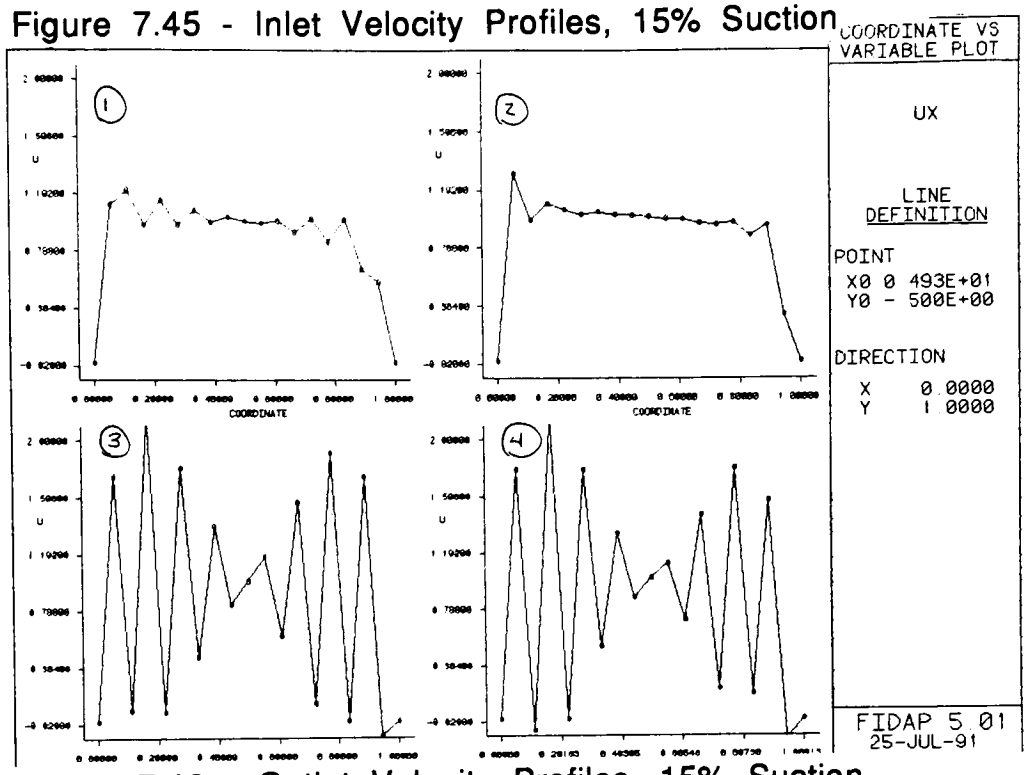

Figure 7.46 - Outlet Velocity Profiles, 15% Suction

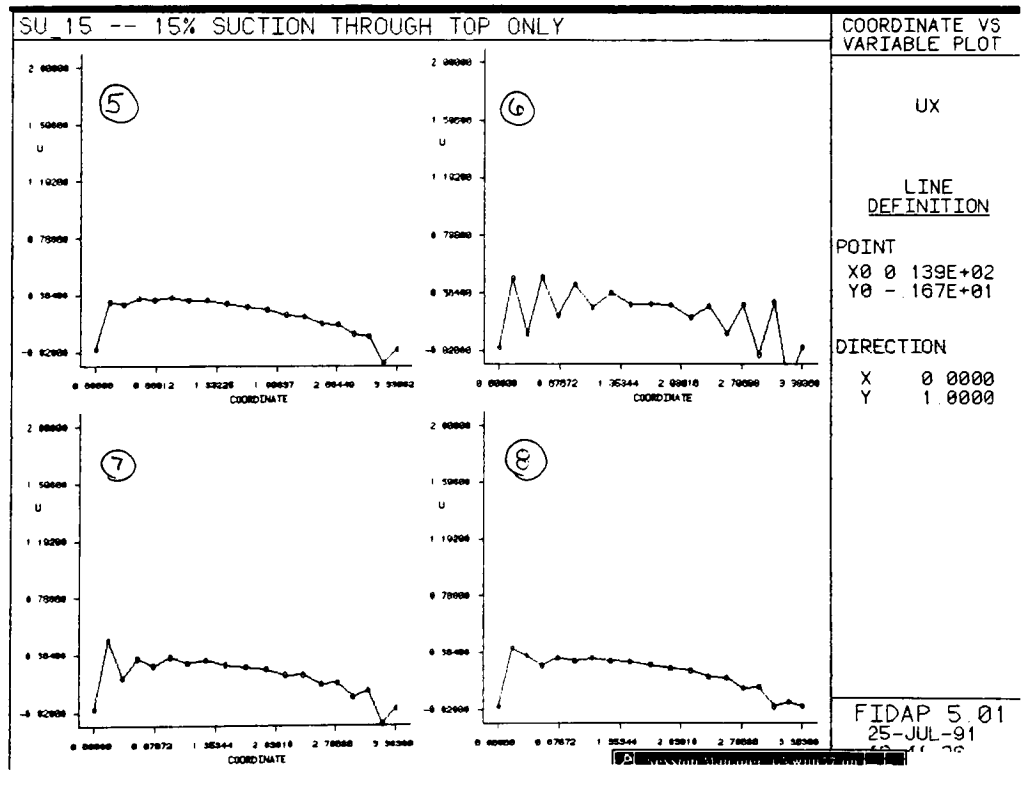

7-3.4 20% Suction

The pressure recovery coefficients of the previous models have steadily increased. In order to try and obtain an 'optimal' suction rate, a suction rate of 20% of the inlet mass flow rate was tested. The streamline contour plot (Figure 7.47) and the velocity vector plot at the outlet (Figure 7.48) are very similar to the 15% suction case. The pressure recovery is slightly lower for this case, though, indicating an optimal suction rate at slightly less than 15% suction (Figure 7.49). The pressure contour plot (Figure 7.50a) and the pressure at the diffuser centerline (Figure 7.50b) indicate a large recovery before the midpoint of the diffuser with a higher pressure at the outlet to cause the flow reversal. The speed contour plot (Figure 7.51) further verifies the well behaved flow in the diffuser.

The kinetic energy plot (Figure 7.52), dissipation plot (Figure 7.53) and the vorticity plot (Figure 7.54) are similar in nature to the plots observed for the 15% suction case. It is interesting to note that the vorticity plot indicates a smaller boundary layer on the inside wall of the turning channel due to the separation observed at the inlet to the turning channel. The velocity profile plots at the inlet (Figure 7.55) and outlet (Figure 7.56) again indicate instabilities of similar locations to the previous tests.

Figure 7.47 - Streamline Contour Plot, 20% Suction

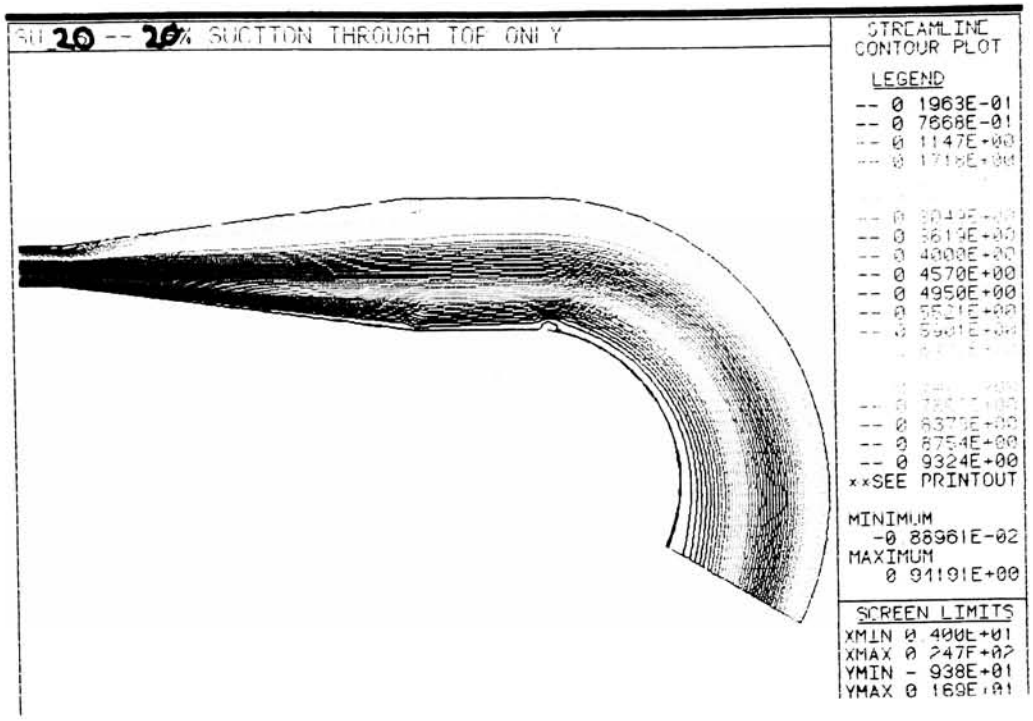

Figure 7.48 - Velocity Vector Plot at Outlet, 20% Suction

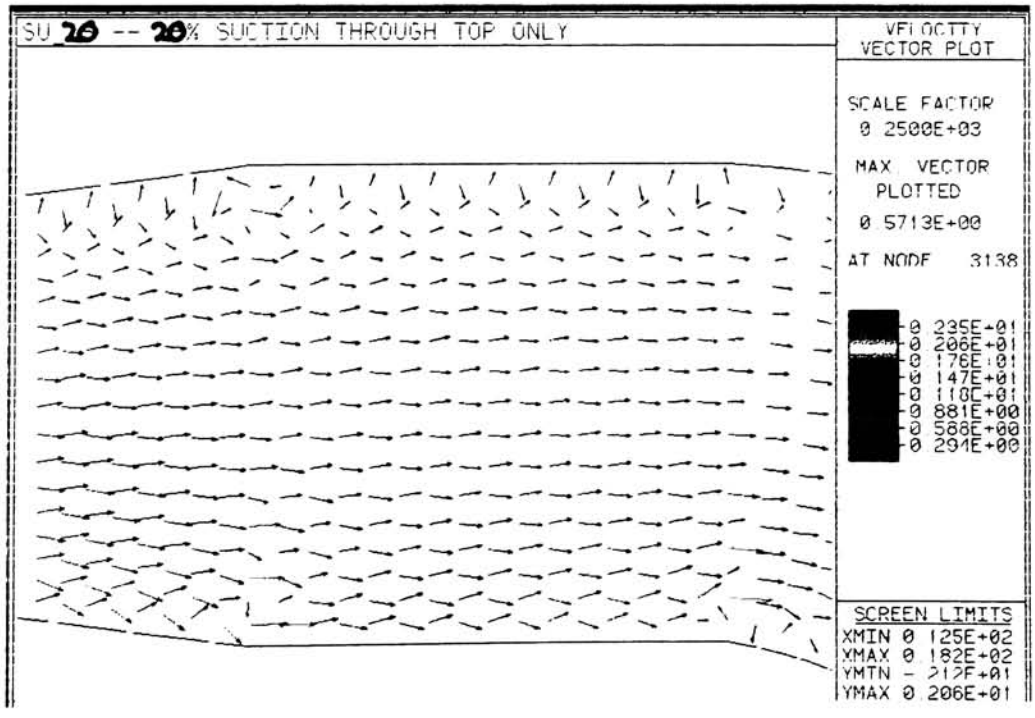

Figure 7.49 - Optimum Pressure Recovery

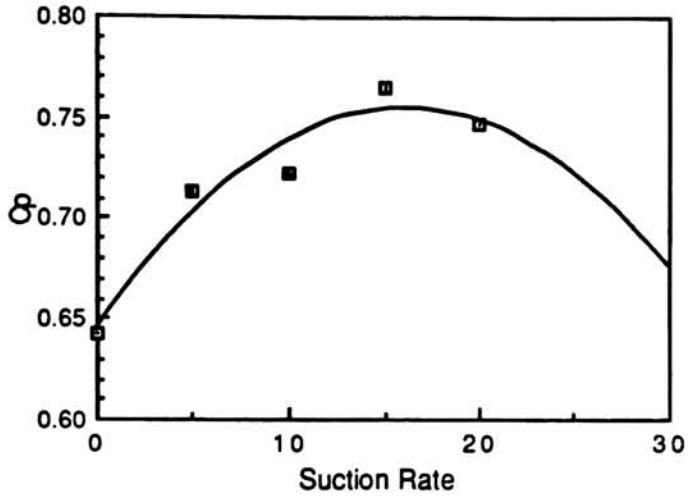

y = 0.64530 + 1.3573e-2x - 4.1886e-4x^2 R^2 = 0.944

Figure 7.50a - Pressure Contour Plot, 20% Suction

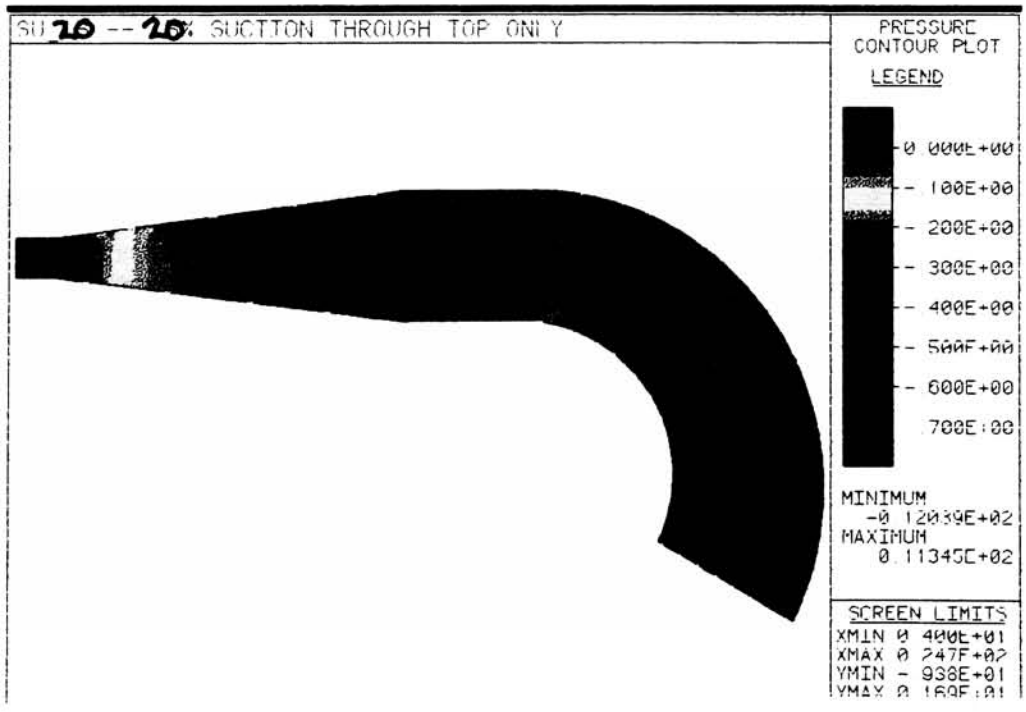

Figure 7.50b - Pressure Along the Diffuser Centerline, 20% Suction

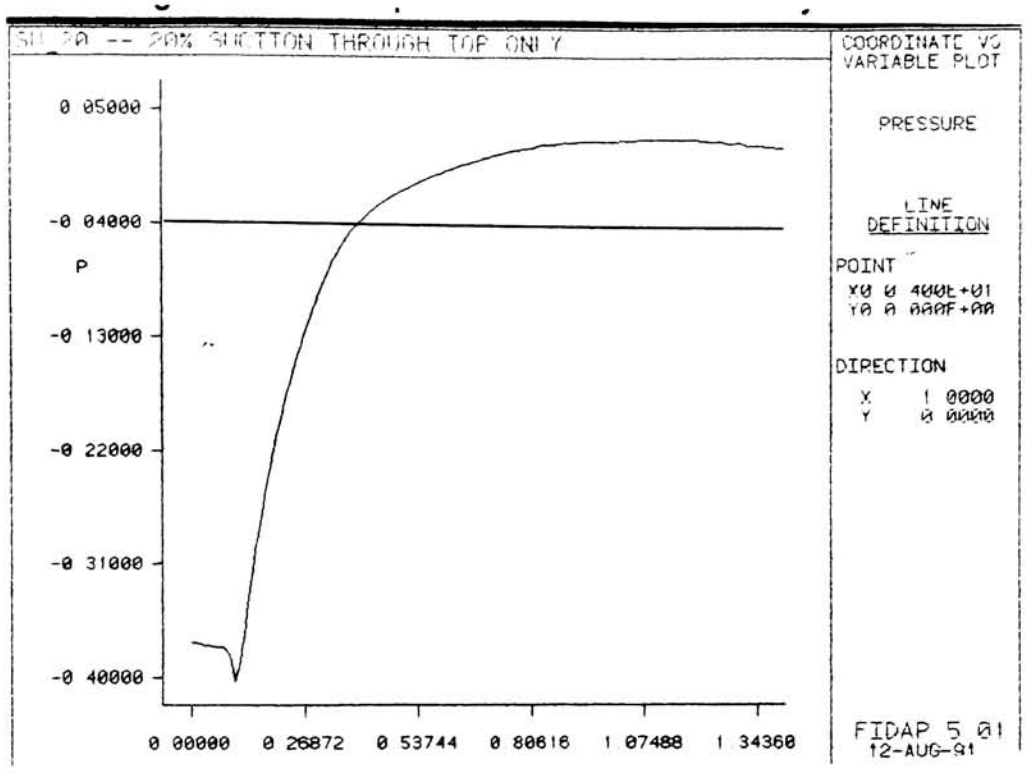

Figure 7.51 - Speed Contour Plot, 20% Suction

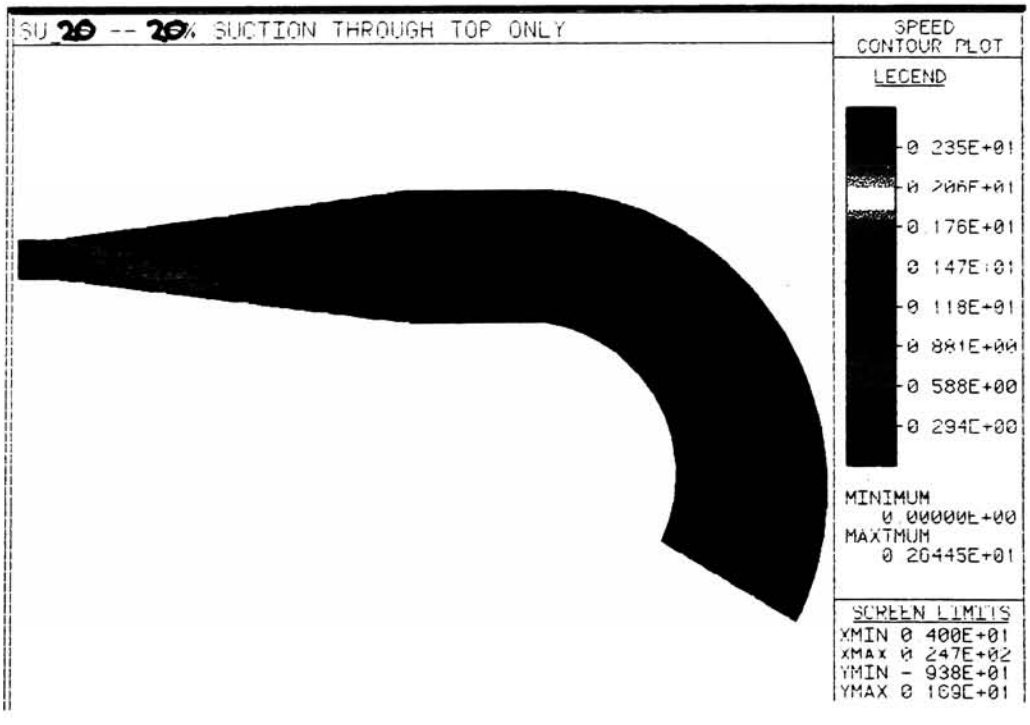

Figure 7.52 - Kinetic Energy Contour Plot, 20% Suction

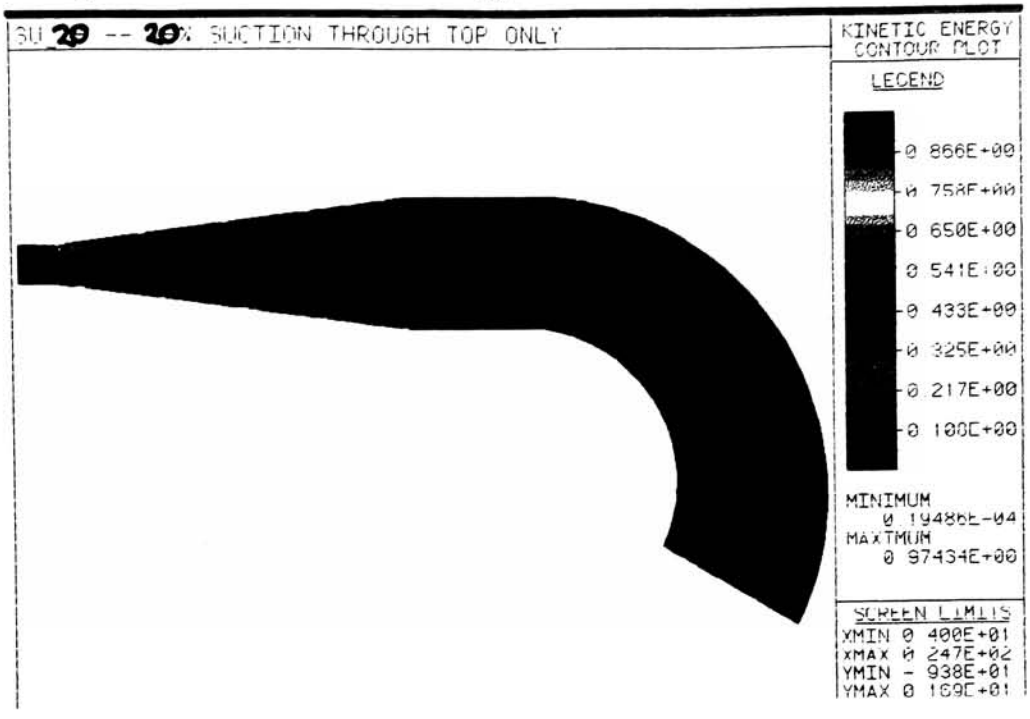

Figure 7.53 - Dissipation Contour Plot, 20% Suction

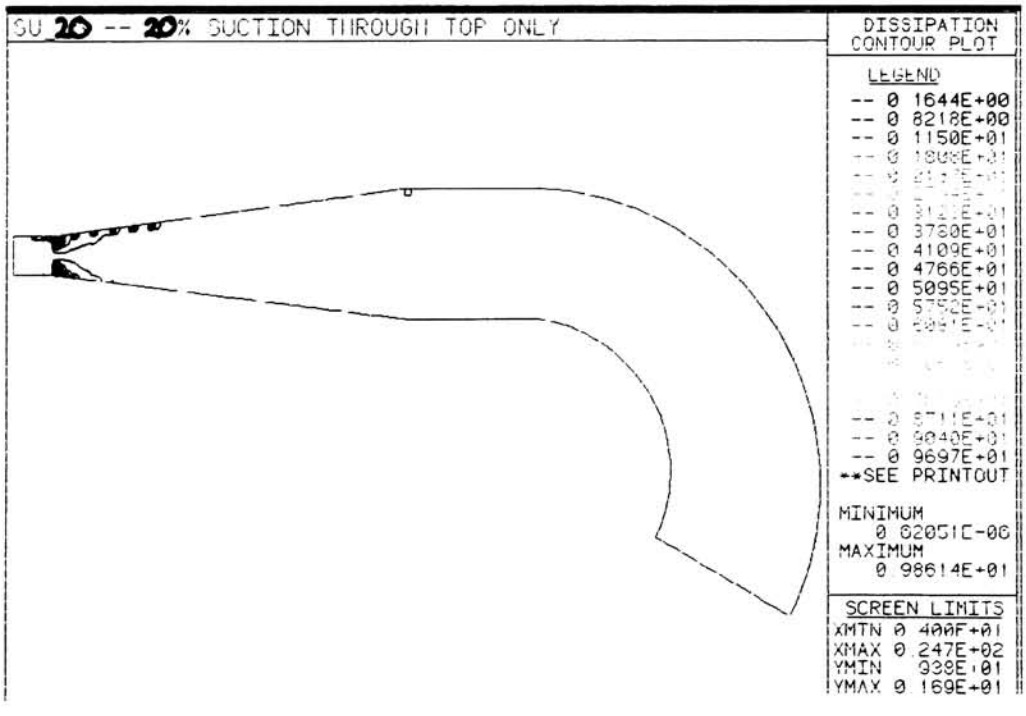

Figure 7.54 - Vorticity Contour Plot, 20% Suction

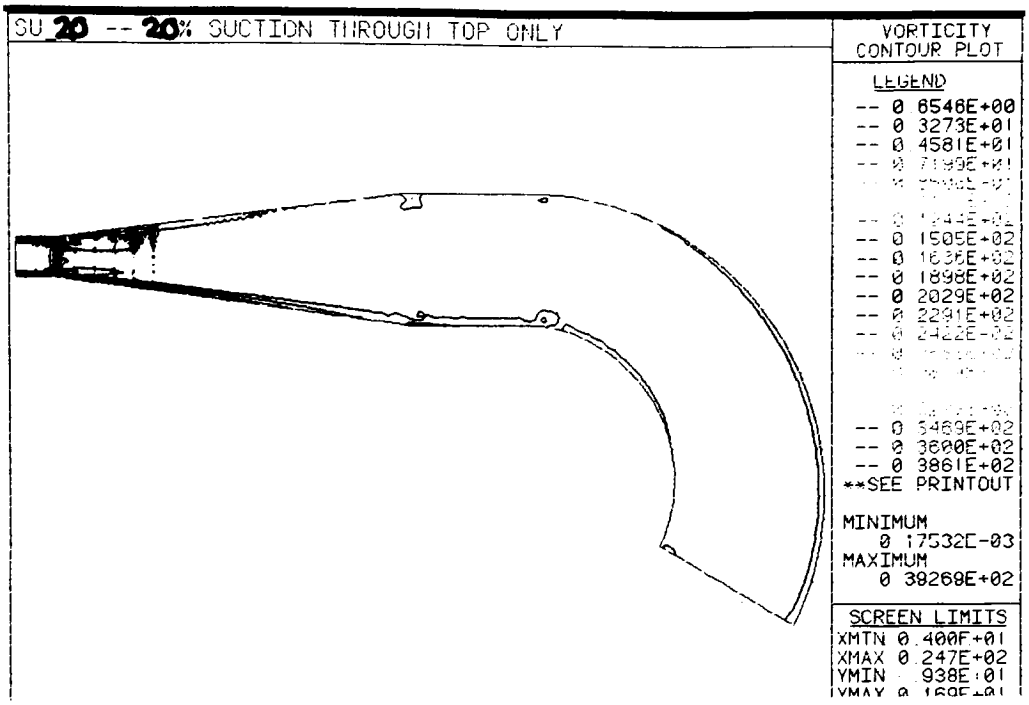

Figure 7.55 - Velocity Profiles at the Inlet, 20% Suction

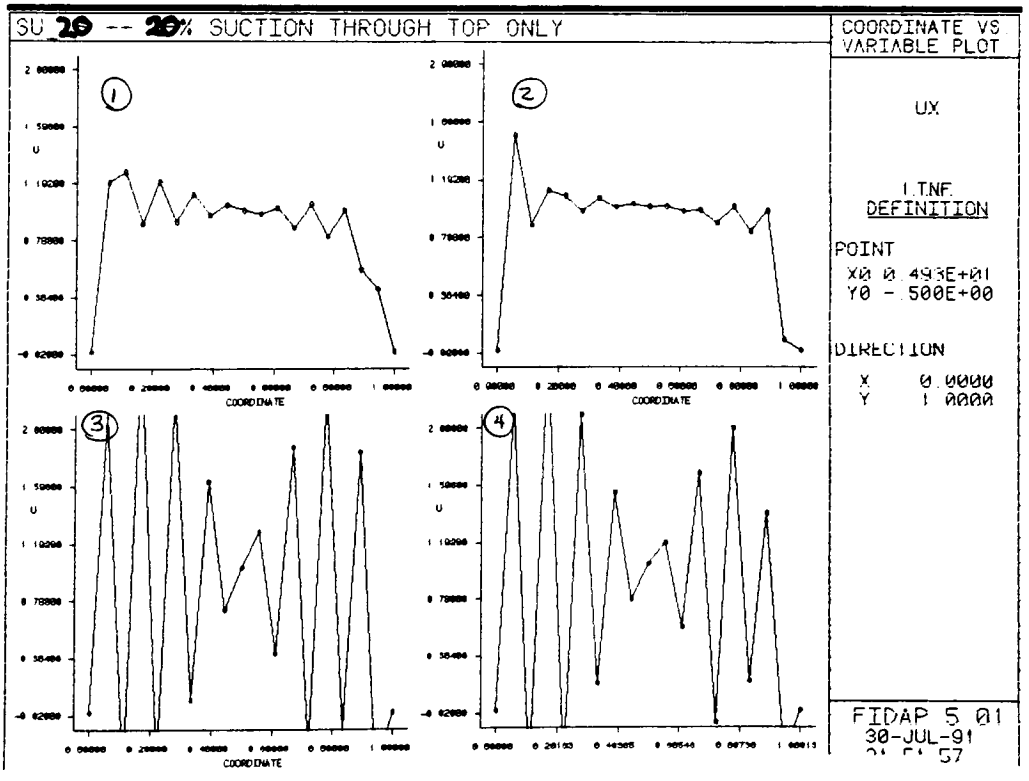

Figure 7.56 - Velocity Profiles at the Outlet, 20% Suction

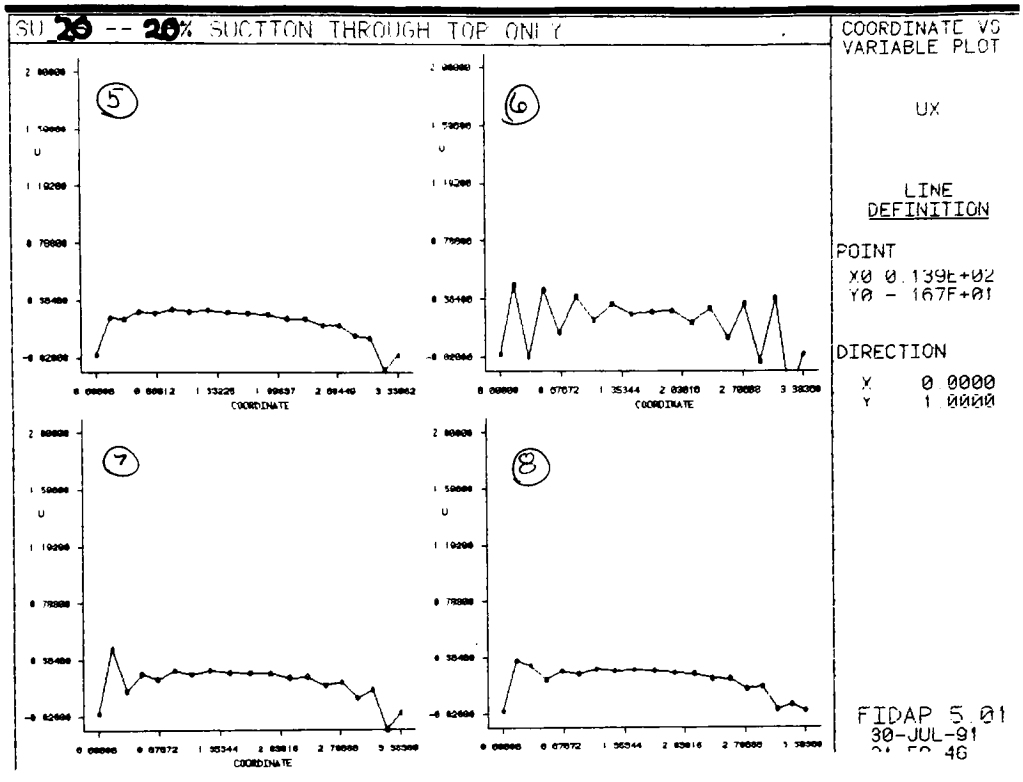

7-4 Blowing

The injection of fluid into the flow field in an attempt to re-energize the boundary layer to preclude separation was also investigated. Less literature is available on prescribed injection rates and injection angles, so this portion of the thesis is undertaken in an attempt to further this technology. Fluid was injected parallel to the centerline of the diffuser into the decelerating flow along the top of the diffuser at rates of 5, 10 and 15% of the inlet mass flow rate.

The results indicate that the injection of fluid after the throat of the diffuser continually increased the efficiency of the diffuser. This result was wholly expected due to the method of determining the pressure recovery coefficient which does not take into consideration the introduction of fluid beyond the diffuser throat.

7-4.1 5% Blowing

The application of 5% blowing through the top wall of the diffuser does not delay the separation and subsequent stall in the diffuser as can be seen by examining the streamline contour plot (Figure 7.57) as well as the velocity vector plot (Figure 7.58). In fact, it appears that the flow reversal area has increased over that of the uncontrolled diffuser. The speed contour plot (Figure 7.59) further verifies the ineffectiveness of the fluid injection by indicating a pronounced jet flow along the bottom of the diffuser.

The pressure recovery of the diffuser (Figure 7.60) resembles that of the diffuser with no controls. A high pressure region is present at the top of the diffuser causing the flow reversal, and a

low pressure region at the bottom allows the flow to move along the wall virtually unimpeded. The pressure recovery coefficient echoes the ineffectiveness of this configuration.

The vorticity (Figure 7.61), kinetic energy generation (Figure 7.62) and the dissipation (Figure 7.63) are quite similar in nature to the uncontrolled case.

The instabilities in the inlet velocity field (Figure 7.64) are more pronounced than in the suction cases indicating that blowing may not be a suitable boundary layer control device when employed at such low rates. The velocity field at the outlet (Figure 7.65) is similar to the previous models.

Figure 7.57 - Streamline Contour Plot, 5% Blowing

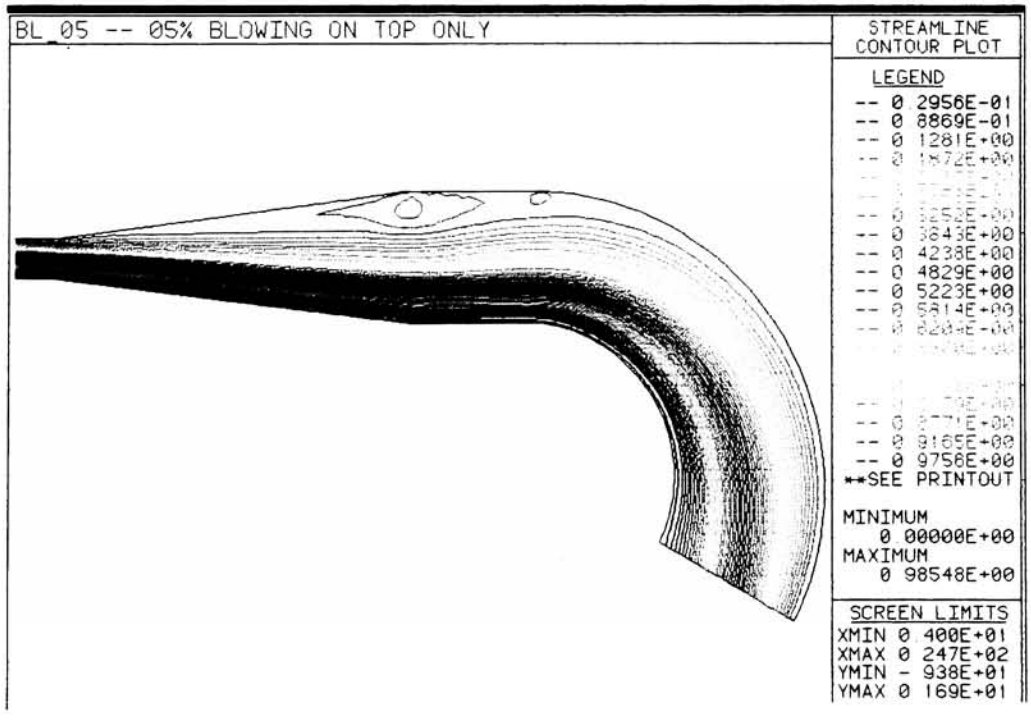

Figure 7.58 - Velocity Vector Plot at the Outlet, 5% Blowing

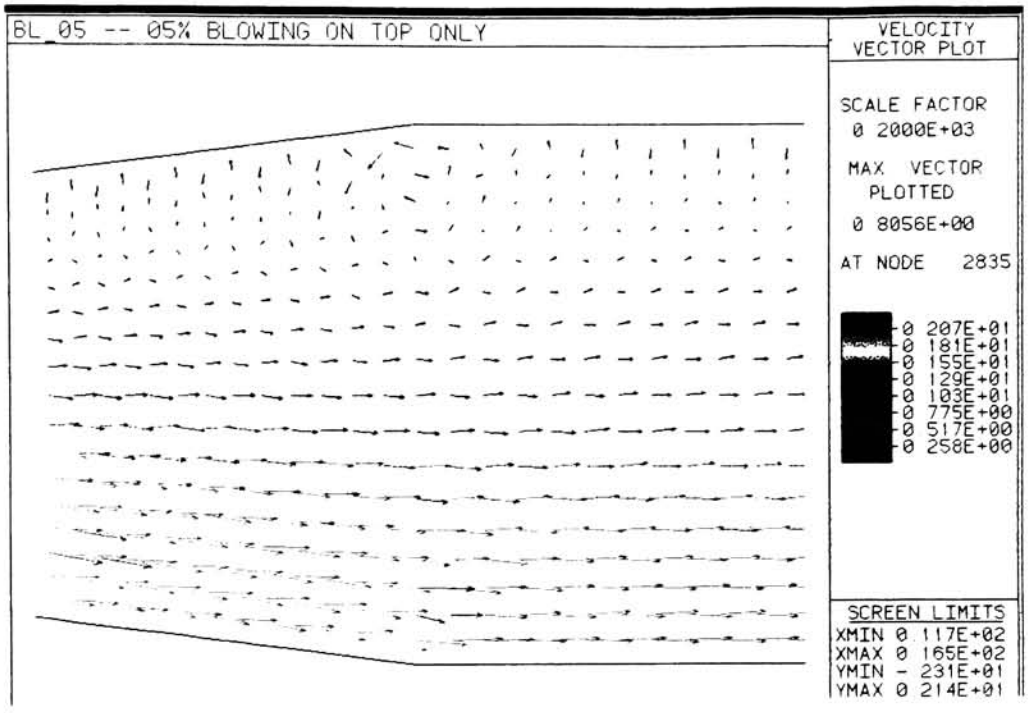

Figure 7.59 - Speed Contour Plot, 5% Blowing

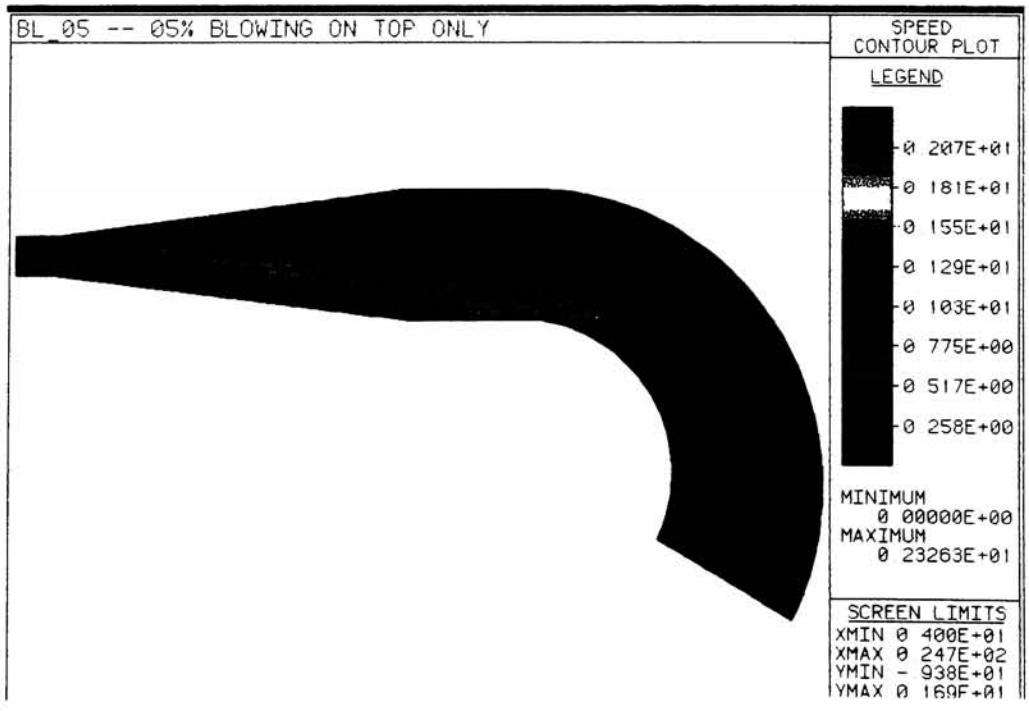

Figure 7.60 - Pressure Contour Plot, 5% Blowing

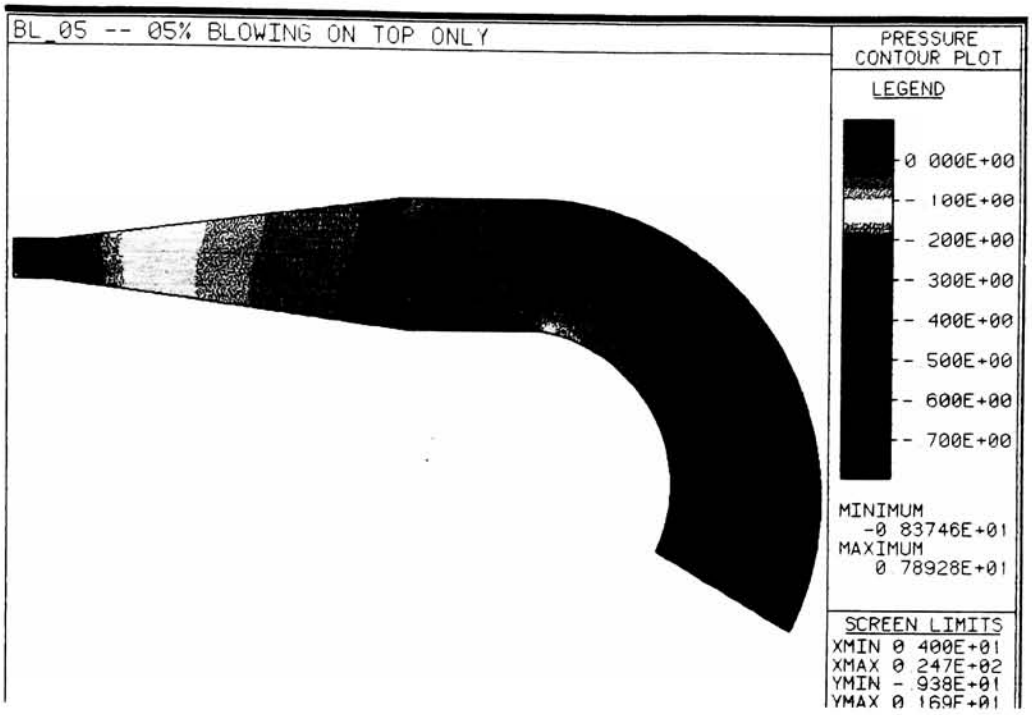

Figure 7.61 - Vorticity Contour Plot, 5% Blowing

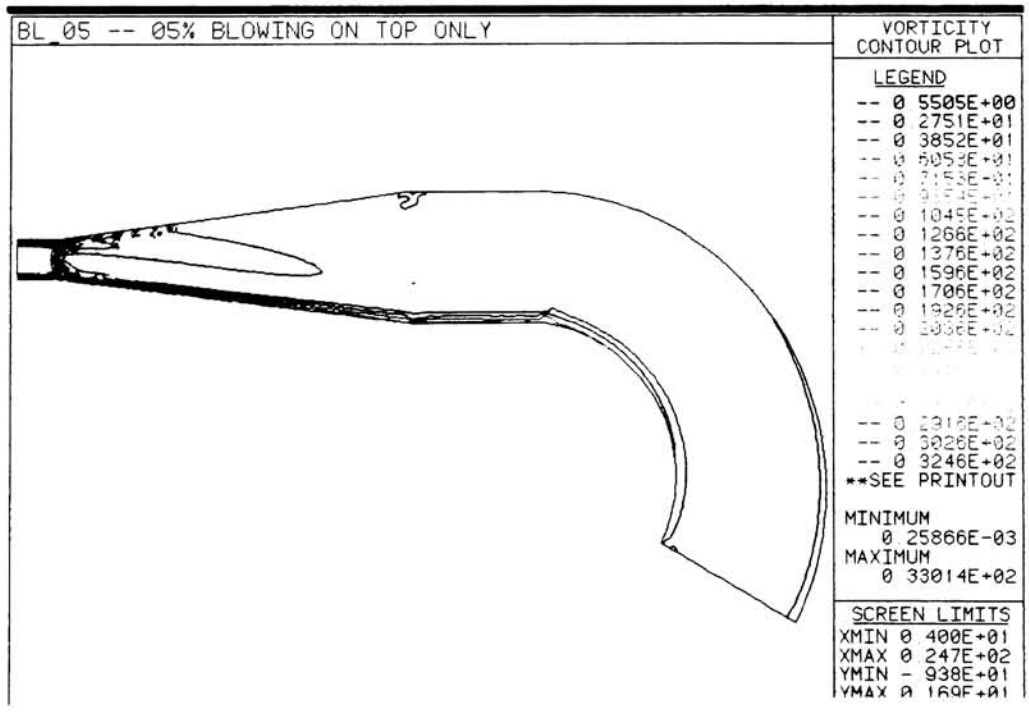

Figure 7.62 - Kinetic Energy Contour Plot, 5% Blowing

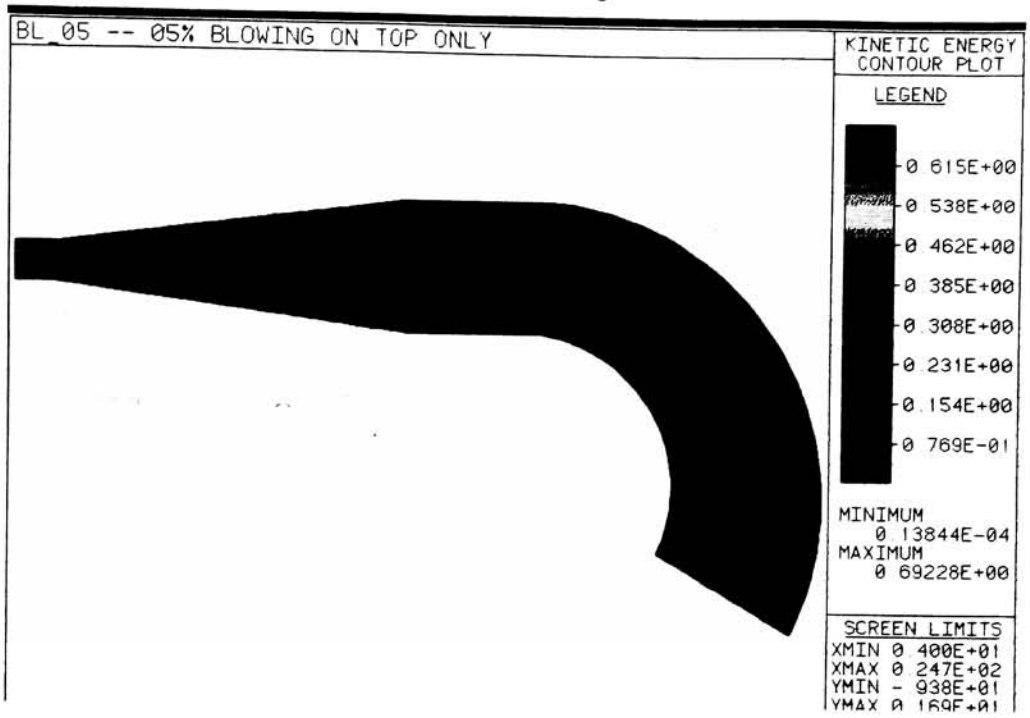

Figure 7.63 - Dissipation Contour Plot, 5% Blowing

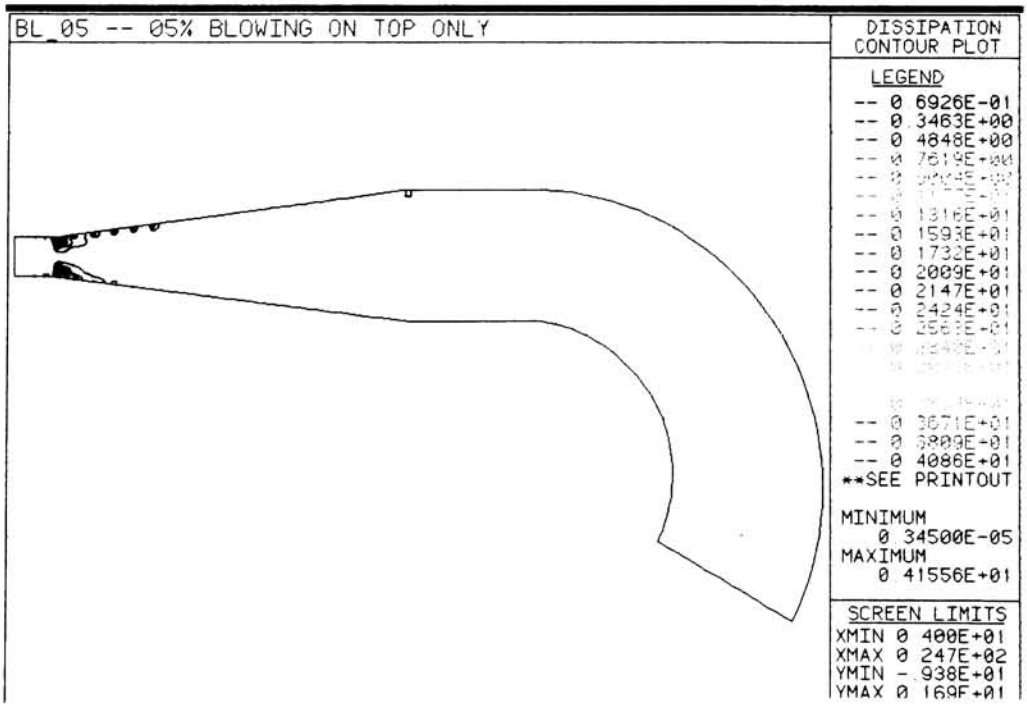

Figure 7.64 - Inlet Velocity Profiles, 5% Blowing

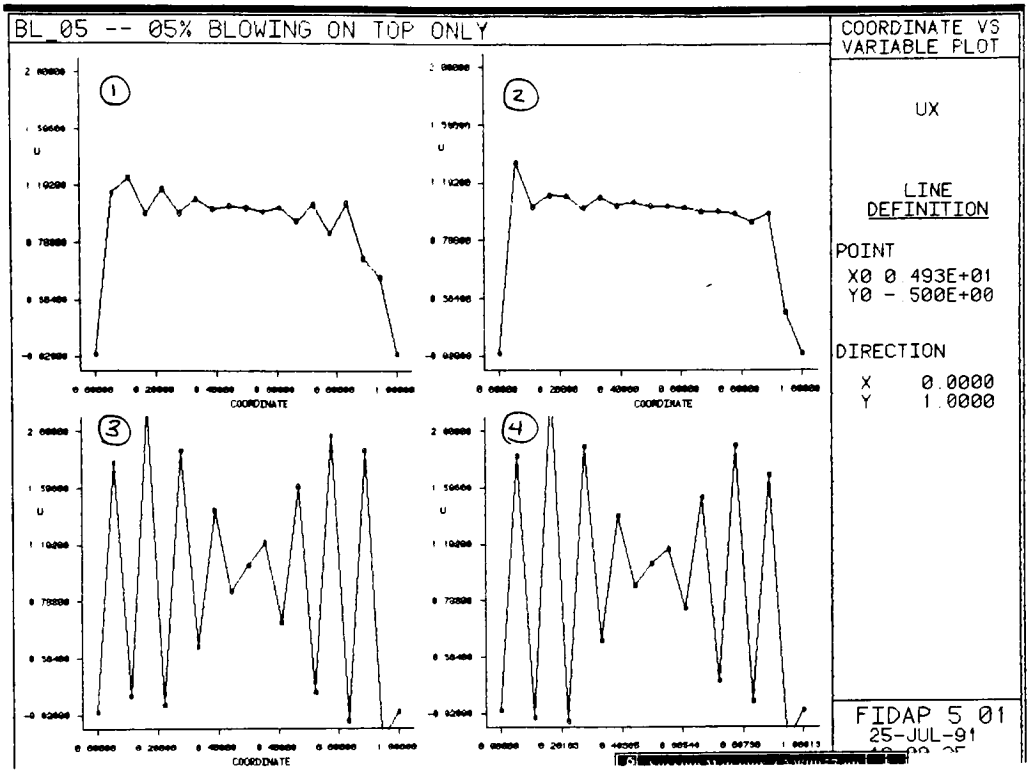

Figure 7.65 - Outlet Velocity Profiles, 5% Blowing

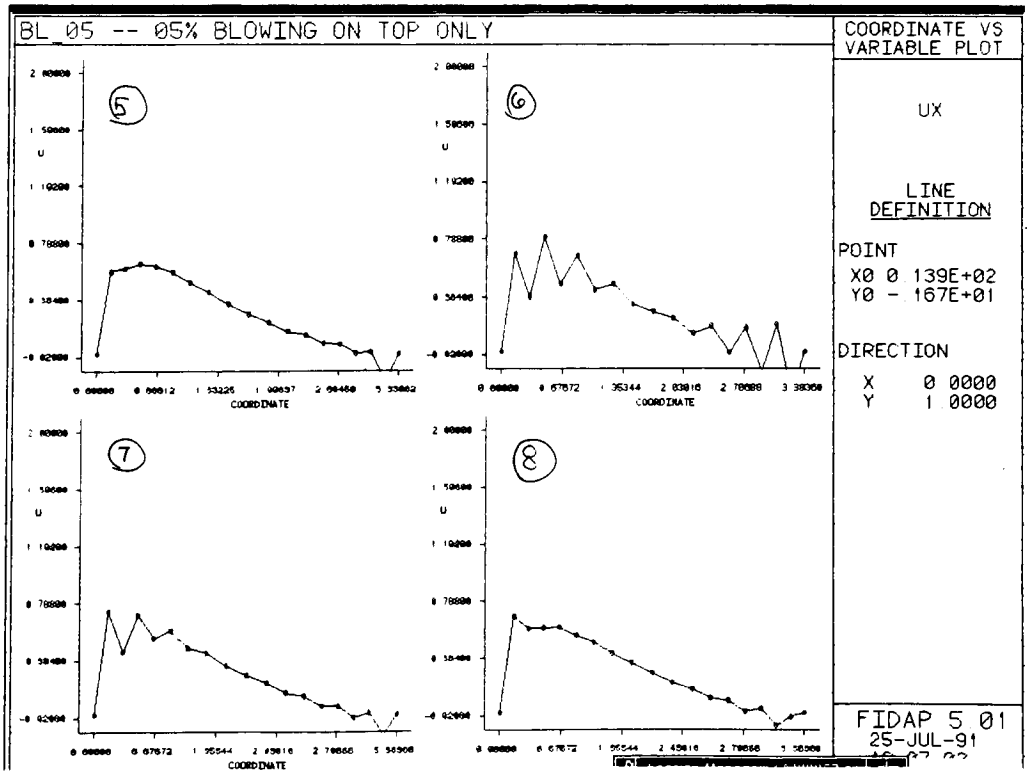

7-4.2 10% Blowing

The application of fluid injection at a rate of 10% shows a marked improvement over the 5% blowing model. The flow reversal area is significantly reduced (Figures 7.66 and 7.67). The separation occurs towards the beginning of the diffuser seemingly providing a layer of fluid for the flow to "glide" along. This could account for the flow field being rather uniform in nature by the end of the diffuser (Figure 7.68). The pressure contour plot (Figure 7.69) further verifies this analysis.

The kinetic energy generation (Figure 7.70) and the dissipation (Figure 7.71) are confined to the areas of high vorticity (Figure 7.72), generally at the inlet of the diffuser. The instabilities of the velocity flow field at the inlet (Figure 7.73) could be a cause of the high shear rate leading the the observed flow characteristics. The flow at the outlet (Figure 7.74) is consistent with previous findings.

Figure 7.66 - Streamline Contour Plot, 10% Blowing

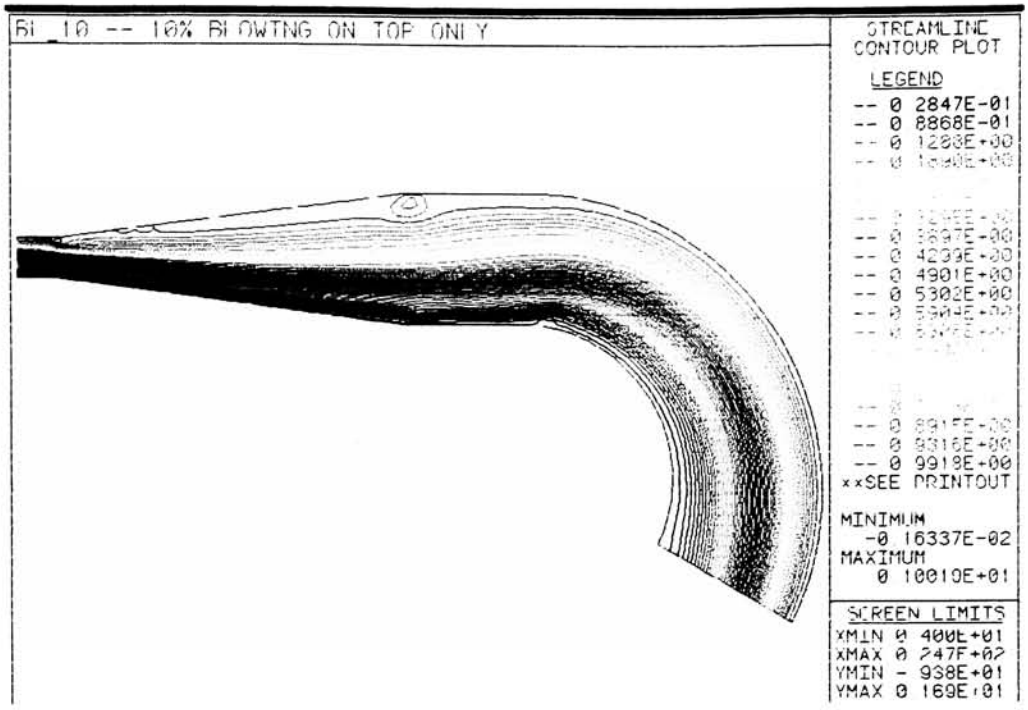

Figure 7.67 - Velocity Vector Plot at the Outlet, 10% Blowing

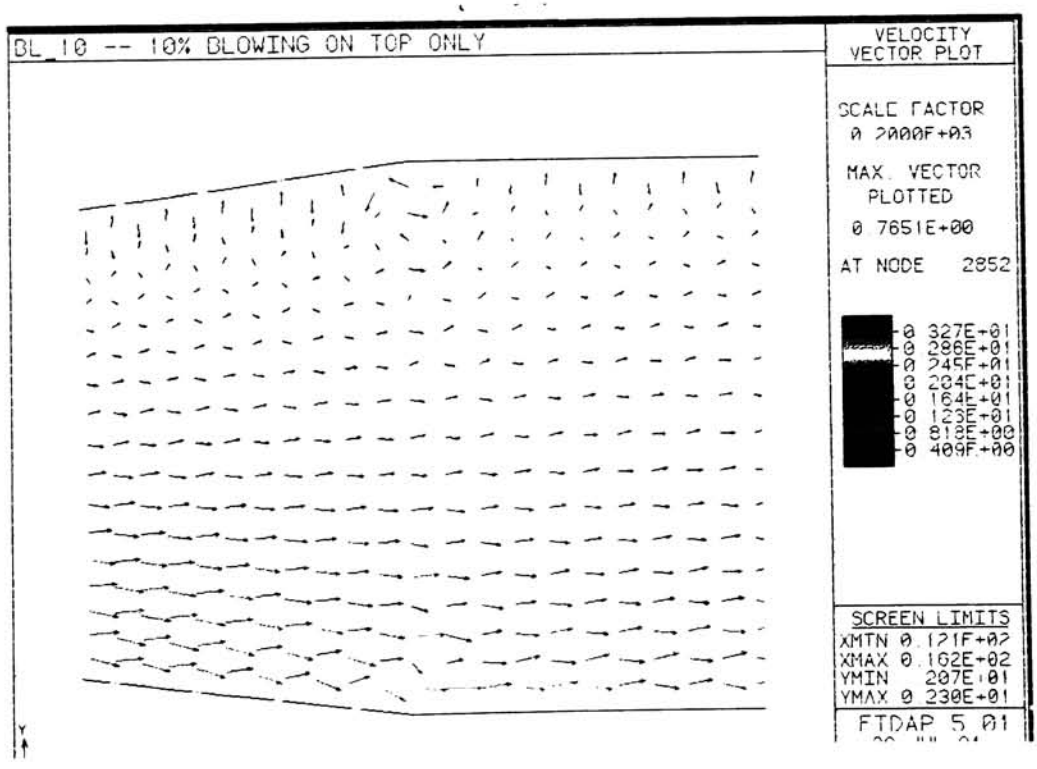

Figure 7.68 - Speed Contour Plot, 10% Blowing

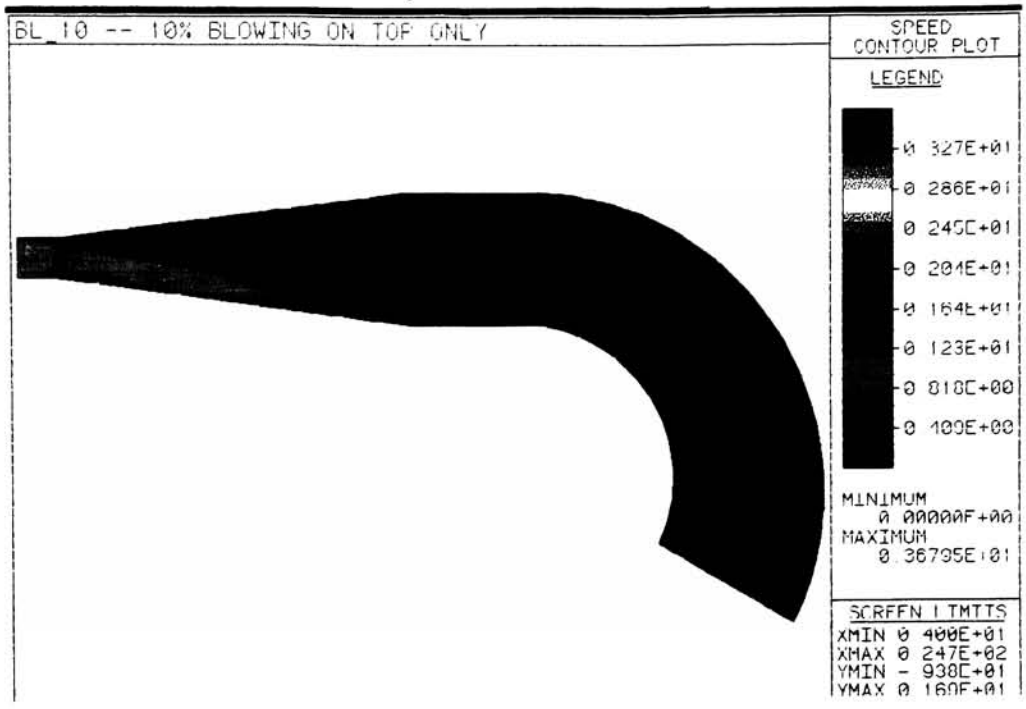

Figure 7.69 - Pressure Contour Plot, 10% Blowing

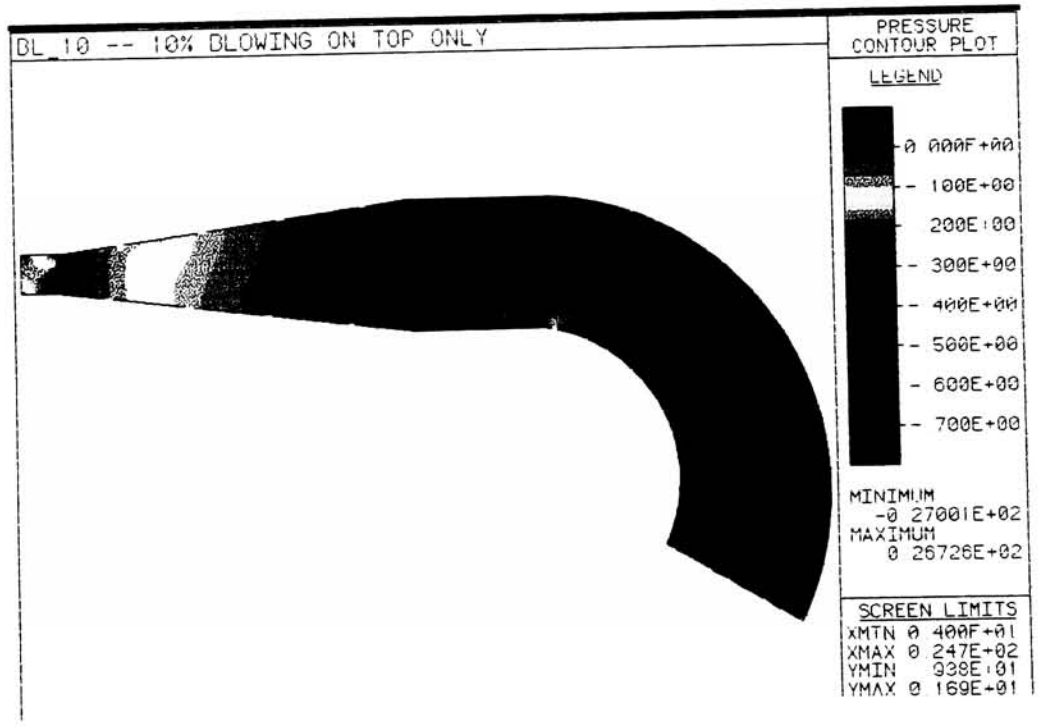

Figure 7.70 - Vorticity Contour Plot, 10% Blowing

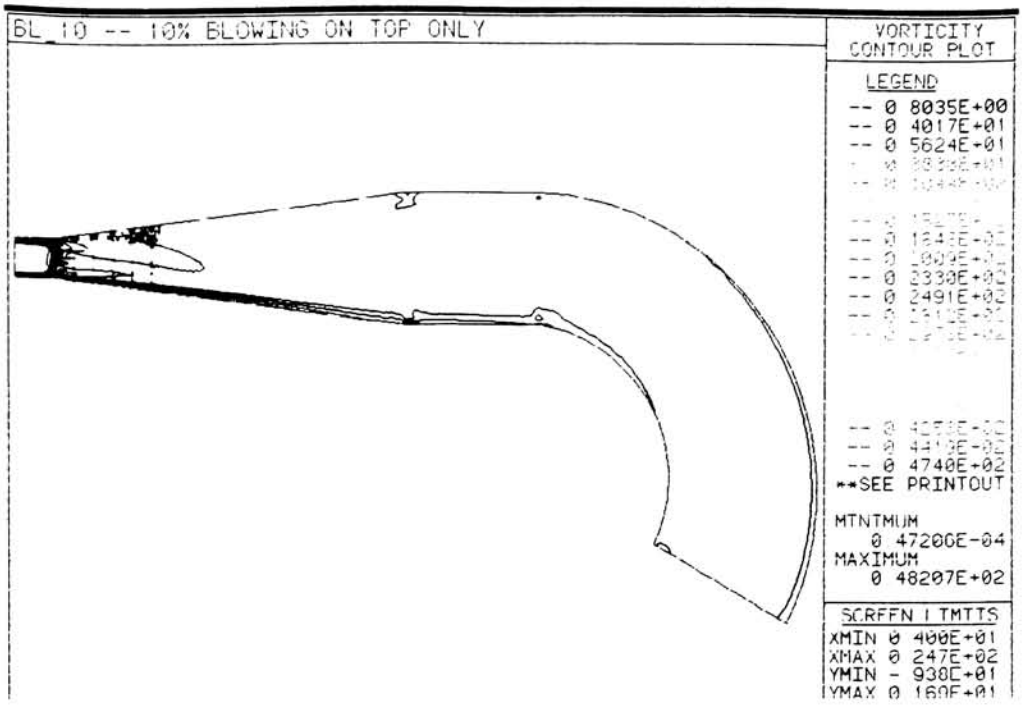

Figure 7.71 - Kinetic Energy Contour Plot, 10% Blowing

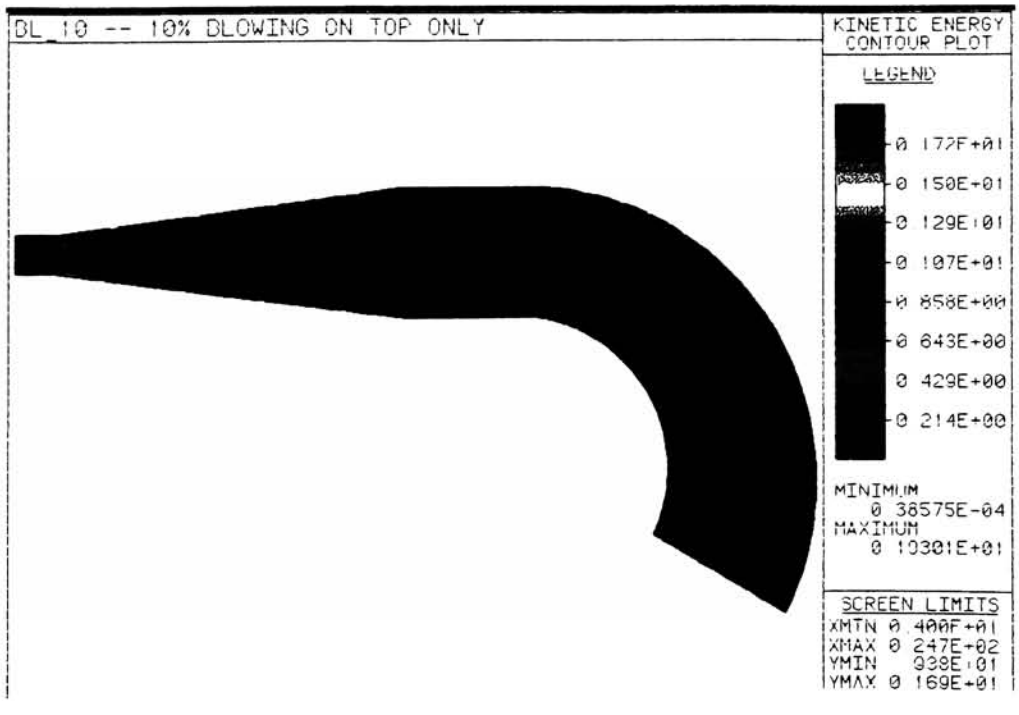

Figure 7.72 - Dissipation Contour Plot, 10% Blowing

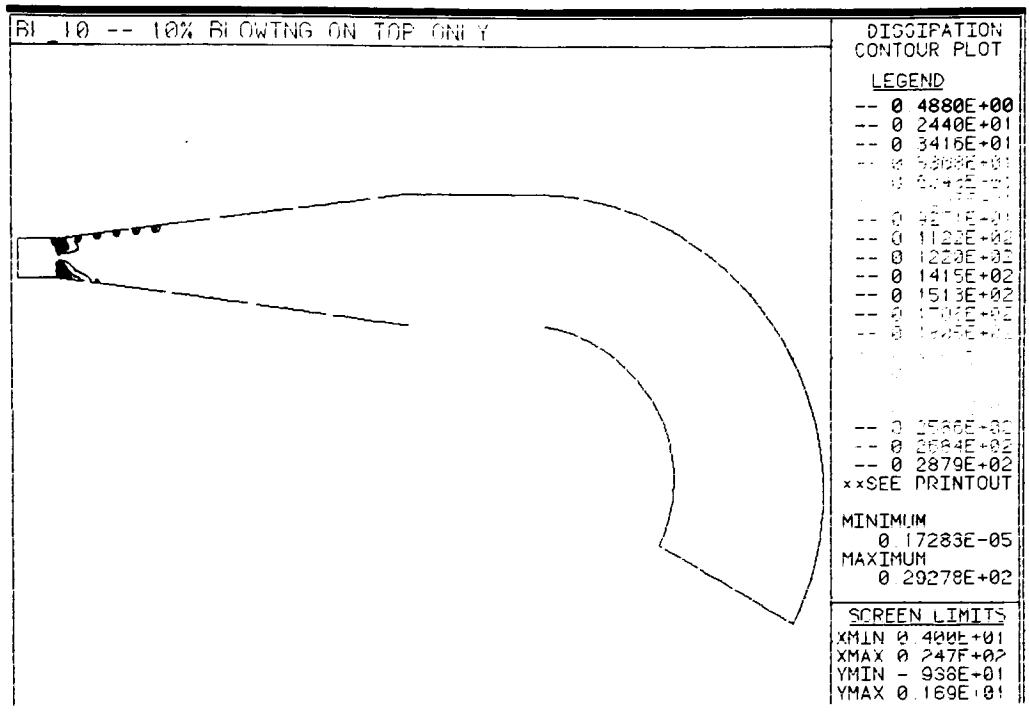

Figure 7.73 - Inlet Velocity Profiles, 10% Blowing

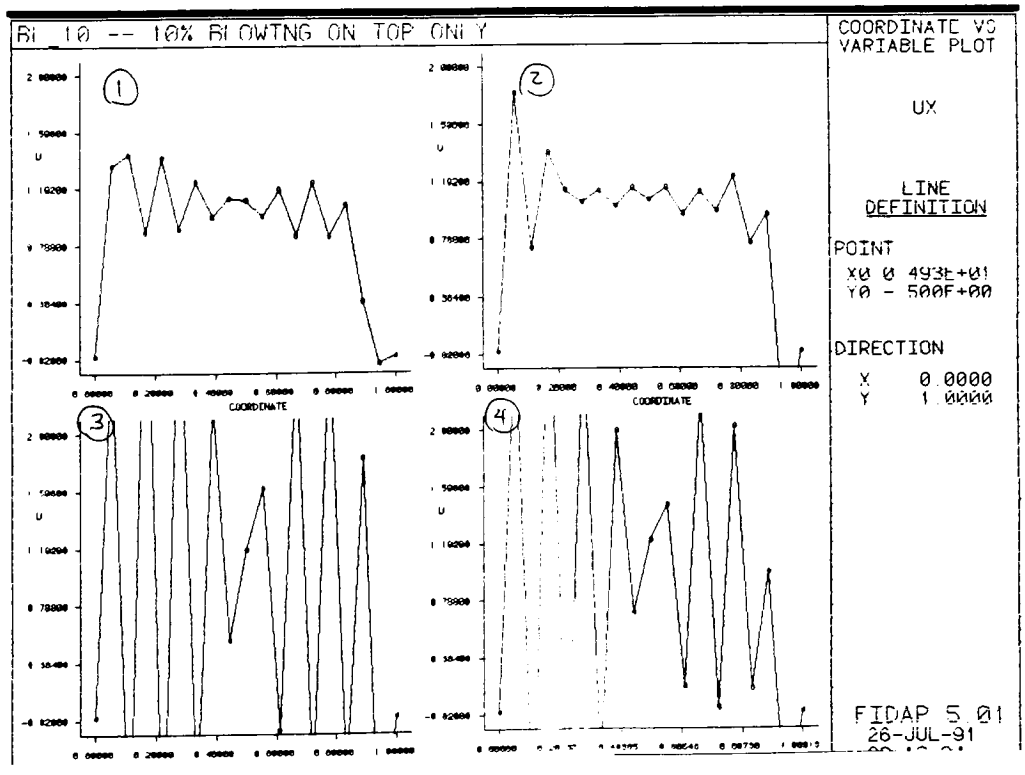

Figure 7.74 - Outlet Velocity Profiles, 10% Blowing

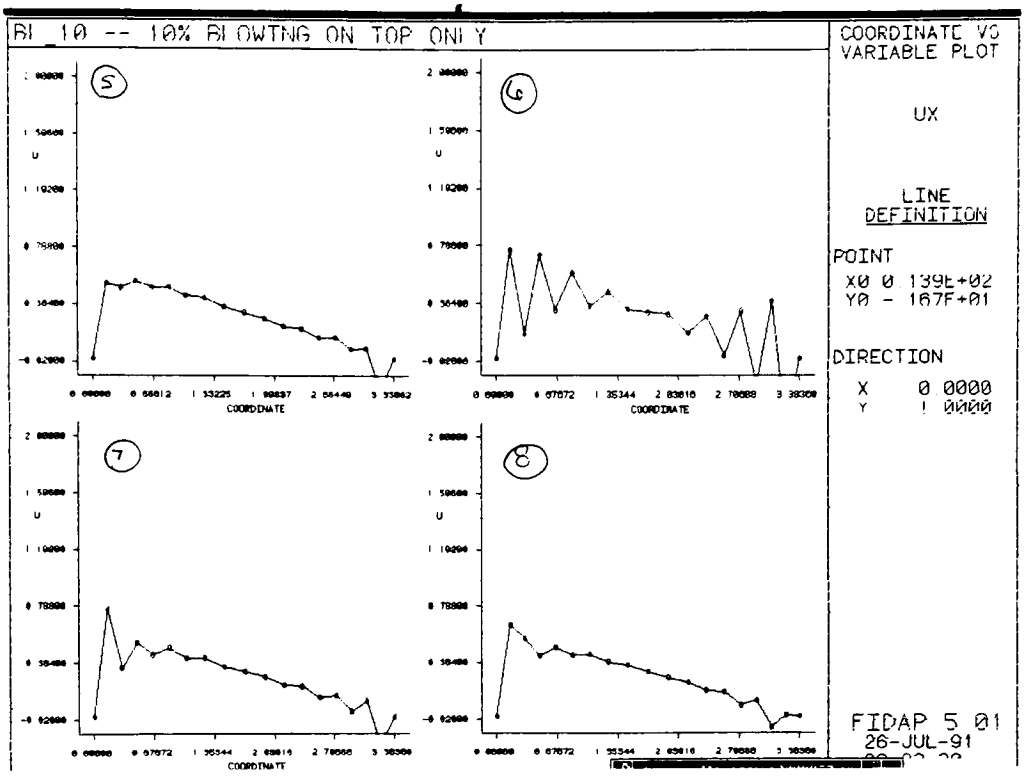

7-4.3 15% Blowing

Just as the application of 5% blowing into the diffuser was shown to be ineffectual, 15% blowing rate seems to disturb the flow field significantly. The streamline contour plot (Figure 7.75) reveals an increased number of areas of separation at the inlet as well as the lower portion of the outlet. The pressure contour plot (Figure 7.76) indicates a large pressure at the throat, causing the separation in that location. The flow reversal at the inlet can be seen in the velocity vector plot at the inlet (Figure 7.77) and the reversal at the outlet is seen in Figure 7.78. The pressure recovery appears to be rather uniform despite the increase in separation locations, and the speed throughout the diffuser (Figure 7.79) is also uniform and relatively laminarized beyond the center of the diffuser.

The vorticity (Figure 7.80) at the separation regions is high in accordance with the higher shear rates that should be present. Correspondingly, the kinetic energy generation (Figure 7.81) and the dissipation (Figure 7.82) are high at the inlet in the highly turbulent regions.

The instabilities introduced in this model are the highest yet. the velocity profiles at the inlet (Figure 7.83) indicate a widely erratic flow pattern that seems to be caused by the introduction of fluid into the diffuser at such a high rate. The flow at the outlet (Figure 7.84) seems to be effected as well. These profiles do show a more uniform laminar velocity profile though.

Figure 7.75 - Streamline Contour Plot, 15% Blowing

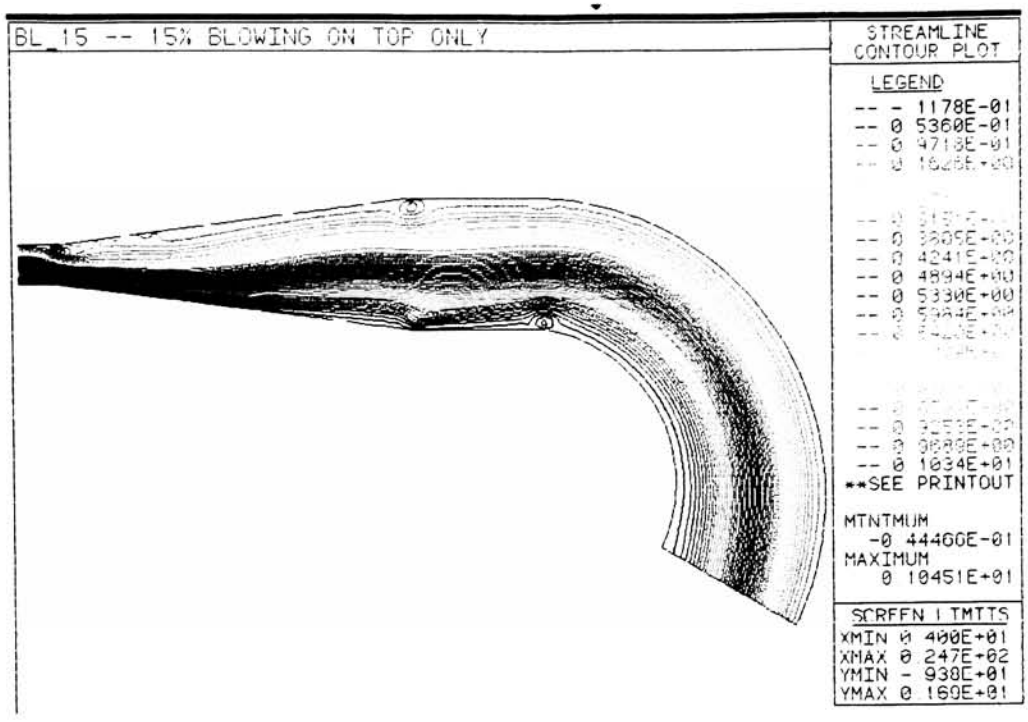

Figure 7.76 - Pressure Contour Plot, 15% Blowing

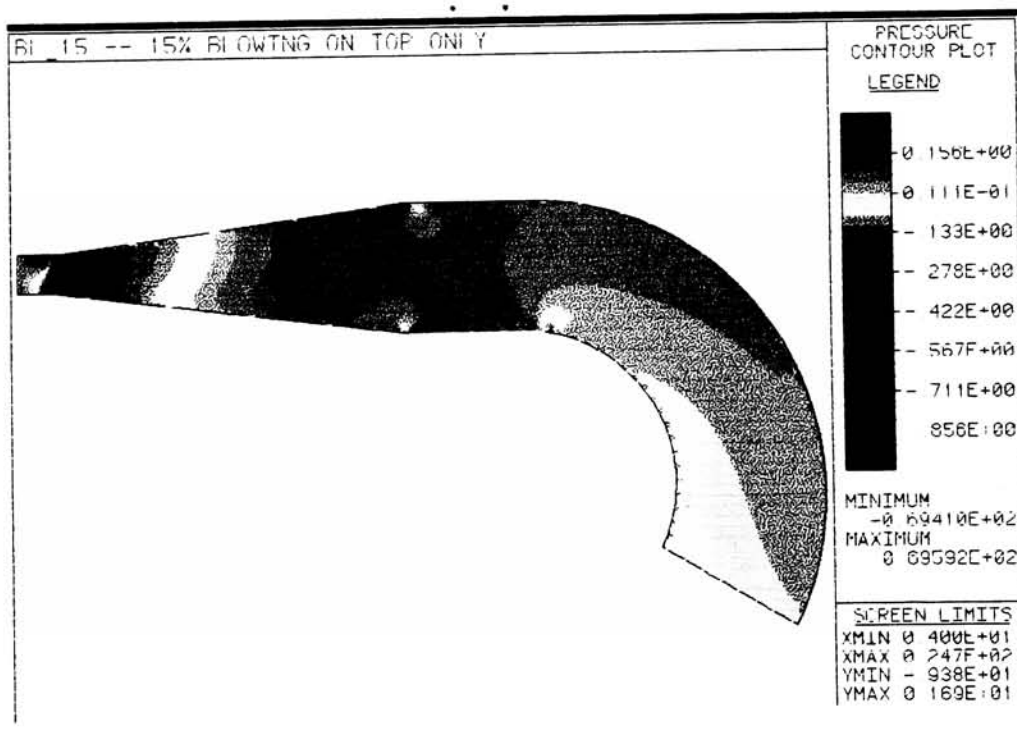

Figure 7.77 - Velocity Vector Plot at Inlet, 15% Blowing

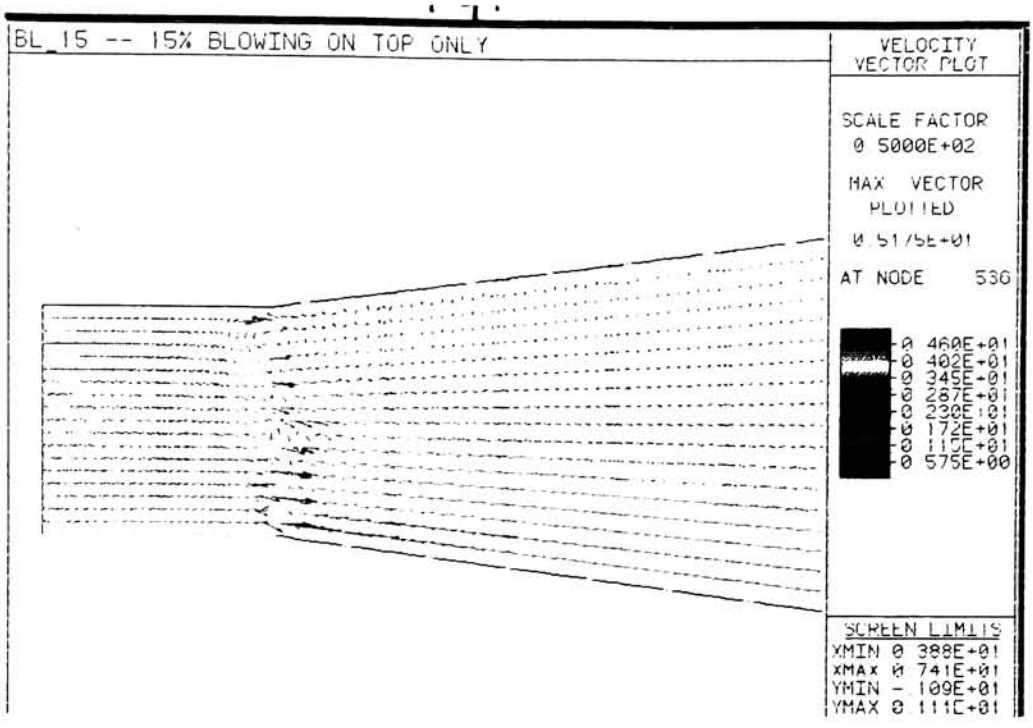

Figure 7.78 - Velocity Vector Plot at the Outlet, 15% Blowing

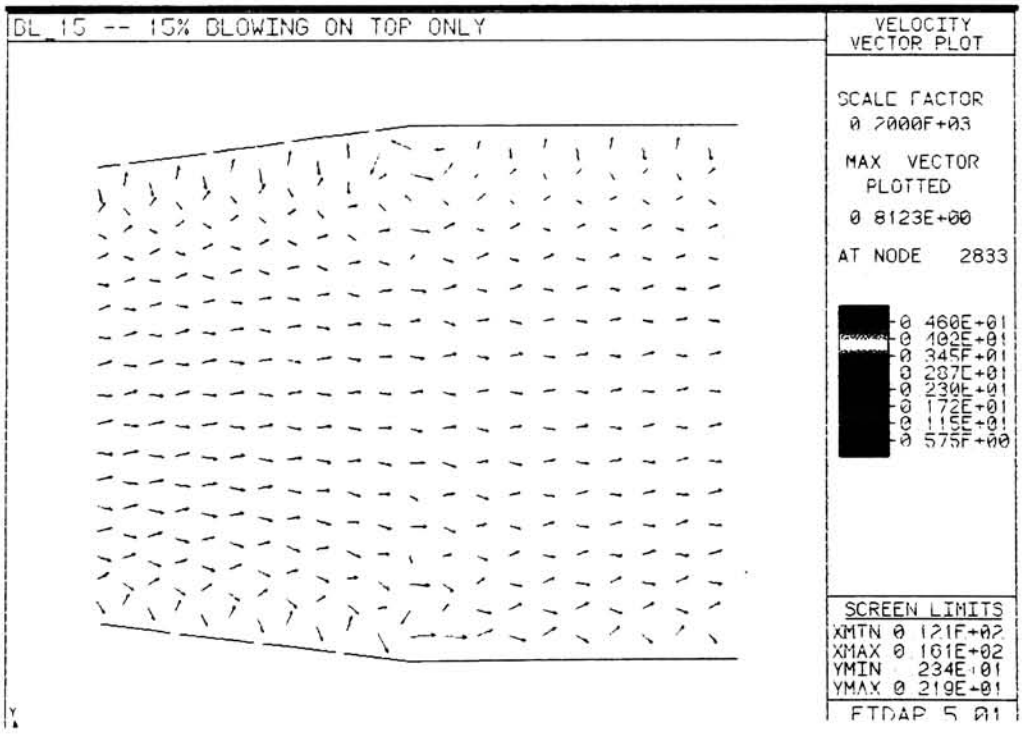

Figure 7.79 - Speed Contour Plot, 15% Blowing

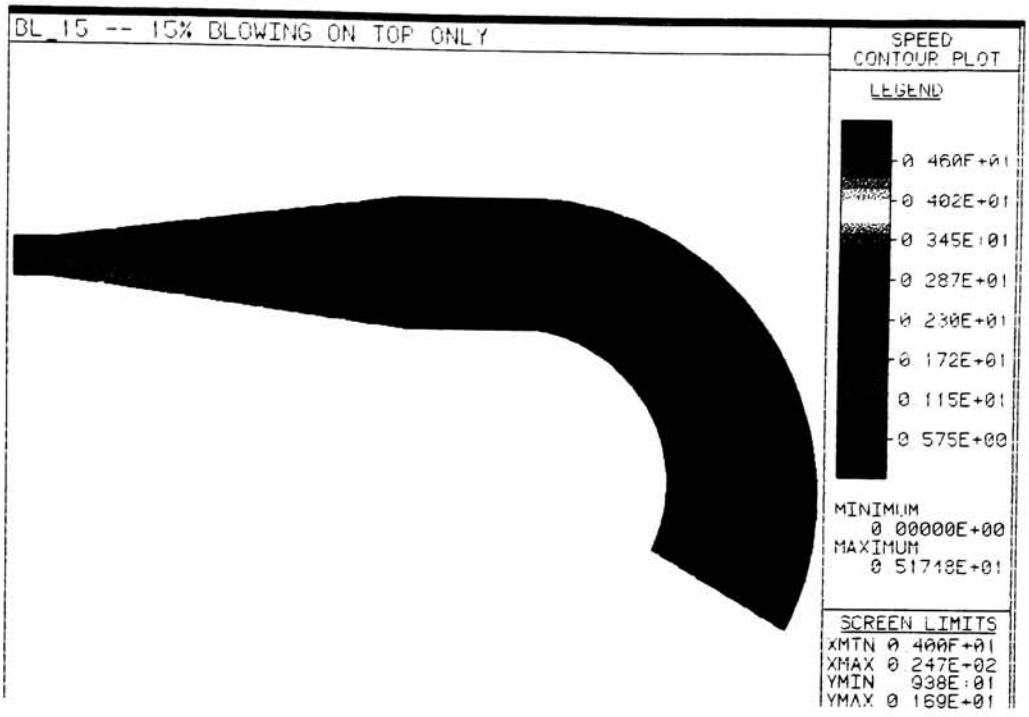

Figure 7.80 - Vorticity Contour Plot, 15% Blowing

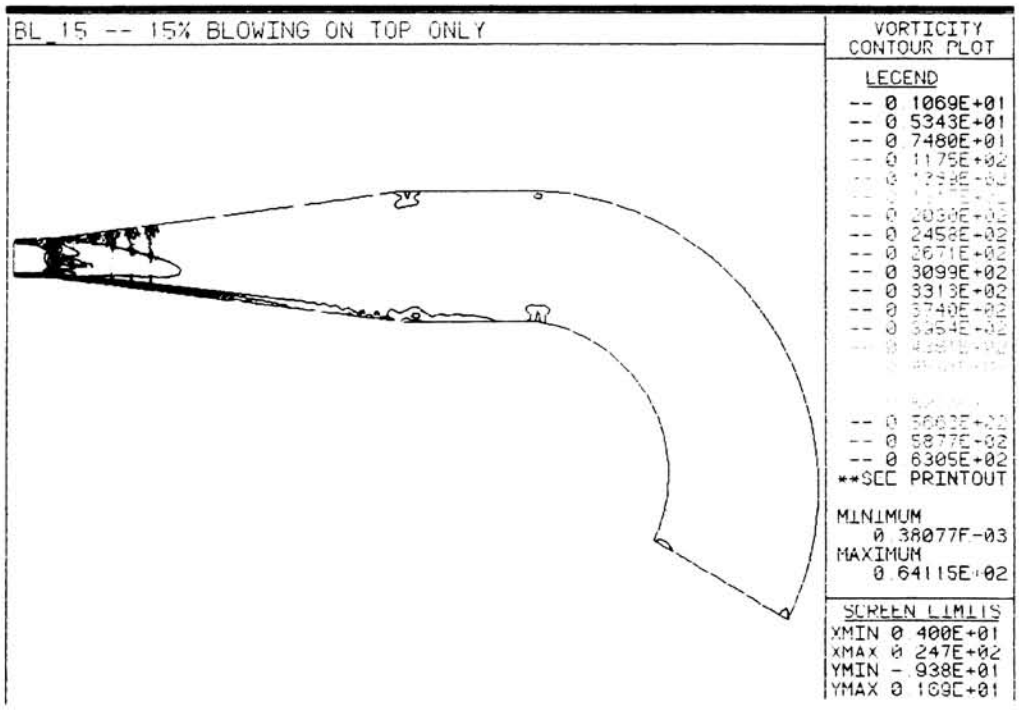

Figure 7.81 - Kinetic Energy Contour Plot, 15% Blowing

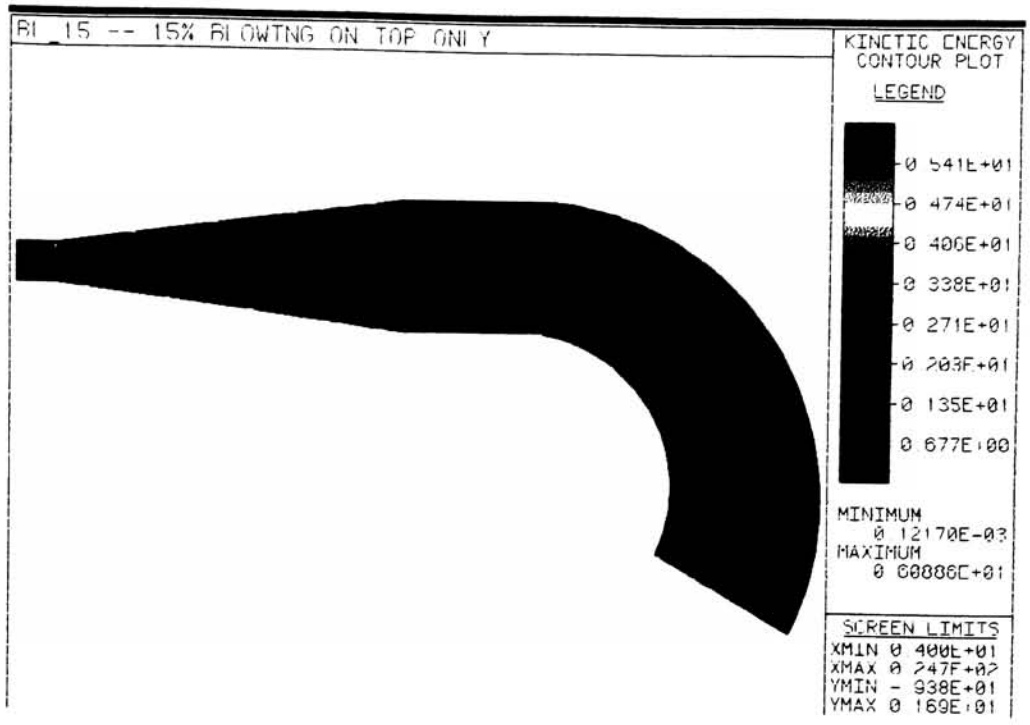

Figure 7.82 - Dissipation Contour Plot, 15% Blowing

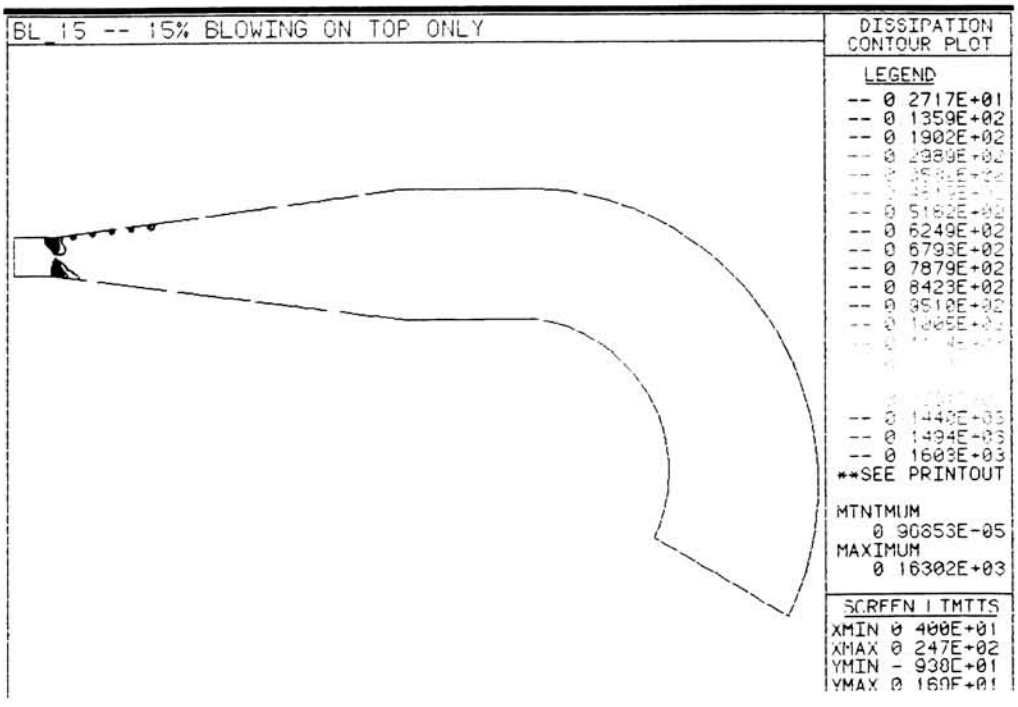

Figure 7.83 - Velocity Profiles at the Inlet, 15% Blowing

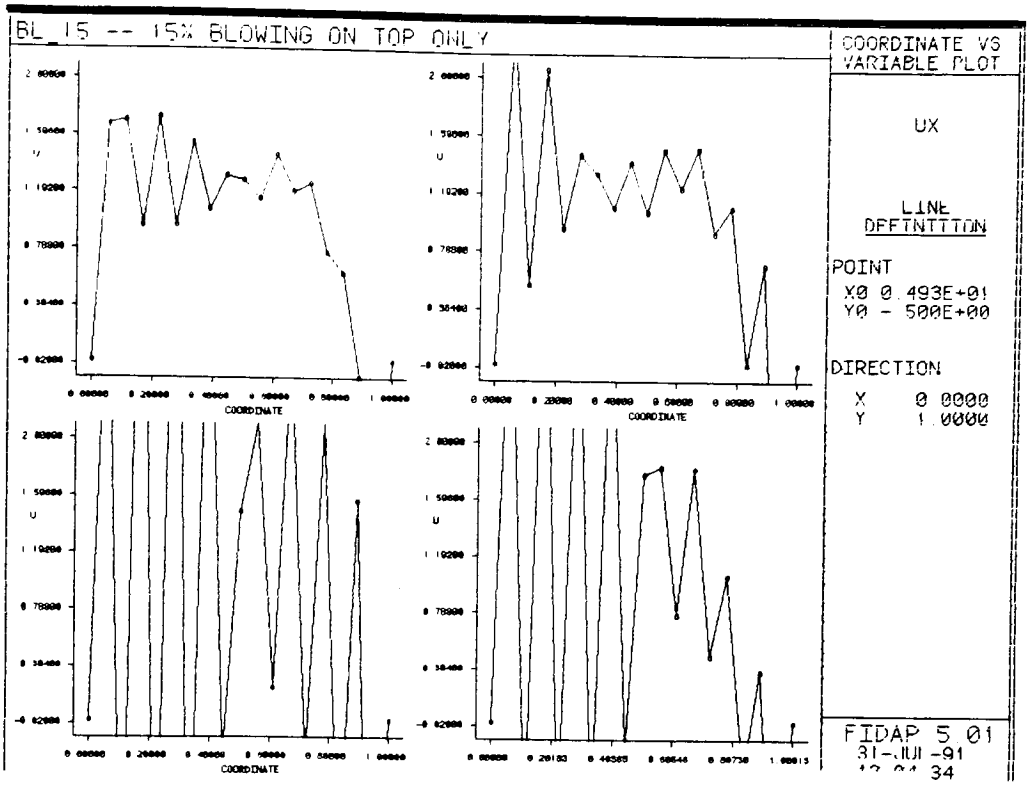

Figure 7.84 - Velocity Profiles at the Outlet, 15% Blowing

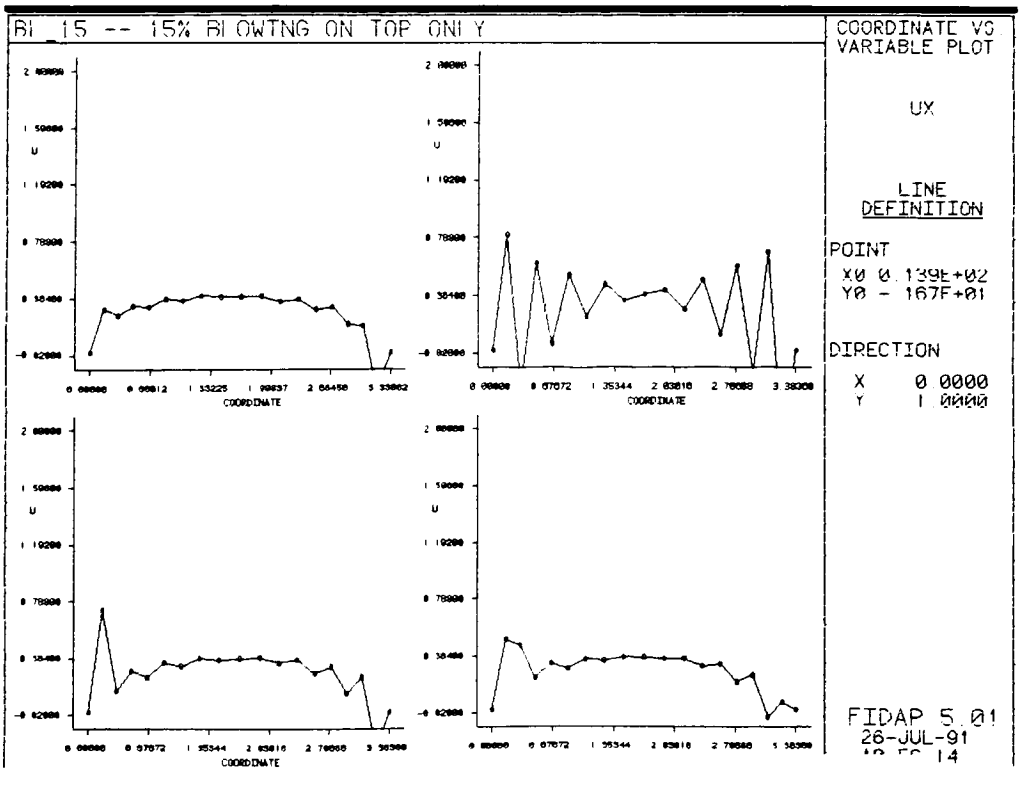

8 CONCLUSIONS

The results of the numerical tests showed that FIDAP is capable of simulating the flow conditions that are present in a 2-dimensional diffuser with adverse pressure gradients as well as the implementation of boundary layer control devices that can be used to correct the resulting flow separation at off-design flow conditions. Specifically, the results indicated that implementing suction at about a rate of 15% of the inlet mass flow rate through the upper wall of the diffuser successfully counteracted the incidence effects that are present in a typical turbopump diffuser at off-design flow rates. Blowing was shown to effectively reenergize the boundary layer and reduce flow separation at rates of 10% of the inlet mass flow rate with injection through the top wall of the diffuser.

8-1.0 Design and Off-Design Flow Models

The Design and Off-Design models were generated as benchmarks to compare the effectiveness of the suction and blowing with regard to the performance of the diffuser. They were also used as test cases to show that FIDAP was capable of modeling the adverse pressure gradient flows found in turbopump diffusers. The results, as indicated in sections 7-1 and 7-2, seemed sufficiently accurate to continue with the modeling.

Before suction and blowing are discussed specifically, it is necessary to discuss some of the results that pertain to all of the models.

1. Table 7.1 gives values for the throat blockage for each of the cases under investigation. These values must be taken as rough estimates due to the nature in determining the momentum bondary layer thickness. It is difficult to find a curve fitting routine that will generate turbulent velocity profiles in functional form. The curve fits used (see Appendix D) approximate the profiles well enough to get an idea of the boundary layer thickness but not well enough to obtain an exact profile. Further, when determining δ, the boundary layer thickness, the assumption was made that the flow near the wall resembled turbulent flow over a plate at both the inlet and the outlet using a 1/7 velocity profile. This assumption may be adequate owing to the nature of the near wall region, but a more adequate model may yet be determined.

2. The concepts developed in chapter three predicted that the diffuser of interest would operate in the large transitory stall region. Unfortunately, the data available for describing and comparing diffusers was for zero incidence effects. Owing to the induced incidence effects, it appears from the results that the diffuser is actually operating in the fully developed stall region when running at the off-design flow rates. As the suction and blowing is implemented, it appears that the flow shows more of the large transitory stall characteristics, leaning towards no appreciable stall.

8-2.0 Suction

When suction was applied to the off-design flow model, it was shown that the flow separation was reduced significantly and the flow became more uniform for mass suction rates as low as 5% of the inlet mass flow rate through the top of the diffuser. Some interesting phenomena occured in the model that are worthy of further discussion.

1. As is indicated on the pressure contour plots as well as the pressure line plots along the centerline for all of the suction rates, the majority of the pressure recovery occurs well before the end of the diffuser. This would tend to indicate that the little flow separation that does occur has little effect on the output characteristics of the diffuser at each suction rate. The implementation of suction itself does tend to increase the performance of the diffuser to a point, after which, more suction becomes detrimental to the diffuser performance.

2. The suction not only benefits the flow before the separation but also forces the flow properties to become more uniform throughout the diffuser. This situation in essence negates the effect of the pronounced incidence angle at off-design flow rates.

3. The amount of suction applied to the model seems to have an "optimum" value at around 15%. Examining the relationship

between the pressure recovery coefficients and the suction rate (Figure 7.49), it is obvious that this phenomenon exists. With this in mind, the future 3-D modeling should be conducted with suction rates between 13 and 17 percent.

4. A review of the location of the suction slits and their interaction with the flow field indicates that a more appropriate location of the first slit in the diffuser might be at the entrance to the diffuser throat. This location would keep the flow from having a chance to gain momentum towards separation that might be occuring in the current model. This change might lead to a lower suction rate requirement and therefore a lower power requirement to maintain the suction.

5. The instabilities that appear to exist at the inlet of the diffuser need to be investigated further by laboratory testing. When they were noticed, it was thought that they might be caused by an insufficient mesh density or an inadequate choice of inlet flow rate. Extensive testing involving varying both of those parameters was undertaken to determine if these factors might be the cause. Unfortunately, all of the tests revealed the same instabilities indicating the need for laboratory testing.

8-3.0 Blowing

The application of blowing to control flow separation in the diffuser is not as well defined or as widely used as suction. The

results presented here are a beginning to this study and indicate that more research and modelling is required to determine its actual effectiveness and applicability to the turbopump design. The results suggest that blowing implemented at too low a rate is simply not effective and blowing at too high a rate is not practical. Some interesting results are worthy of further discussion.

1. The concept of blowing was implemented in an attempt to reenergize the decelerating fluid particles in the vicinity of the separation. Another concept that could be investigated in an attempt to counteract the effects of the incidence. For example, in the off-design flow case, perhaps blowing through the bottom wall of the diffuser would act in the same manner as the suction at the top of the diffuser.

2. Blowing is rather impractical from an implementation stand point. Additional fluid is required that is not in the normal flow field. This may lead to prohibitive expenses to provide additional fuel that would be necessary.

3. Particular difficulty arises when attempting to interpret the pressure recovery coefficient. The definition as it exists is based on the assumption of conservation of mass of the system. Since blowing introduces mass into the system, perhaps a new relationship is needed to describe this flow case effectively considering the coefficient that was determined to be larger than one for the 15% blowing case.

REFERENCES

1. "MK-49F Fuel Diffuser and Crossover Design," Rockwell International, Rocketdyne Division R/H 1173-4126.

2. "Turbulent Flow with FIDAP, Seminar Notes," Fluid Dynamics International. Evanston, IL

3. Fox, Robert W. and McDonald, Alan T. Introduction to Fluid Mechanics. John Wiley and Sons, New York, 1985.

4. Panton, Ronald L. Incompressible Flow. John Wiley and Sons, New York, 1984.

5. Tennekes, H. and Lumley, J. L. A First Course in Turbulence. The MIT Press, Cambridge, 1972.

6. Reynolds, A. J. Turbulent Flows In Engineering. John Wiley and Sons, New York, 1974.

7. Hinze, J. O. Turbulence. McGraw-Hill Book Company, Inc., New York, 1959.

8. Schlicting, H. Boundary Layer Theory. McGraw-Hill Book Company, Inc., New York, 1960.

9. Reneau, L. R., Johnston, J. P., and Kline, S. J. "Performance and Design of Straight, Two-Dimensional Diffusers." Report PD-8, Thermosciences Division, Stanford University, 1964.

10. Runstadler, P. W., Francis, D. X., and Dean, R. C. "Diffuser Data Book." TN-186, Creare, Inc, 1975.

11. Ball, W. H., "Experimental Investigation of the Effects of Wall Suction and Blowing on the Performance of Highly Offset Diffusers," AIAA, SAE, and ASME, Joint Propulstion Conference, 19th, Seattle, 1983.

12. Nelson, C. D., Hudson, W. G. and T. Yang, "The Design and Performance of Axially Symmetrical Contoured Wall Diffusers Employing Suction Boundary Layer Control," ASME Gas Turbine Conference and Products Show, Zurich, 1974.

13. Stepanenko, A. P., "Effect of Boundary Layer Suction on the Performance of a Curvilinear Annular Diffuser," Fiziko-Tekhnichni Matematichni Nauki, Vol. 33, 1971.

14. Fujimoto, T., Furuya, Y., Nichiura, I., Tsuzuki, I., and E. Yamazato, "Pressure Recovery and Energy Loss Efficiencies of Two Dimensional Diffusers with Suction at Entrance," JSME Bulletin, Vol. 13, 1977, pp 264-271.

15. Yang, T., "Design and Experimental Performance of Short Curved Wall Diffusers with Axial Symmetry Utilizing Slot Suction," NASA-TN-D-7237, 1973.

16. Fiedler, R. A. and B. F. Gessner, "Influence of Tangential Fluid Injeciton on the Performance of Two-Dimensional Diffusers."

17. Reddy, J. N. An Introduction to the Finite Element Method. McGraw-Hill Book Company, Inc., New York, 1984.

18. FIDAP Theory Manual. Fluid Dynamics International, Evanston, IL.

19. Pourahmadi, F. and Humphrey, J. "Prediction of Curved Channel Flow with an Extended k-ε Model of Turbulence." AIAA Journal, Vol 21, Oct 1983, pp. 1365-1373.

20. Veres, J. and Chang, T. "CFD Analysis of a Crossover Diffuser within a Centrifugal Pump." NASA/AIEE Propulsion Conference for Space Exploration Initiative, Sept. 4-6, 1991.

Additional References

Sohn, J. L. "Numerical Analysis of Laminar and Turbulent Incompressible Flows Using the Finite Element 'Fluid Dynamics Analysis Package (FIDAP)'" NASA CR-179390, Aug 1988.

Antonia, R. A., Fulachier, L., Krishnamoorthy, L. V., Benabid, T. and Anselmet, F. "Influence of Wall Suction on the Organized Motion in a Turbulent boundary Layer." Journal of Fluid Mechanics, Vol 190, 1988.

Olson, R. M. and Eckert, E. R. G. "Experimental Studies of Turbulent Flow in a Porous circular Tube With Uniform fluid Injection Through the Tube Wall." Journal of Applied Mechanics, March 1966.

Schildknecht, M., Miller, J. A., and Meier, G. E. A. "The Influence of Suction on the Structure of Trubulence in Fully Developed Pipe Flow." Journal of Fluid Mechanics, Vol 90, 1979.

Merkine, L., Solan, A., and Winograd, Y. "Turbulent Flow in a Tube With Wall Suction." Journal of Heat Transfer, May 1971.

Ashjaee, J. and Johnston, J. P. "Straight-Walled, Twi-Dimensional Diffusers - Transitory Stall and Peak Pressure Recovery." Journal of Fluids Engineering, Vol. 102, 1980.

Kline, S. J. "On the Nature of Stall." Journal of Basic Engineering, September, 1959.

Reynolds, G. A. and Saric, W. S. "Experiments on the Stability of the Flat-Plate Boundary Layer with Suction." AIAA Journal, Vol. 24, 1986.

Kinney, R. B. and Sparrow, E. M. "Turbulent Flow, Heat Transfer, and Mass Transfer in a Tube with Surface Suction." Journal of Heat Transfer, Feb 1970.

Lin, S. P. and Tobak, M. "Reversed Flow Above a Plate with Suction." AIAA Journal, Vol 24, 1986.

Kline, S. J., Abbott, D. E. and Fox, R. W. "Optimum Design of Straight Wall Diffusers." Journal of Basic Engineering, Sept 1959.

Sabnis, J., Madabhushi, R., Gibeling, H. and McDonald, H. "On the Use of k-ε Turbulence Model for Computation of Solid Rocket Internal Flows." AIAA 89-2558, AIAA/ASME/SAE/ASEE 25th Joint Propulsion Conference, July 10-12, 1989.

Rink, L. and Carroll, M. "Computational Analysis of Turbomachinery Flows Using FLOFIVE." AIAA 89-2559, AIAA/ASME/SAE/ASEE 25th Joint Propulsion Conference, July 10-12, 1989.

APPENDIX A - Flow Conditions

This appendix defines the flow constants and determines the inlet flow parameters for the design flow rate model as well as the off-design and boundary layer control models. The values for the non-dimensional suction and blowing velocities calculated using the following procedure are given in Table A.1

Flow Constants

$$\rho = 1.94 \frac{slug}{ft^3} \qquad \mu = 2.089e\text{-}5 \frac{lbf\ s}{ft^2} \qquad D_H = 1\ in$$

100% Design Flow Rate

Re = 16667

$$v_i = \frac{\mu\ Re}{\rho\ D_{Hi}} = \frac{2.089e\text{-}5 * 16667}{1.94 * (1/12)} = 2.1537 \frac{ft}{s}$$

$$m_i = \rho\ v_i\ A_i \Rightarrow \frac{m}{ft} = \rho\ v_i\ D_{Hi} = 1.94 * 2.1537 * \frac{1}{12} = 0.3482 \frac{slug}{s}$$

incidence angle = 1.49° (From Talbe 1.1)

60% Design Flow Rate

Re = 10,000

$$v_i = \frac{\mu\ Re}{\rho\ D_{Hi}} = \frac{2.089e\text{-}5 * 10000}{1.94 * (1/12)} = 1.292 \frac{ft}{s}$$

$$m_i = \rho\ v_i\ A_i \Rightarrow \frac{m}{ft} = \rho\ v_i\ D_{Hi} = 1.94 * 1.292 * \frac{1}{12} = 0.20887 \frac{slug}{s}$$

Incidence angtle = 4.19° (From Table 1.1)

Suction

Number of slits = NS = 7 (along the top for suction)

Width of slits = w_s = 0.05 in

Assumptions: (1) suction rate is the same through each slit.

(2) suction is at a 37.5 deg angle to the axis of the diffuser.

(3) total suction is distributed equally accross each slit.

Blowing

NS = 5 (along the top of the diffuser)

w_s = 0.05 in

Assumptions (1) Blowing rate is the same through each slit.

(2) Blowing is tangential to centerline of the diffuser.

(3) Total blowing is distributed equally across each slit.

Example - 5% Suction

$m_{5\%}$ = mass flow rate for 5% suction = $0.05 * m_i$ = $0.05 * 0.20887$

$= 0.01044 \frac{slug}{s}$

$\frac{m_{5\%}}{ft}$ = m at each slit = $\frac{m_5}{7} = \frac{0.01044}{7} = 0.0014919 \frac{slug}{s}$

$U_{5\%}$ = velocity at each slit = $\frac{m_{5\%}}{ft\ \rho\ A} = \frac{0.0014919}{1.94 \frac{0.05}{12}} = 0.1846 \frac{ft}{s}$

$u_{5\%}^* = \frac{U \cos(37.5)}{1.292} = 0.1134$

$v_{5\%}^* = \frac{U \sin(37.5)}{1.292} = 0.08697$

Table A.1 - Suction and Blowing Velicties

Model	u^*	v^*
5% Suction	0.1134	0.08697
10% Suction	0.2267	0.1739
15% Suction	0.3400	0.2609
20% Suction	0.4533	0.3479
5% Blowing	0.1999	0.0
10% Blowing	0.3999	0.0
15% Blowing	0.5999	0.0

APPENDIX B - Determination of C_p and Reynolds Number

Determination of Pressure Recovery Coefficient

The determination of the pressure recovery coefficient is rather straight forward. The definition is given by

$$C_p = \frac{\Delta P}{\frac{1}{2}\rho v^2} \qquad (3.1)$$

where ΔP is the change in pressure accross the diffuser, ρ is the liquid density and v is the inlet velocity.

The solution procedure employed a nondimension approach. The nondimensional pressure is defined by FIDAP as

$$P^* = \frac{P}{\rho v^2} \qquad (6.1c)$$

Rearranging and solving for the dimensional pressure yields:

$$P = P^* \rho v^2$$

Substituting this result into (3.1) gives the pressure recovery coefficient as a function of P^*

$$C_p = 2\,\Delta P^*$$

The coefficients tabulated on Table 7.1 are calculated in this manner from the nondimensional pressures tabulated on Table B1. The inlet and outlet P^* were calculated using the program 'AVE,'

given at the end of this appendix. The graphs of the pressure distributions at the inlet and outlet (Figures A.1-A.9) are given to verify the calculated values as well as to provide a visualization of the pressures of interest.

Table B.1 - Nondimensional Pressures

Model	P_i^*	P_o^*
100% Flow	-0.3924	-2.5296E-2
60% Flow	-0.3575	-3.6261e-2
5% Suction	-0.3752	-1.8349e-2
10% Suction	-0.3680	-6.3551e-3
15% Suction	-0.3739	-8.5118e-3
20% Suction	-0.3525	-1.9793e-2
5% Blowing	-0.3143	-2.6825e-2
10% Blowing	-0.4041	-2.2376e-2
15% Blowing	-0.7987	7.6942e-2

Figure B.1 - Design Flow, Pressure Line Plots

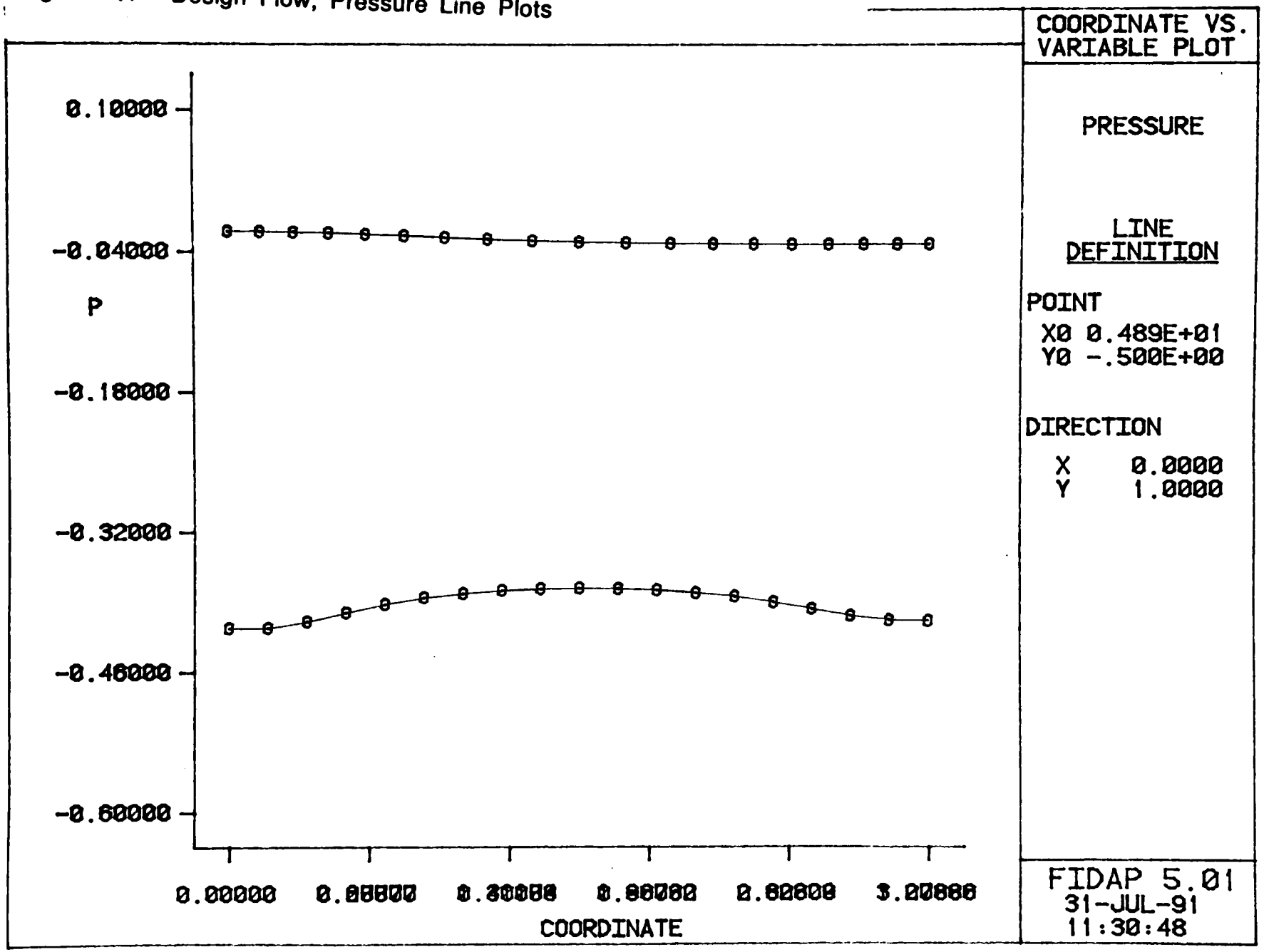

Figure B.2 - 60% Design Flow, Pressure Line Plots

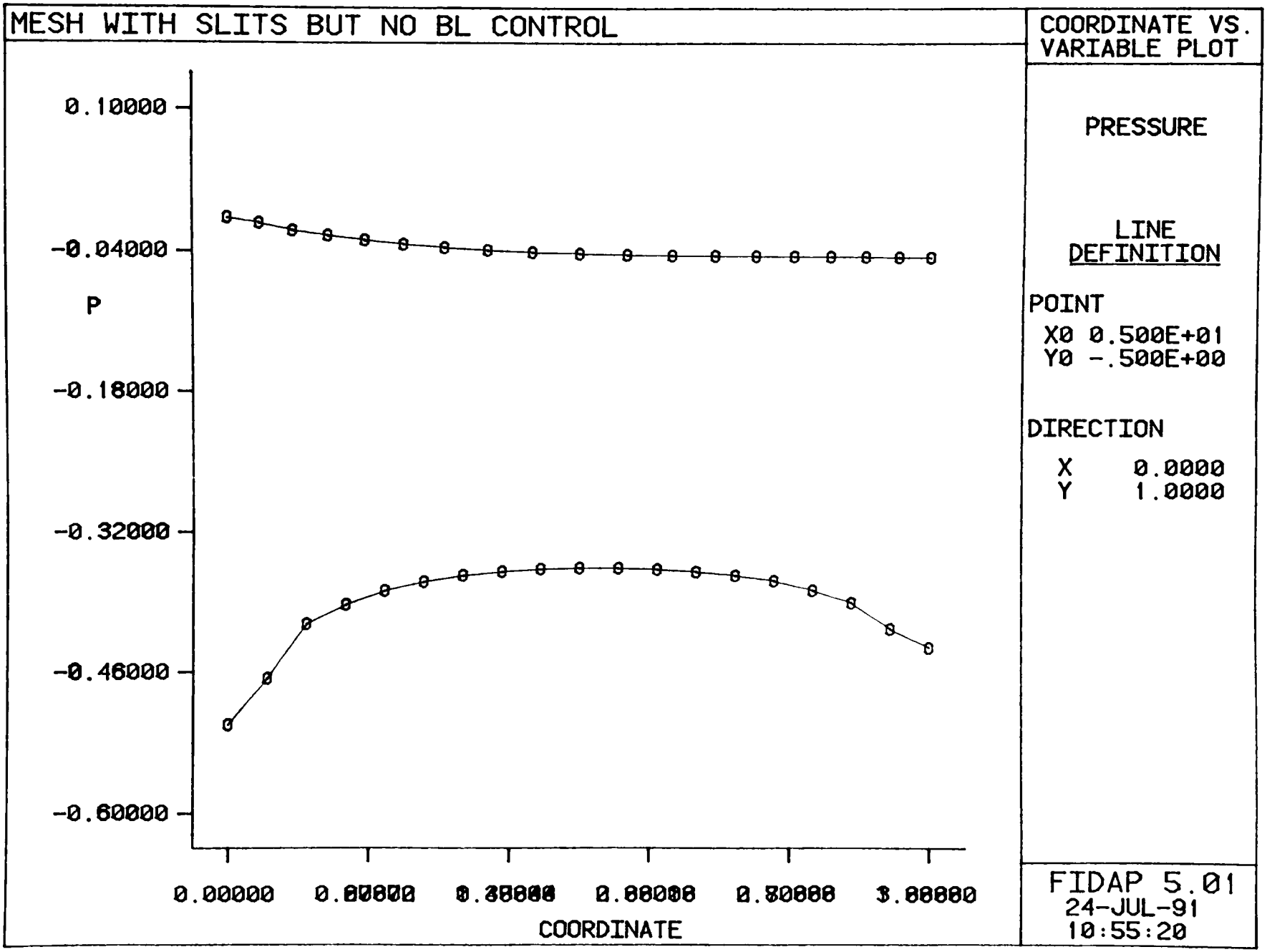

Figure B.3 - 5% Suction, Pressure Line Plots

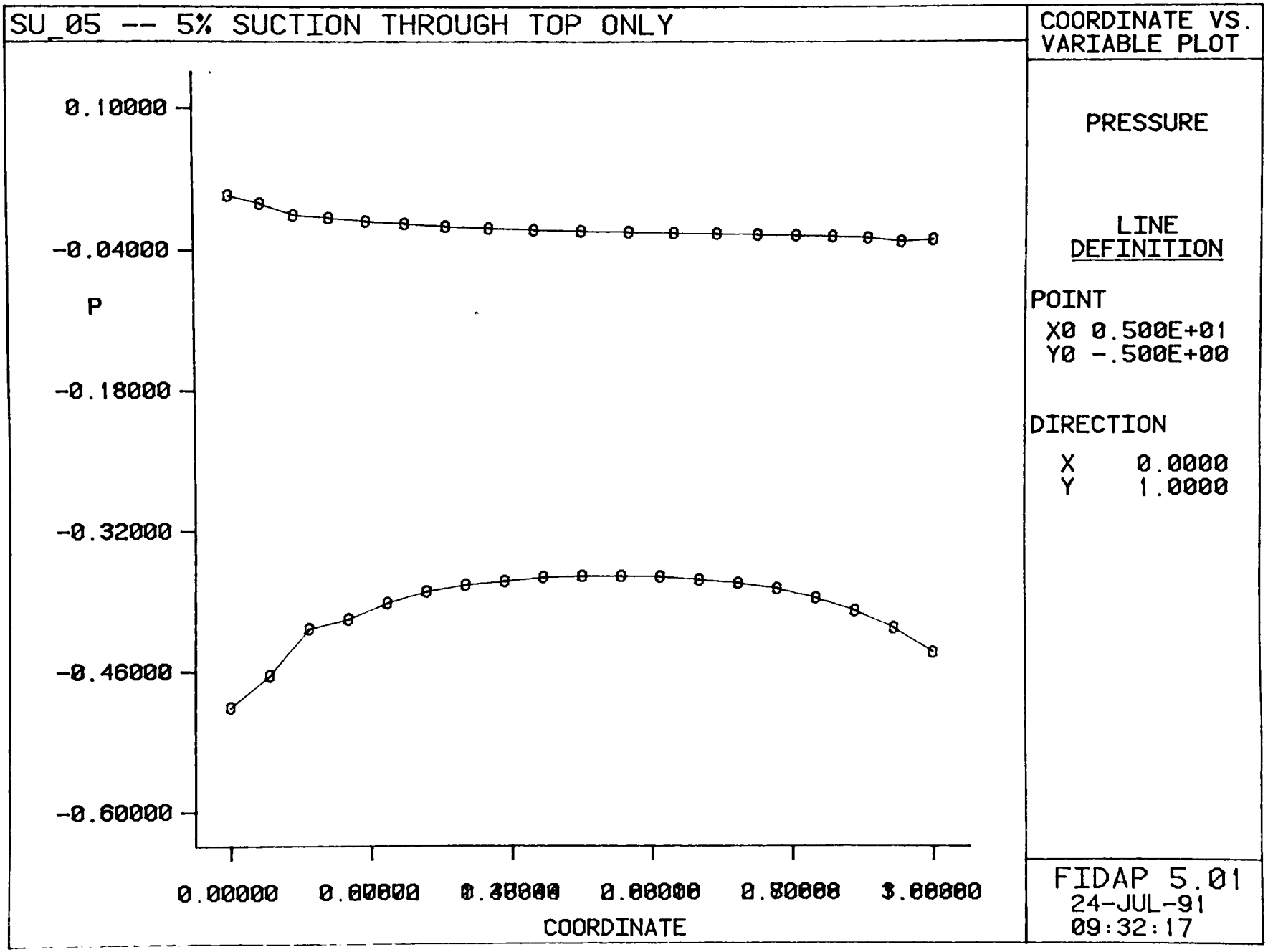

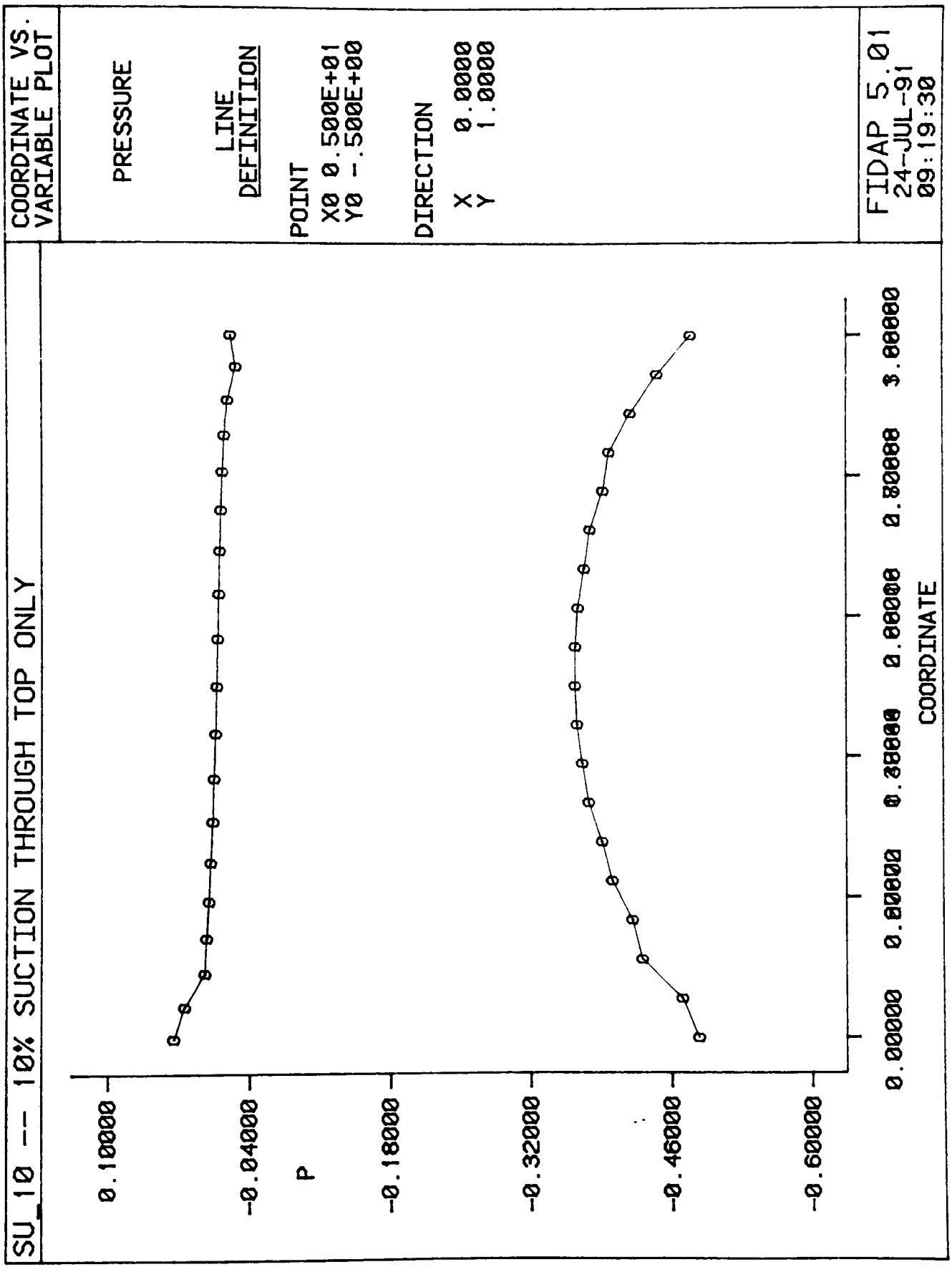

Figure B.4 - 10% Suction, Pressure Line Plots

Figure B.5 - 15% Suction, Pressure Line Plots

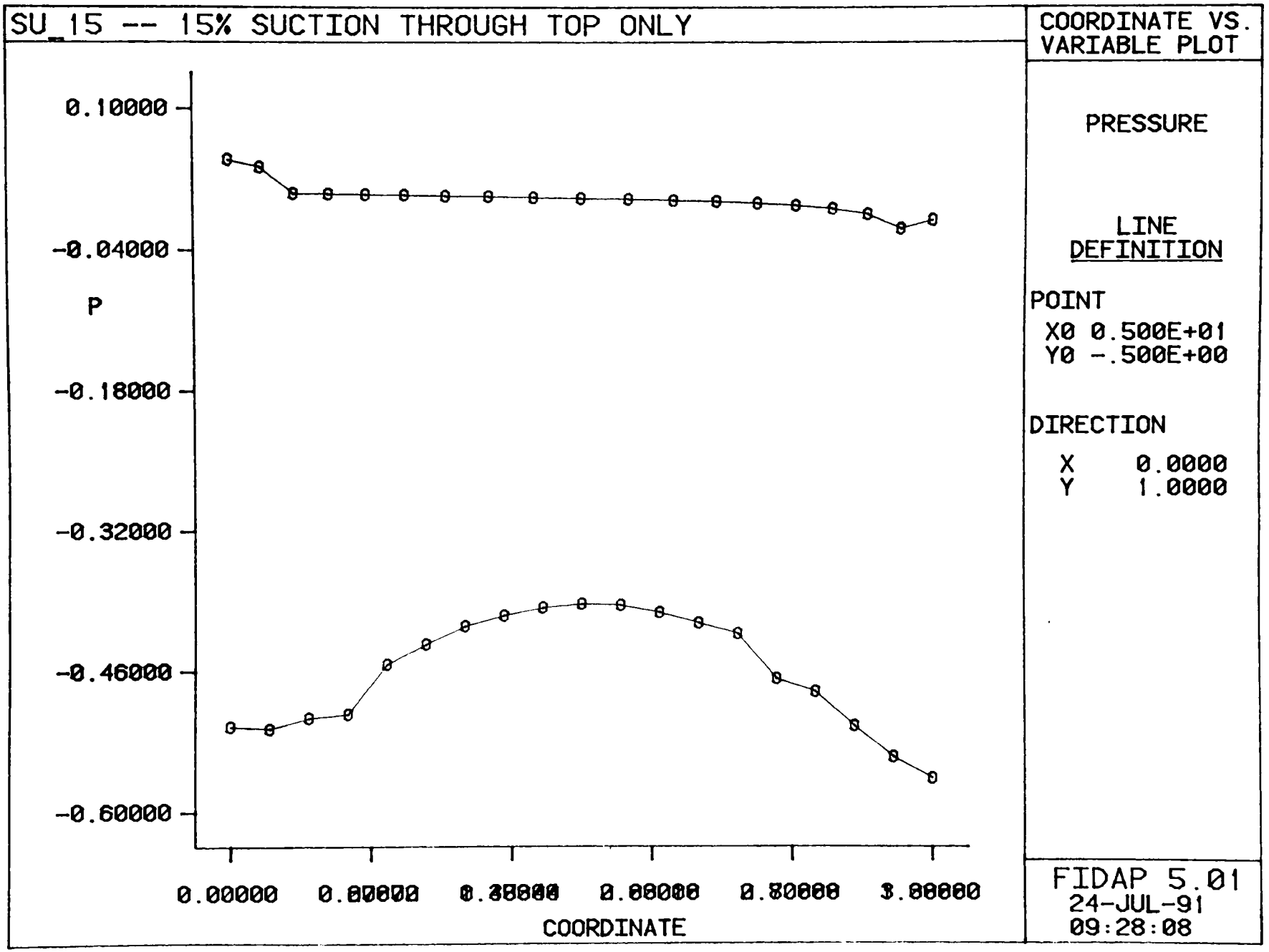

Figure B.6 - 20% Suction, Pressure Line Plots

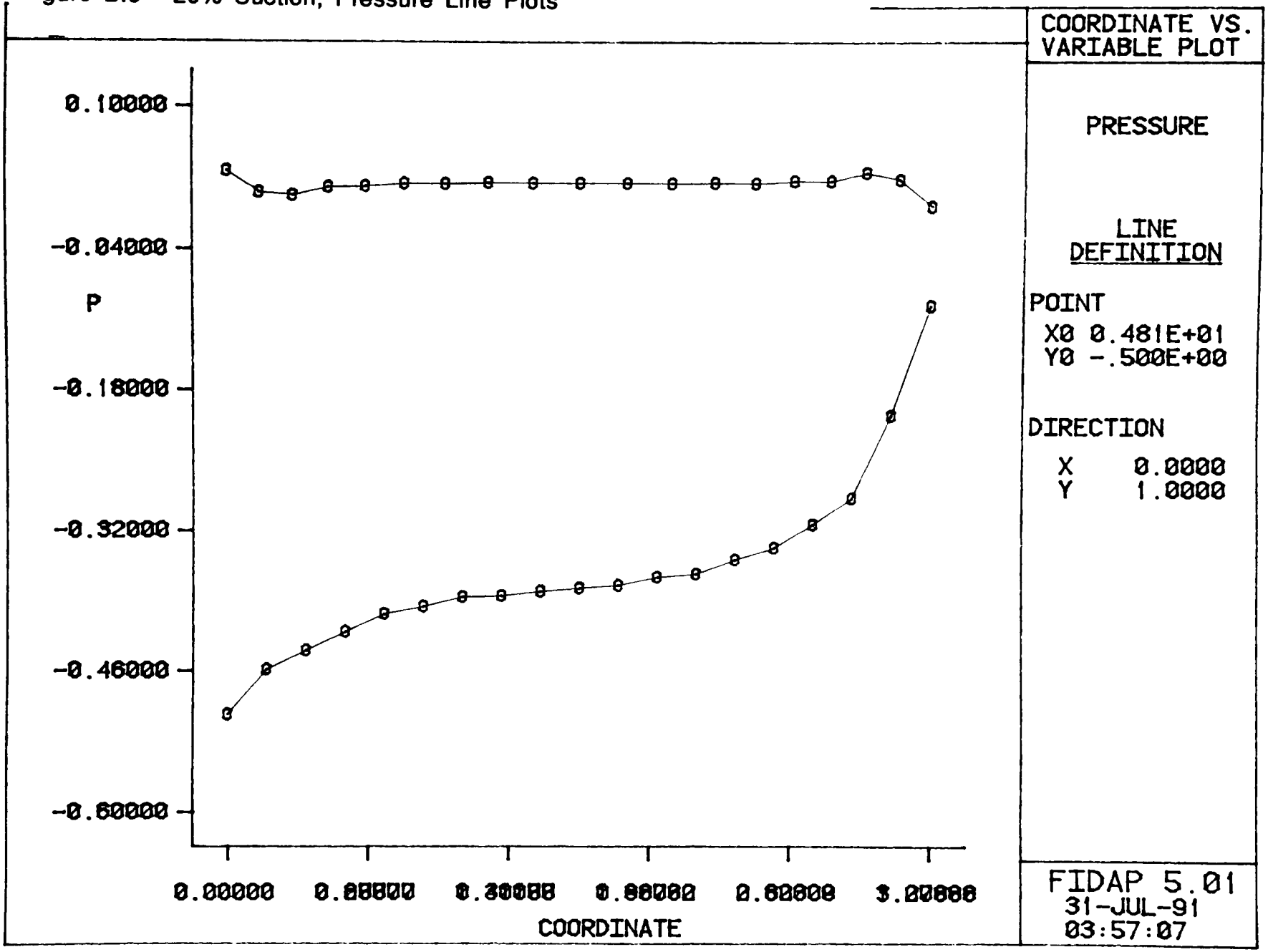

Figure B.7 - 5% Blowing, Pressure Line Plots

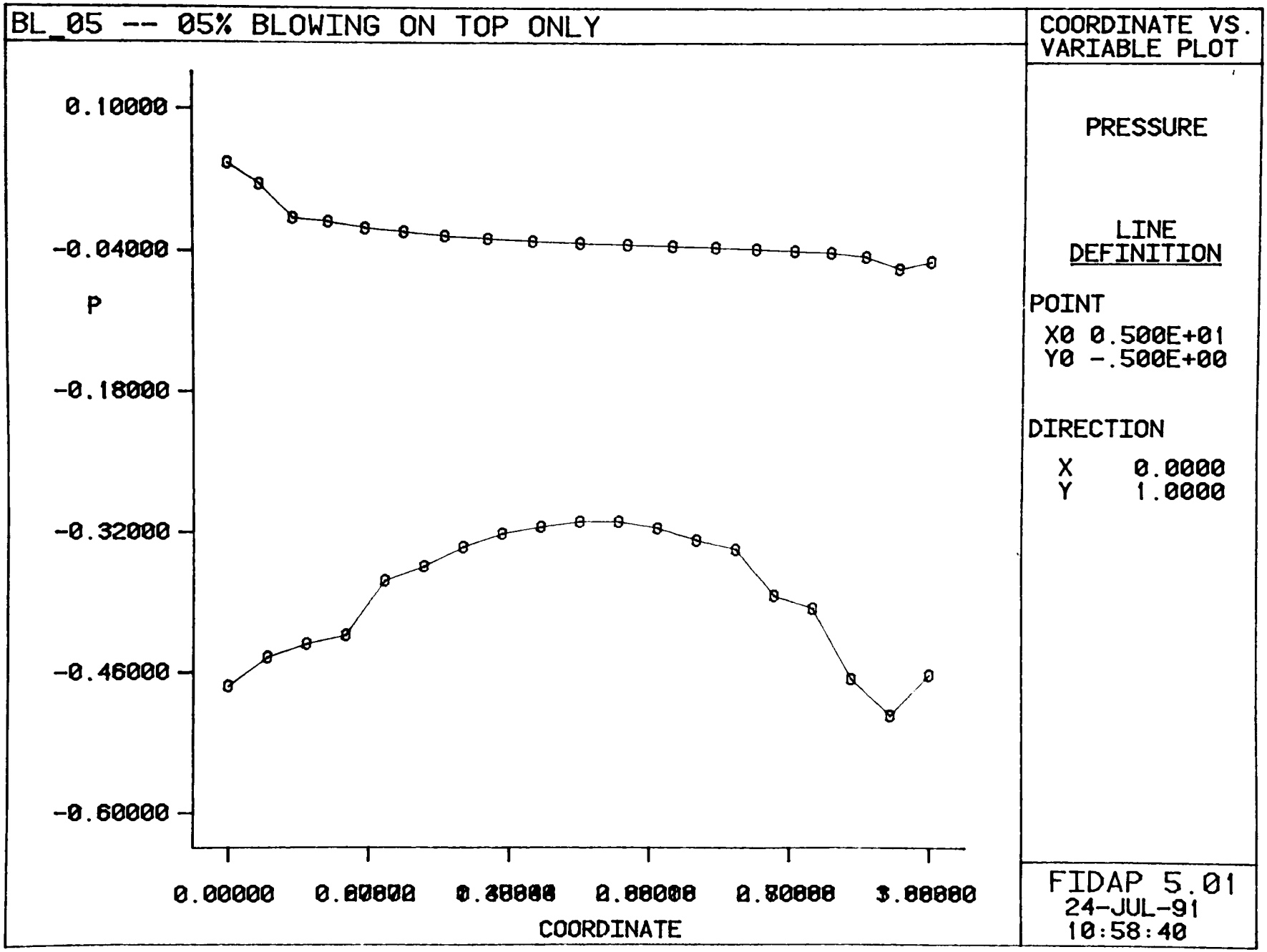

Figure B.8 - 10% Blowing, Pressure Line Plots

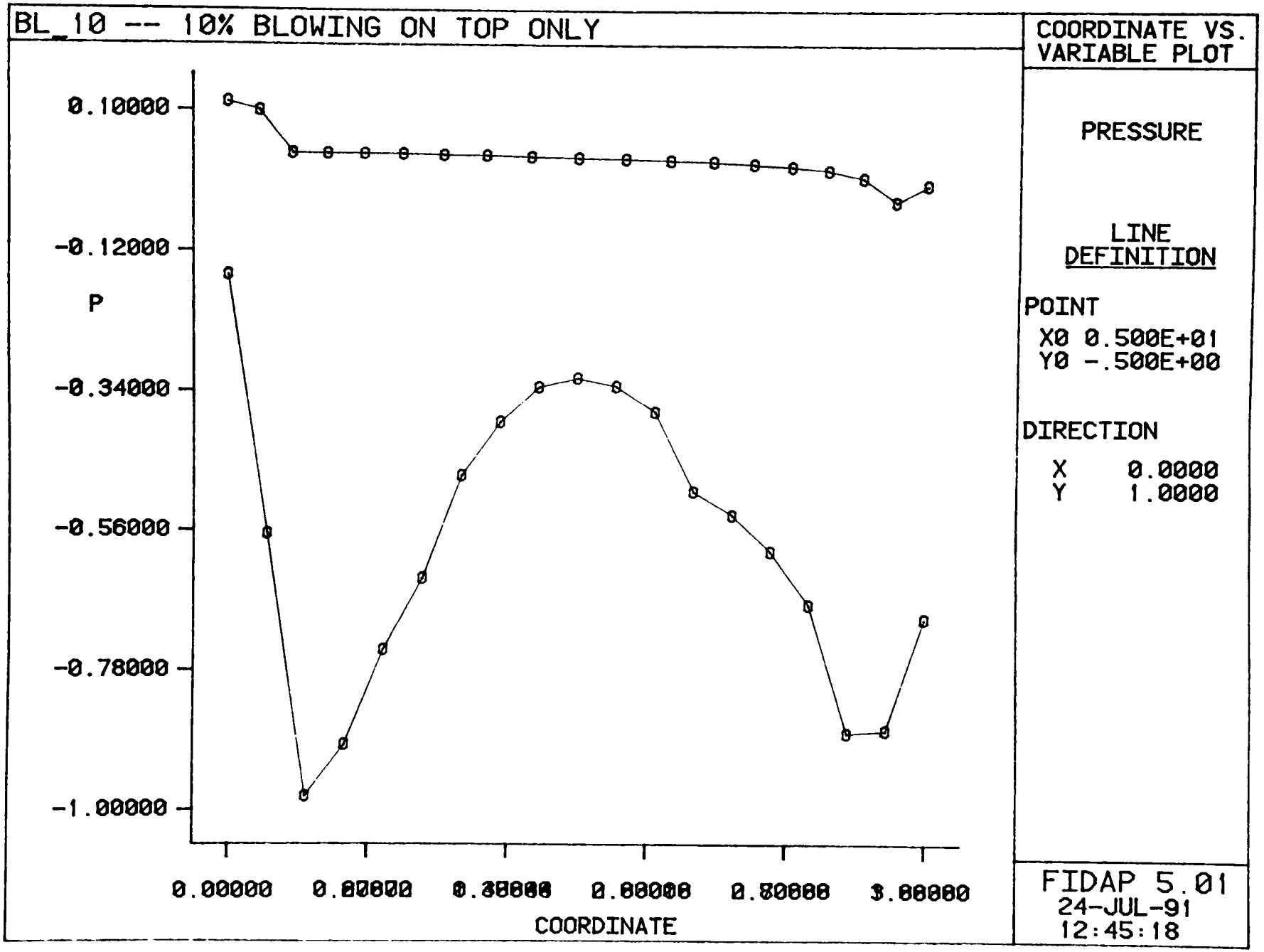

Figure B.9 - 15% Blowing, Pressure Line Plots

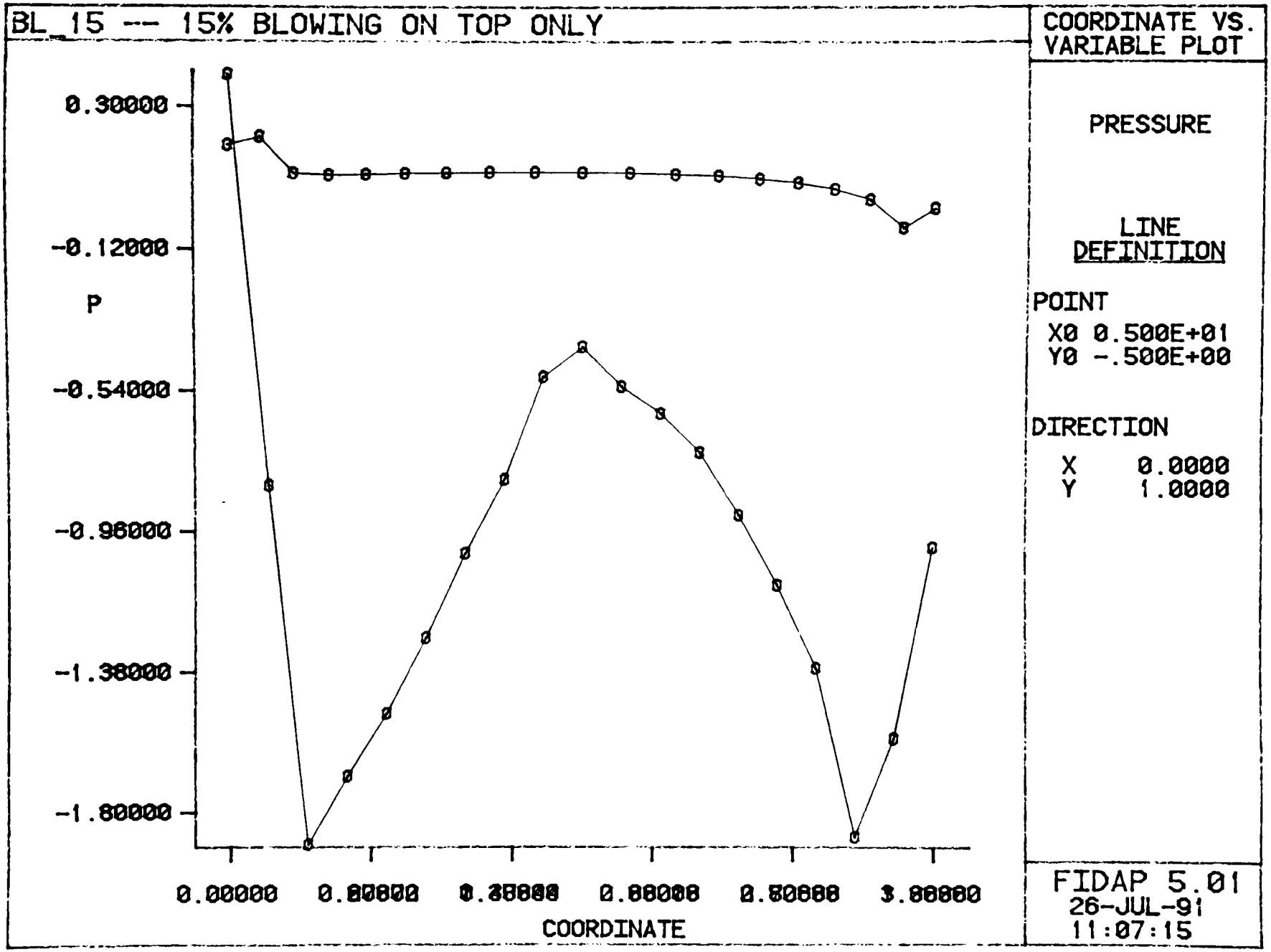

Determinataion of Outlet Reynolds Number

In a similar manner the Reynolds number is calculated from the average speed either at the inlet or outlet. The speed is calculated from

$$s = (\sqrt{u_1^2 + u_2^2})\ v_c \frac{ft}{s}$$

The values for the Reynolds numbers tabulated in Table 7.2 were calculated from the average inlet and outlet velocities shown on Table B.2 using the program 'AVE2' given at the end of this appendix. The velocities used in the calculations were taken from locations one and six of Figure 7.8.

Table B.2 - Inlet and Outlet Speeds

Model	$S_i \frac{ft}{s}$	$S_o \frac{ft}{s}$
100% Flow	1.9265	0.5709
60% Flow	1.1529	0.3594
5% Suction	1.1349	0.3398
10% Suction	1.1177	0.3284
15% Suction	1.1293	0.3189
20% Suction	1.1247	0.3099
5% Blowing	1.1553	0.3898
10% Blowing	1.1821	0.4048
15% Blowing	1.4579	0.4379

```
*
      implicit none
      dimension pa(2)
      real ps, x, y, z, e, p, pa, ps1
      integer i, j, n

      write (6,*) '-----------------------------------------'
*
      do 100, j = 1,2
*
      read (9+j,*) n
      p = 0
*
      do 50, i = 1,n
            read (9+j,*) e, x, y, z, ps
            p = p + ps
 50   continue
*
      pa(j) = p/n
*
 100  continue
*
      ps1 = 2*(pa(2)-pa(1))
*
      write (6,*) 'Average Pressure In =',pa(1)
      write (6,*) 'Average Pressure Out =',pa(2)
      write (6,*)
      write (6,*) 'Cp =',ps1
      write (6,*) '-----------------------------------------'
*
      stop
      end
```

```
*
      implicit none
      dimension pa(2)
      real ps, x, y, z, e, p, pa, ps1, vx, vy, s, s1
      integer i, j, n

      write (6,*) '-------------------------------------------'
*
      do 100, j = 1,2
*
      read (9+j,*) n
      s = 0
*
      do 50, i = 1,n
            read (9+j,*) e, x, y, z, vx, vy
            s1 = (vx**2 + vy**2)**0.5
            s = s + s1
 50   continue
*
      pa(j) = s/n
*
 100  continue
*
*
      write (6,*) 'Average Speed In =',pa(1)
      write (6,*) 'Average Speed Out =',pa(2)
      write (6,*) '-------------------------------------------'
*
      stop
      end
```

Appendix C - FIDAP Input Files

- DIV.FIECHI
- SU_05.FIECHI
- BL_05.FIECHI

Note: The only changes to each file is the boundary condition on the suction or blowing slits in accordance with the values given in Appendix A, Table A.1.

```
/---------->>> title   'DIV.FIECHI'  (Turbulent)              1/25/91
/
/       This is the 2D model of a diffuser with an angle of divergence
/       equal to 15 deg and with 4.19 incidence angle at the inlet, and
/       turning channel.
/
/                Created by
/
/                G. Wissinger
/                Rochester Institute of Technology
/                April, 1991
/
/       dimensionLESS Analysis
/                Vin = 1.292 ft/s
/                incid = 4.19 deg
/
/                Re = 10.0e3
/
/                Fluid = Water
/                density = 1.94 slug/ft^3
/                abs viscosity = 2.089e-5 lbf s/ft^2
/
/
/
*TITLE
Mesh with slits but NO BL Control
*FIMESH(2-D,IMAX=39,JMAX=3,MXPOINT=2000)
EXPI(DELTAS)
1 0 12 0 2 0 6 0 2 0 6 0 11 0 2 0 10 0 2 0 10 0 2 0 10,
0 2 0 10 0 2 0 60 0 16 0 40
EXPJ(DELTAS)
1 0 18
/
/       Spacial dimensions in IN
POINT
/  i j k    x       y         z
/
/       MAJOR key points
1    1    1   1   4.0       -0.5
20   1    3   1   4.0        0.5
6    11   1   1   5.0       -0.5
25   11   3   1   5.0        0.5
17   33   1   1   14.053    -1.6918
36   33   3   1   14.053     1.6918
18   35   1   1   17.4366   -1.6918
37   35   3   1   17.4366    1.6918
19   37   1   1   20.4266   -7.3201
38   37   3   1   23.8836   -9.3789
40   0    0   0   16.9266   -5.8105
/
/       SUCTION HOLE key points
21    3   3   1   4.475      0.5
22    5   3   1   4.525      0.5
2     3   1   1   4.475     -0.5
3     5   1   1   4.525     -0.5
23    7   3   1   4.725      0.5
24    9   3   1   4.775      0.5
4     7   1   1   4.725     -0.5
5     9   1   1   4.775     -0.5
26   13   3   1   5.4709     0.5620
```

```
/---------->>> title   'SU_05.FIECHI'  (Turbulent)                1/25/91
/
/       This is the 2D model of a diffuser with an angle of divergence
/       equal to 15 deg and with 4.19 incidence angle at the inlet, and
/       turning channel. This model implements suction with the velocity
/       at each hole Vo=0.1845 ft/s @ a 45 deg angle to the diffuser.
/       The config is such that 5% of the inlet mass flow rate is sucked
/       out through the bottom only.
/
/               Created by
/
/               G. Wissinger
/               Rochester Institute of Technology
/               January, 1991
/
/       dimensionLESS Analysis
/               Vin = 1.292 ft/s
/               incid = 4.19 deg
/
/               mass flow rate in = mi = 0.20887 slug/s/ft
/               mass flow rate suction = ms (5%) = 0.010443 slug/s/ft
/               mass flow rate suction/slit/ft = 0.0014919 slug/s slit/ft
/
/               y-vel at a slit = 0.1134  (nondim)
/               x-vel at a slit = 0.08698  (nondim)
/
/               Lst = Total suction length = 0.3265 in
/               Length of each slit = Ls = 0.05 in
/               Ns = Number of slits = Lst/Ls = 7
/                       Each slit is spaced at 0.5 in intervals
/               Re = 10.0e3
/
/               Fluid = Water
/               density = 1.94 slug/ft^3
/               abs viscosity = 2.089e-5 lbf s/ft^2
/
/
/
*TITLE
SU_05 -- 5% Suction through TOP only
*FIMESH(2-D,IMAX=39,JMAX=3,MXPOINT=2000)
EXPI(DELTAS)
1 0 12 0 2 0 6 0 2 0 6 0 11 0 2 0 10 0 2 0 10 0 2 0 10,
0 2 0 10 0 2 0 60 0 16 0 40
EXPJ(DELTAS)
1 0 18
/
/       Spacial dimensions in IN
POINT
/  i j k    x        y         z
/
/       MAJOR key points
1   1   1   1   4.0       -0.5
20  1   3   1   4.0        0.5
6   11  1   1   5.0       -0.5
25  11  3   1   5.0        0.5
17  33  1   1   14.053    -1.6918
36  33  3   1   14.053     1.6918
18  35  1   1   17.4366   -1.6918
37  35  3   1   17.4366    1.6918
```

```
27  15  3  1  5.5205   0.5685
7   13  1  1  5.4709  -0.5620
8   15  1  1  5.5205  -0.5685
28  17  3  1  5.9667   0.6273
29  19  3  1  6.0162   0.6338
9   17  1  1  5.9667  -0.6273
10  19  1  1  6.0162  -0.6338
30  21  3  1  6.4624   0.6925
31  23  3  1  6.5119   0.6991
11  21  1  1  6.4624  -0.6925
12  23  1  1  6.5119  -0.6991
32  25  3  1  6.9581   0.7578
33  27  3  1  7.0077   0.7643
13  25  1  1  6.9581  -0.7578
14  27  1  1  7.0077  -0.7643
34  29  3  1  7.4538   0.8231
35  31  3  1  7.5034   0.8296
15  29  1  1  7.4538  -0.8231
16  31  1  1  7.5034  -0.8296
/
/       Mesh is graduated towards the edges
LINE
/
/       Vertical lines
1  20 1.0 3 1.0 .5
6  25 1.0 3 1.0 .5
17 36 1.5 3 1.5 .5
18 37 1.5 3 1.5 .5
19 38 1.5 3 1.5 .5
/
/       Bottom
1  2
2  3
3  4
4  5
5  6
6  7  1.5 3
7  8
8  9
9  10
10 11
11 12
12 13
13 14
14 15
15 16
16 17  4 3
17 18
/
/       Top
20 21
21 22
22 23
23 24
24 25
25 26  1.5 3
26 27
27 28
28 29
29 30
```

```
30 31
31 32
32 33
33 34
34 35
35 36   4 3
36 37
/
/
ARC
37 38 40
18 19 40
/
/
SURFACE
1 38
/
/
ELEMENTS(QUAD,NODES=4,ALL)
ELEMENTS(boundary,EDGE,NODES=2)
1  2
3  4
5  6
6  7
8  9
10 11
12 13
14 15
16 19
20 21
22 23
24 25
25 26
27 28
29 30
31 32
33 34
35 38
/
/       Velocities in FT/S
BCNODE(UX)
/       Inlet
1 20  0.99732
/       no slip
1  2
3  4
5  6
6  7
8  9
10 11
12 13
14 15
16 19
20 21
22 23
24 25
25 26
27 28
29 30
31 32
```

```
33 34
35 38
/       Suction
2  3
4  5
7  8
9  10
11 12
13 14
15 16
21 22
23 24
26 27
28 29
30 31
32 33
34 35
/
BCNODE(UY)
/       Inlet
1 20  -0.073065
/       no slip
1  2
3  4
5  6
6  7
8  9
10 11
12 13
14 15
16 19
20 21
22 23
24 25
25 26
27 28
29 30
31 32
33 34
35 38
/       Suction
2  3
4  5
7  8
9  10
11 12
13 14
15 16
21 22
23 24
26 27
28 29
30 31
32 33
34 35
/
/       k is in FT^2/S^2
BCNODE(KINETIC)
1 20  0.005
/
```

```
/       epsilon is in FT^2/S^3
BCNODE(DISSIPATION)
1 20  0.0010591
/
number
2 1
/
END
/
/
*PROBLEM(NONLINEAR,TURB)
*EXEC(newjob)
/                                /
/       NONdimensionalize the problem using values at the INLET to the
/       test section as characteristic
/
/               Lc = 1 IN               : (L*=L/Lc)
/               Vc = 1.292   FT/S       : (V*=V/Vc)
/               Kc =           S^2/FT^2 : (K*=K*Kc=K/U^2;    Kc=1/U^2)
/               Ec =           S^3/FT^2 : (E*=E*Ec=E*Lc/U^3; Ec=Lc/U^3)
/
/
/       Invoke non-dimensional model
*DENSITY(CONSTANT=1.0)
*VISCOSITY(K.E.)
1.0e-5
/
/
/       the 'mixed' keyword tells FIDAP to solve for pressure also
*PRESSURE(MIXED=1E-15)
/
/       This method of solving the system is recommended for turbulent cases.
/       It doesn't converge as fast but it uses less storage space.
*SOLUTION(segr=500)
/
/       Give initial guesses to the solution
*ICNODE(UX,CONSTANT= 0.997329)
*ICNODE(UY,CONSTANT=-0.073065)
*ICNODE(KINETIC,CONSTANT=0.005)
*ICNODE(DISSIPATION,CONSTANT=0.0010591)
/
/
*OPTIONS(UPWINDING)
/
/       Invoke the relaxation parameters to help convergence
*relaxation
/ux  uy  uz  P    T    s    k    e    c1   c2   ?
0.2 0.2 0.2 0.2 0.05 0.0 0.15 0.15 0.05 0.05 0.2
/
/
*POSTPROCESS(ALL)
/
/       allows ALL parameters to be written to the .FDOUT file
*PRINTOUT(ALL)
/
/
*NODES(FIMESH)
*ELEMENTS(QUAD,NODES=4,FIMESH)
*ELEMENTS(WALL,NODES=2,FIMESH)
*ELEMENTS(WALL,NODES=2,FIMESH)
```

```
*ELEMENTS(WALL,NODES=2,FIMESH)
*ELEMENTS(WALL,NODES=2,FIMESH)
*ELEMENTS(WALL,NODES=2,FIMESH)
*ELEMENTS(WALL,NODES=2,FIMESH)
*ELEMENTS(WALL,NODES=2,FIMESH)
*ELEMENTS(WALL,NODES=2,FIMESH)
*ELEMENTS(WALL,NODES=2,FIMESH)
*ELEMENTS(WALL,NODES=2,FIMESH)
*ELEMENTS(WALL,NODES=2,FIMESH)
*ELEMENTS(WALL,NODES=2,FIMESH)
*ELEMENTS(WALL,NODES=2,FIMESH)
*ELEMENTS(WALL,NODES=2,FIMESH)
*ELEMENTS(WALL,NODES=2,FIMESH)
*ELEMENTS(WALL,NODES=2,FIMESH)
*ELEMENTS(WALL,NODES=2,FIMESH)
*print(all)
*END
```

```
19  37  1  1  20.4266  -7.3201
38  37  3  1  23.8836  -9.3789
40  0   0  0  16.9266  -5.8105
/
/       SUCTION HOLE key points
21   3  3  1  4.475    0.5
22   5  3  1  4.525    0.5
2    3  1  1  4.475   -0.5
3    5  1  1  4.525   -0.5
23   7  3  1  4.725    0.5
24   9  3  1  4.775    0.5
4    7  1  1  4.725   -0.5
5    9  1  1  4.775   -0.5
26  13  3  1  5.4709   0.5620
27  15  3  1  5.5205   0.5685
7   13  1  1  5.4709  -0.5620
8   15  1  1  5.5205  -0.5685
28  17  3  1  5.9667   0.6273
29  19  3  1  6.0162   0.6338
9   17  1  1  5.9667  -0.6273
10  19  1  1  6.0162  -0.6338
30  21  3  1  6.4624   0.6925
31  23  3  1  6.5119   0.6991
11  21  1  1  6.4624  -0.6925
12  23  1  1  6.5119  -0.6991
32  25  3  1  6.9581   0.7578
33  27  3  1  7.0077   0.7643
13  25  1  1  6.9581  -0.7578
14  27  1  1  7.0077  -0.7643
34  29  3  1  7.4538   0.8231
35  31  3  1  7.5034   0.8296
15  29  1  1  7.4538  -0.8231
16  31  1  1  7.5034  -0.8296
/
/       Mesh is graduated towards the edges
LINE
/
/       Vertical lines
1  20 1.0 3 1.0 .5
6  25 1.0 3 1.0 .5
17 36 1.5 3 1.5 .5
18 37 1.5 3 1.5 .5
19 38 1.5 3 1.5 .5
/
/       Bottom
1  2
2  3
3  4
4  5
5  6
6  7 1.5 3
7  8
8  9
9  10
10 11
11 12
12 13
13 14
14 15
15 16
```

```
16 17   4 3
17 18
/
/        Top
20 21
21 22
22 23
23 24
24 25
25 26 1.5 3
26 27
27 28
28 29
29 30
30 31
31 32
32 33
33 34
34 35
35 36   4 3
36 37
/
/
ARC
37 38 40
18 19 40
/
/
SURFACE
1 38
/
/
ELEMENTS(QUAD,NODES=4,ALL)
ELEMENTS(boundary,EDGE,NODES=2)
1  2
3  4
5  6
6  7
8  9
10 11
12 13
14 15
16 19
20 21
22 23
24 25
25 26
27 28
29 30
31 32
33 34
35 38
/
/        Velocities in FT/S
BCNODE(UX)
/        Inlet
. 20  0.99732
/        no slip
1  2
3  4
```

```
5  6
6  7
8  9
10 11
12 13
14 15
16 19
20 21
22 23
24 25
25 26
27 28
29 30
31 32
33 34
35 38
/        Suction
2  3
4  5
7  8
9  10
11 12
13 14
15 16
21 22   0.1134
23 24   0.1134
26 27   0.1134
28 29   0.1134
30 31   0.1134
32 33   0.1134
34 35   0.1134
/
BCNODE(UY)
/         Inlet
1 20   -0.073065
/         no slip
1  2
3  4
5  6
6  7
8  9
10 11
12 13
14 15
16 19
20 21
22 23
24 25
25 26
27 28
29 30
31 32
33 34
35 38
/        Suction
2  3
4  5
7  8
9  10
11 12
```

```
13 14
15 16
21 22   0.08698
23 24   0.08698
26 27   0.08698
28 29   0.08698
30 31   0.08698
32 33   0.08698
34 35   0.08698
/
/       k is in FT^2/S^2
BCNODE(KINETIC)
1 20   0.005
/
/       epsilon is in FT^2/S^3
BCNODE(DISSIPATION)
1 20   0.0010591
/
number
2 1
/
END
/
/
*PROBLEM(NONLINEAR,TURB)
*EXEC(newjob)
/
/       NONdimensionalize the problem using values at the INLET to the
/       test section as characteristic
/
/               Lc = 1 IN               : (L*=L/Lc)
/               Vc = 1.292   FT/S       : (V*=V/Vc)
/               Kc =           S^2/FT^2 : (K*=K*Kc=K/U^2;    Kc=1/U^2)
/               Ec =           S^3/FT^2 : (E*=E*Ec=E*Lc/U^3; Ec=Lc/U^3)
/
/
/       Invoke non-dimensional model
*DENSITY(CONSTANT=1.0)
*VISCOSITY(K.E.)
1.0e-4
/
/
/       the 'mixed' keyword tells FIDAP to solve for pressure also
*PRESSURE(MIXED=1E-15)
/
/       This method of solving the system is recommended for turbulent cases.
/       It doesn't converge as fast but it uses less storage space.
*SOLUTION(segr=500)
/
/       Give initial guesses to the solution
*ICNODE(UX,CONSTANT=0.997329)
*ICNODE(UY,CONSTANT=-0.073065)
*ICNODE(KINETIC,CONSTANT=0.005)
*ICNODE(DISSIPATION,CONSTANT=0.0010591)
/
/
*OPTIONS(UPWINDING)
/
/       Invoke the relaxation parameters to help convergence
*relaxation
```

```
/ux   uy   uz   P     T    s     k     e    c1    c2    ?
0.2 0.2 0.2 0.2 0.05 0.0 0.15 0.15 0.05 0.05 0.2
/
/
*POSTPROCESS(ALL)
/
/       allows ALL parameters to be written to the .FDOUT file
*PRINTOUT(ALL)
/
/
*NODES(FIMESH)
*ELEMENTS(QUAD,NODES=4,FIMESH)
*ELEMENTS(WALL,NODES=2,FIMESH)
*ELEMENTS(WALL,NODES=2,FIMESH)
*ELEMENTS(WALL,NODES=2,FIMESH)
*ELEMENTS(WALL,NODES=2,FIMESH)
*ELEMENTS(WALL,NODES=2,FIMESH)
*ELEMENTS(WALL,NODES=2,FIMESH)
*ELEMENTS(WALL,NODES=2,FIMESH)
*ELEMENTS(WALL,NODES=2,FIMESH)
*ELEMENTS(WALL,NODES=2,FIMESH)
*ELEMENTS(WALL,NODES=2,FIMESH)
*ELEMENTS(WALL,NODES=2,FIMESH)
*ELEMENTS(WALL,NODES=2,FIMESH)
*ELEMENTS(WALL,NODES=2,FIMESH)
*ELEMENTS(WALL,NODES=2,FIMESH)
*ELEMENTS(WALL,NODES=2,FIMESH)
*ELEMENTS(WALL,NODES=2,FIMESH)
*ELEMENTS(WALL,NODES=2,FIMESH)
*print(all)
*END
```

```
/---------->>> title    ' bl_05.FIECHI'  (Turbulent)              1/25/91
/
/       This is the 2D model of a diffuser with an angle of divergence
/       equal to 15 deg and with 4.19 incidence angle at the inlet, and
/       turning channel. This model implements blowing with the velocity
/       at each hole Vo=0.2583 ft/s tangential to the flow in the diffuser.
/       The config is such that 5% of the inlet mass flow rate is blown
/       in through the BOTTOM only.
/
/               Created by
/
/               G. Wissinger
/               Rochester Institute of Technology
/               January, 1991
/
/       dimensionLESS Analysis
/               Vin = 1.292 ft/s
/               incid = 4.19 deg
/
/               mass flow rate in = mi = 0.20887 slug/s/ft
/               mass flow rate blowing = mb (10%) = 0. slug/s/ft
/               mass flow rate blowing/slit/ft = 0. slug/s slit/ft
/
/               y-vel at a slit = 0.0  (nondim)
/               x-vel at a slit = 0.1999  (nondim)
/
/               Lst = Total blowing length = 0.3265 in
/               Length of each slit = Ls = 0.05 in
/               Ns = Number of slits = Lst/Ls = 7
/                       Each slit is spaced at 0.5 in intervals
/               Re = 10.0e3
/
/               Fluid = Water
/               density = 1.94 slug/ft^3
/               abs viscosity = 2.089e-5 lbf s/ft^2
/
/
/
*TITLE
BL_05 -- 05% blowing on TOP only
*FIMESH(2-D,IMAX=39,JMAX=3,MXPOINT=2000)
EXPI(DELTAS)
1 0 12 0 2 0 6 0 2 0 6 0 11 0 2 0 10 0 2 0 10 0 2 0 10,
0 2 0 10 0 2 0 60 0 16 0 40
EXPJ(DELTAS)
1 0 18
/
/       Spacial dimensions in IN
POINT
/  i  j  k    x        y         z
/
/       MAJOR key points
1    1    1   1   4.0        -0.5
20   1    3   1   4.0         0.5
6    11   1   1   5.0        -0.5
25   11   3   1   5.0         0.5
17   33   1   1   14.053     -1.6918
36   33   3   1   14.053      1.6918
18   35   1   1   17.4366    -1.6918
37   35   3   1   17.4366     1.6918
```

```
19   37   1   1   20.4266   -7.3201
38   37   3   1   23.8836   -9.3789
40   0    0   0   16.9266   -5.8105
/
/        SUCTION HOLE key points
21    3   3   1   4.475      0.5
22    5   3   1   4.525      0.5
2     3   1   1   4.475     -0.5
3     5   1   1   4.525     -0.5
23    7   3   1   4.725      0.5
24    9   3   1   4.775      0.5
4     7   1   1   4.725     -0.5
5     9   1   1   4.775     -0.5
26   13   3   1   5.4709     0.5620
27   15   3   1   5.5205     0.5685
7    13   1   1   5.4709    -0.5620
8    15   1   1   5.5205    -0.5685
28   17   3   1   5.9667     0.6273
29   19   3   1   6.0162     0.6338
9    17   1   1   5.9667    -0.6273
10   19   1   1   6.0162    -0.6338
30   21   3   1   6.4624     0.6925
31   23   3   1   6.5119     0.6991
11   21   1   1   6.4624    -0.6925
12   23   1   1   6.5119    -0.6991
32   25   3   1   6.9581     0.7578
33   27   3   1   7.0077     0.7643
13   25   1   1   6.9581    -0.7578
14   27   1   1   7.0077    -0.7643
34   29   3   1   7.4538     0.8231
35   31   3   1   7.5034     0.8296
15   29   1   1   7.4538    -0.8231
16   31   1   1   7.5034    -0.8296
/
/        Mesh is graduated towards the edges
LINE
/
/        Vertical lines
1   20 1.0 3 1.0 .5
6   25 1.0 3 1.0 .5
17  36 1.5 3 1.5 .5
18  37 1.5 3 1.5 .5
19  38 1.5 3 1.5 .5
/
/        Bottom
1   2
2   3
3   4
4   5
5   6
6   7   1.5 3
7   8
8   9
9   10
10  11
11  12
12  13
13  14
14  15
15  16
```

```
16 17   4 3
17 18
/
/        Top
20 21
21 22
22 23
23 24
24 25
25 26   1.5 3
26 27
27 28
28 29
29 30
30 31
31 32
32 33
33 34
34 35
35 36   4 3
36 37
/
/
ARC
37 38 40
18 19 40
/
/
SURFACE
1 38
/
/
ELEMENTS(QUAD,NODES=4,ALL)
ELEMENTS(boundary,EDGE,NODES=2)
1  2
3  4
5  6
6  7
8  9
10 11
12 13
14 15
16 19
20 21
22 23
24 25
25 26
27 28
29 30
31 32
33 34
35 38
/
/        Velocities in FT/S
BCNODE(UX)
/        Inlet
1 20   0.99732
/        no slip
1  2
3  4
```

```
5  6
6  7
8  9
10 11
12 13
14 15
16 19
20 21
22 23
24 25
25 26
27 28
29 30
31 32
33 34
35 39
/        Blowing
2  3
4  5
7  8
9  10
11 12
13 14
15 16
21 22
23 24
26 27   0.1999
28 29   0.1999
30 31   0.1999
32 33   0.1999
34 35   0.1999
/
BCNODE(UY)
/         Inlet
1 20   -0.073065
/         no slip
1  2
3  4
5  6
6  7
8  9
10 11
12 13
14 15
16 19
20 21
22 23
24 25
25 26
27 28
29 30
31 32
33 34
35 38
/         Blowing
2  3    0.0
4  5    0.0
7  8    0.0
9  10   0.0
11 12   0.0
```

```
13 14   0.0
15 16   0.0
21 22
23 24
26 27
28 29
30 31
32 33
34 35
/
/       k is in FT^2/S^2
BCNODE(KINETIC)
1 20   0.005
/
/       epsilon is in FT^2/S^3
BCNODE(DISSIPATION)
1 20   0.0010591
/
number
2 1
/
END
/
/
*PROBLEM(NONLINEAR,TURB)
*EXEC(newjob)
/
/       NONdimensionalize the problem using values at the INLET to the
/       test section as characteristic
/
/               Lc = 1 IN               : (L*=L/Lc)
/               Vc = 1.292   FT/S       : (V*=V/Vc)
/               Kc =           S^2/FT^2 : (K*=K*Kc=K/U^2;     Kc=1/U^2)
/               Ec =           S^3/FT^2 : (E*=E*Ec=E*Lc/U^3; Ec=Lc/U^3)
/
/
/       Invoke non-dimensional model
*DENSITY(CONSTANT=1.0)
*VISCOSITY(K.E.)
1.0e-4
/
/
/       the 'mixed' keyword tells FIDAP to solve for pressure also
*PRESSURE(MIXED=1E-15)
/
/       This method of solving the system is recommended for turbulent cases.
/       It doesn't converge as fast but it uses less storage space.
*SOLUTION(segr=500)
/
/       Give initial guesses to the solution
*ICNODE(UX,CONSTANT=0.997329)
*ICNODE(UY,CONSTANT=-0.073065)
*ICNODE(KINETIC,CONSTANT=0.005)
*ICNODE(DISSIPATION,CONSTANT=0.0010591)
/
/
*OPTIONS(UPWINDING)
/
/       Invoke the relaxation parameters to help convergence
*relaxation
```

```
/ux   uy   uz   P     T    s     k     e    c1    c2    ?
0.2 0.2 0.2 0.2 0.05 0.0 0.15 0.15 0.05 0.05 0.2
/
/
*POSTPROCESS(ALL)
/
/       allows ALL parameters to be written to the .EDOUT file
*PRINTOUT(ALL)
/
/
*NODES(FIMESH)
*ELEMENTS(QUAD,NODES=4,FIMESH)
*ELEMENTS(WALL,NODES=2,FIMESH)
*ELEMENTS(WALL,NODES=2,FIMESH)
*ELEMENTS(WALL,NODES=2,FIMESH)
*ELEMENTS(WALL,NODES=2,FIMESH)
*ELEMENTS(WALL,NODES=2,FIMESH)
*ELEMENTS(WALL,NODES=2,FIMESH)
*ELEMENTS(WALL,NODES=2,FIMESH)
*ELEMENTS(WALL,NODES=2,FIMESH)
*ELEMENTS(WALL,NODES=2,FIMESH)
*ELEMENTS(WALL,NODES=2,FIMESH)
*ELEMENTS(WALL,NODES=2,FIMESH)
*ELEMENTS(WALL,NODES=2,FIMESH)
*ELEMENTS(WALL,NODES=2,FIMESH)
*ELEMENTS(WALL,NODES=2,FIMESH)
*ELEMENTS(WALL,NODES=2,FIMESH)
*ELEMENTS(WALL,NODES=2,FIMESH)
*ELEMENTS(WALL,NODES=2,FIMESH)
*ELEMENTS(WALL,NODES=2,FIMESH)
*ELEMENTS(WALL,NODES=2,FIMESH)
*print(all)
*END
```

APPENDIX D - Determination of δ^*

As was indicated in Section 3-1.0, the boundary layer thickness is an important factor in determining the characteristics of a diffuser's performance. The displacement thicknes δ^* was defined as

$$\delta^* = \int_0^{\delta} (1 - \frac{u}{v_t})\, dy \qquad (3.7)$$

The models run on FIDAP generate velocity vectors at every node. From these vectors, the speed accross the inlet and outlet can be determined (see Appendix B) and plotted as a function of y. The resulting data can then be curve fit using a fifth-order polynomial to determine an aproximation for $\frac{u}{v_t}$. Figures D.1-D.9 are the resulting curve fits generated using Cricket Graph^{tm} for the inlet (top) and outlet (bottom) speeds. (NOTE: u/v_t is on the 2-axis and y^* the 1-axis.)

Further, if the substitution $\eta = \frac{y}{\delta}$ is made and $\frac{u}{v_t} = f(y)$, where f(y) is the curve fit equation, then (3.7) becomes

$$\delta^* = \int_0^1 (1 - f(y))\, \delta\, d\eta$$

Integration and substitution leads to the following result

$$\delta^* = (1\text{-}a) - b\delta - c\delta^2 - d\delta^3 - e\delta^4 - f\delta^5$$

where a, b, c, d, e, f are the coefficients on the polynomial and δ the boundary layer thickness which can be approximated by using the result of turbulent flow over a flat plate given by

$$\delta = \frac{0.340\ x}{Re_x^{0.2}}$$

x is the distance along the plate, in this case 1 in at the inlet and 9 in at the outlet and Re_x is the corresponding Reynolds number.

A FORTRAN program was written to calculate δ^* for each model. The results were used to calculate B_t in Table 7.1 and are given in Table D.1

Table D.1 - Displacement Thickness at Inlet and Outlet

Model	δ_i^*	δ_o^*
100% Flow	0.3132	0.4957
60% Flow	0.1381	0.3305
5% Suction	0.2033	0.4731
10% Suction	0.2376	0.5349
15% Suction	0.2275	0.6174
20% Suction	0.2061	0.6667
5% Blowing	0.2151	0.3761
10% Blowing	0.1460	0.4551
15% Blowing	0.0010	0.5735

Figure D.1 - Design Flow, Speed Curve Fit

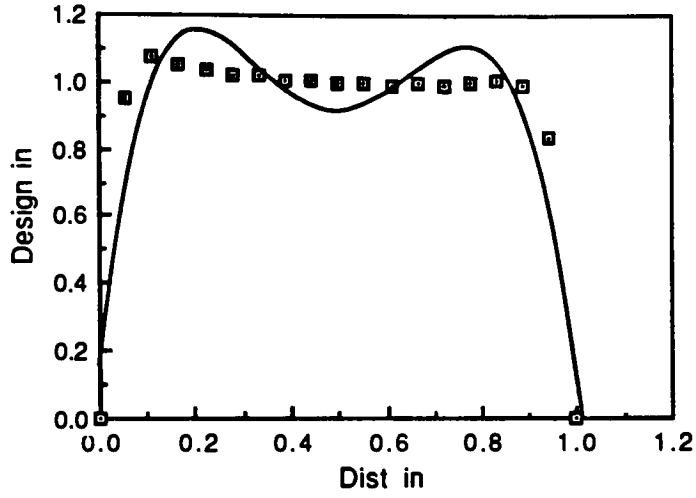

y = 0.15372 + 12.411x - 51.788x^2 + 84.259x^3 - 52.089x^4 + 7.1944x^5

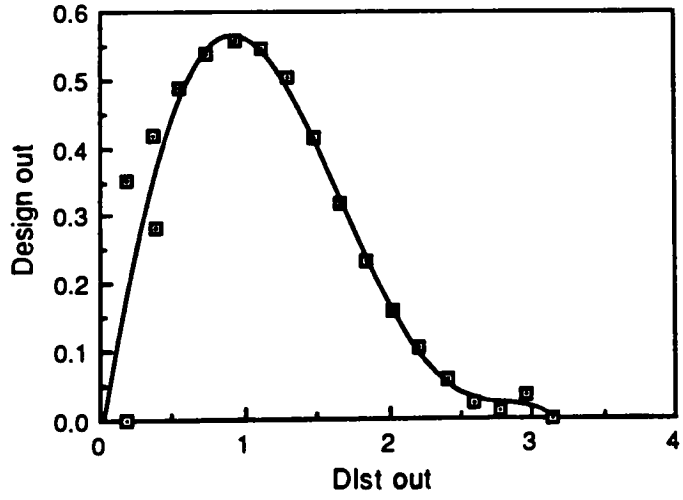

y = - 4.2526e-2 + 1.2801x - 0.46797x^2 - 0.42991x^3 + 0.25858x^4 - 3.66

Figure D.2 - 60% Flow, Speed Curve Fit

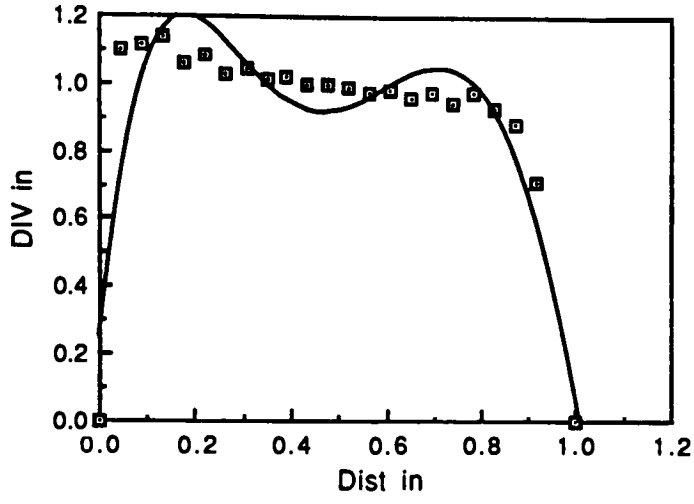

y = 0.24995 + 13.830x - 68.256x^2 + 135.80x^3 - 115.38x^4 + 33.817x^5

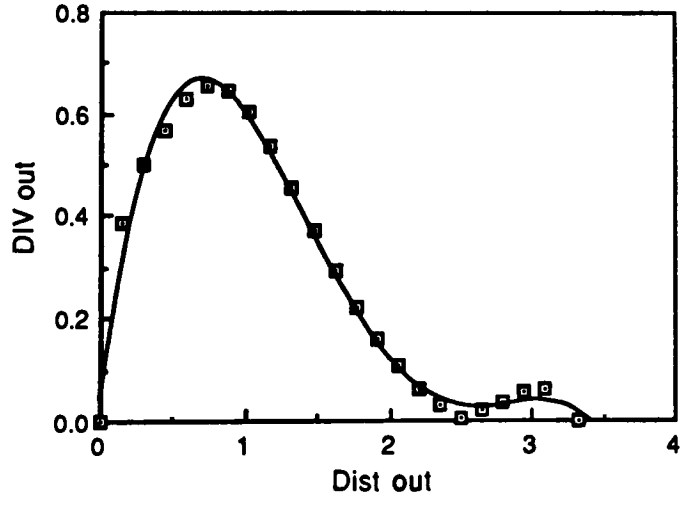

y = 4.0196e-2 + 2.1365x - 2.2867x^2 + 0.80954x^3 - 9.4925e-2x^4 R^2 =

Figure D.3 - 5% Suction, Speed Curve Fit

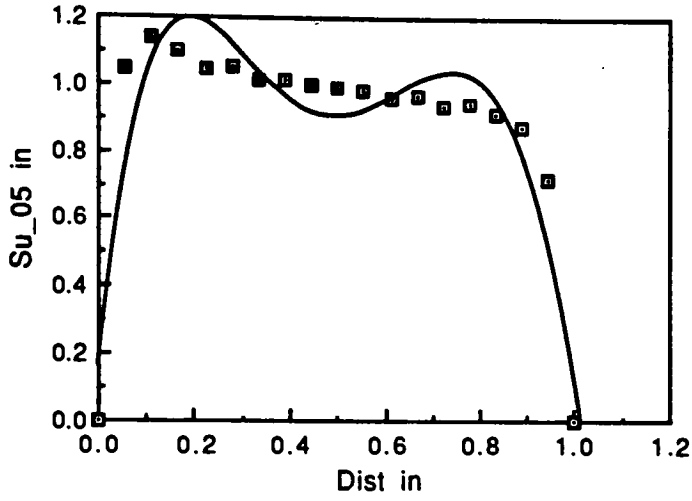

y = 0.16454 + 13.925x - 63.717x^2 + 116.97x^3 - 90.067x^4 + 22.856x^5

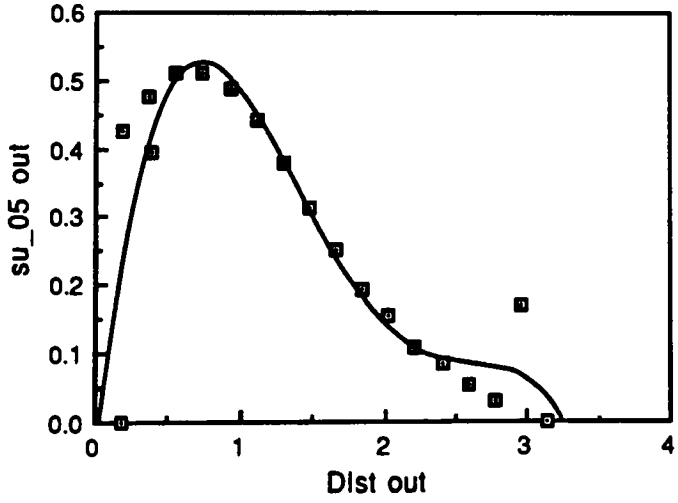

y = - 7.0325e-2 + 1.9664x - 2.0784x^2 + 0.76460x^3 - 9.5114e-2x^4 R^2

Figure D.4 - 10% Suction, Speed Curve Fit

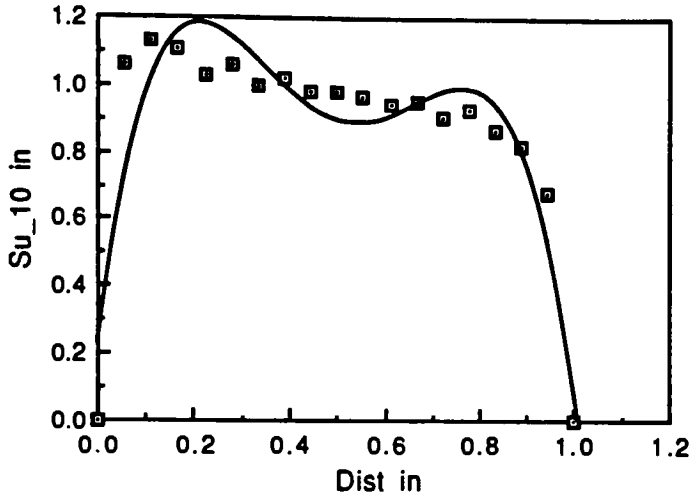

y = 0.22603 + 11.334x - 44.364x^2 + 64.650x^3 - 31.783x^4 R^2 = 0.852

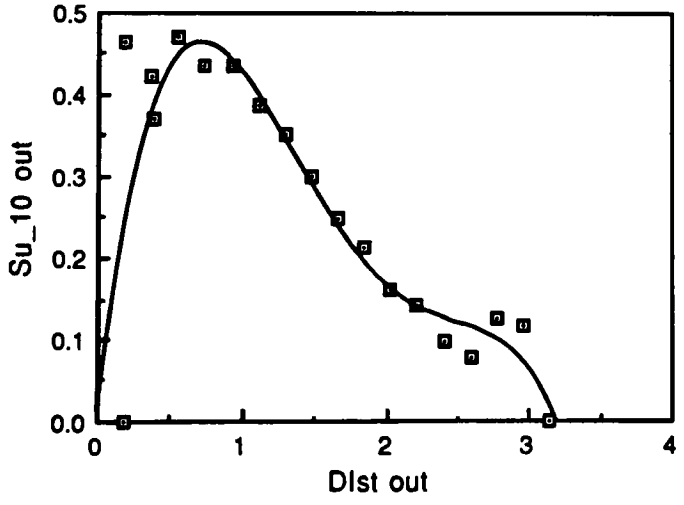

y = 1.4076e-2 + 1.5214x - 1.6524x^2 + 0.62757x^3 - 8.1307e-2x^4 R^2 =

Figure D.5 - 15% Suction, Speed Curve Fit

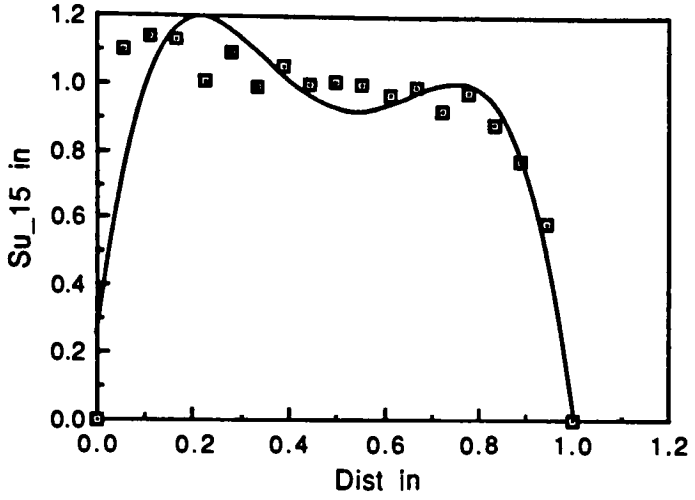

y = 0.24540 + 11.140x - 43.402x^2 + 63.333x^3 - 31.298x^4 R^2 = 0.858

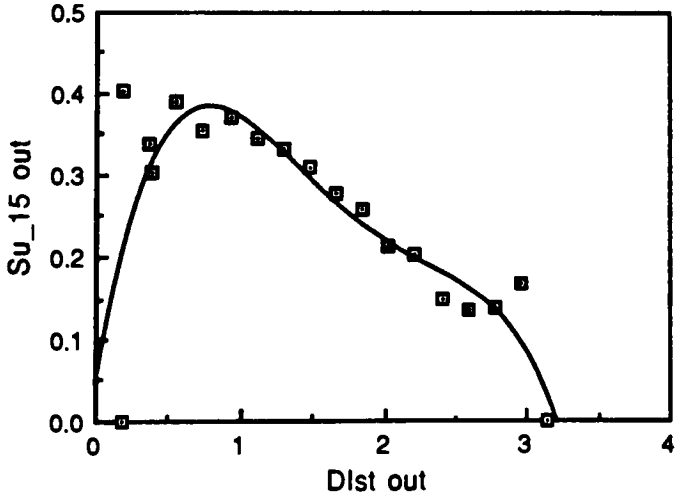

y = 4.5332e-2 + 1.0714x - 1.1097x^2 + 0.42185x^3 - 5.6494e-2x^4 R^2 =

Figure D.6 - 20% Suction, Speed Curve Fit

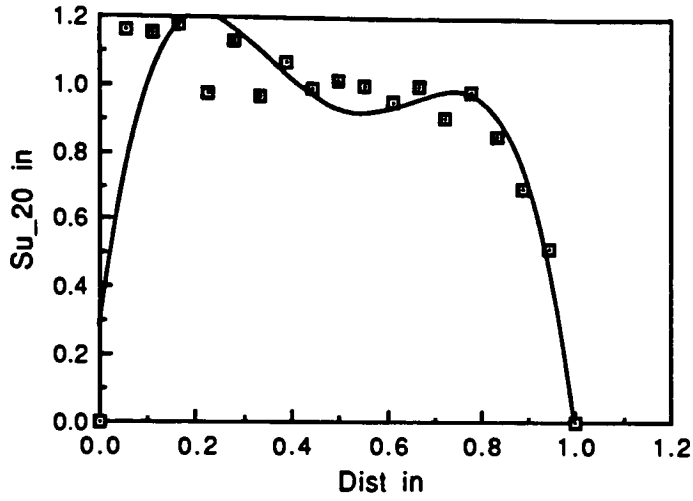

y = 0.27651 + 10.932x - 42.608x^2 + 62.022x^3 - 30.639x^4 R^2 = 0.834

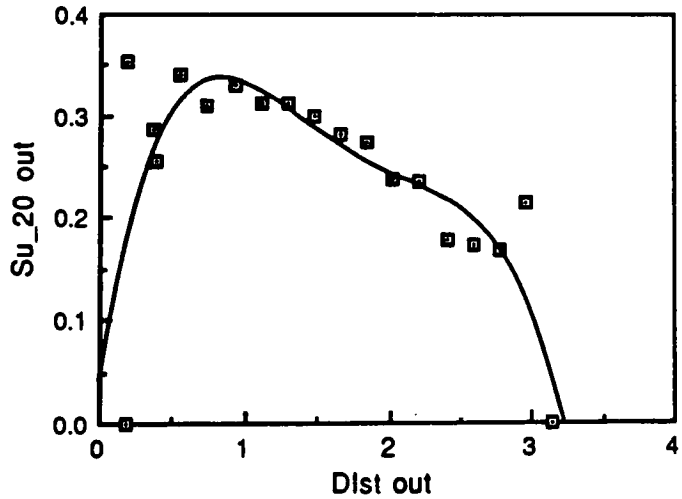

y = 4.1123e-2 + 0.90606x - 0.93090x^2 + 0.36864x^3 - 5.2180e-2x^4 R^2

Figure D.7 - 5% Blowing, Speed Curve Fit

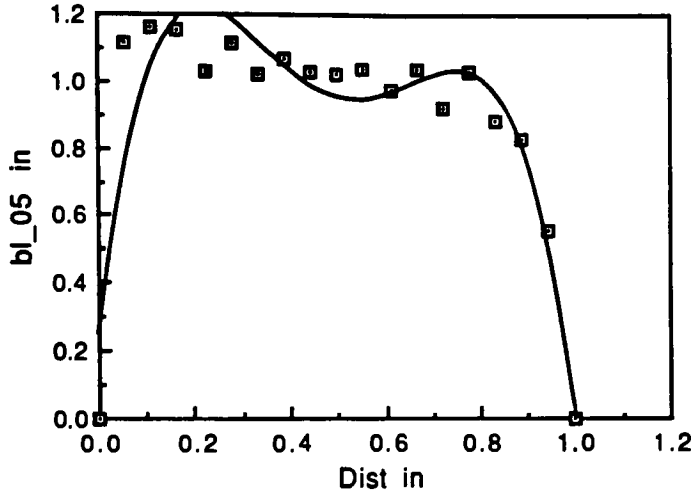

y = 0.25089 + 11.325x - 44.124x^2 + 64.536x^3 - 31.981x^4 R^2 = 0.859

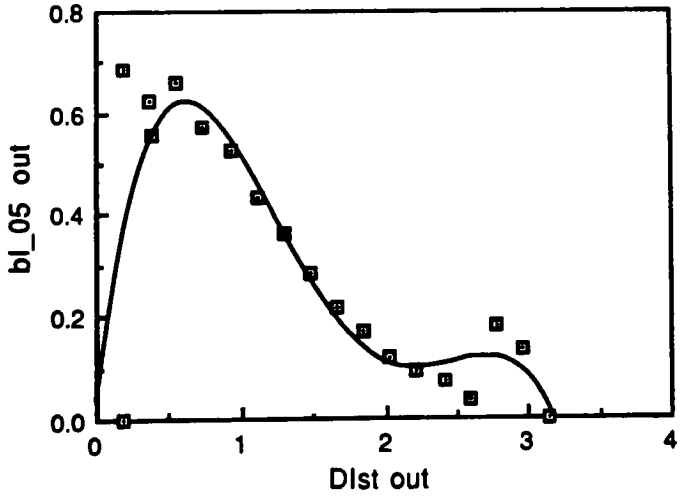

y = 3.8154e-2 + 2.2497x - 2.7294x^2 + 1.1104x^3 - 0.14960x^4 R^2 = 0.

Figure D.8 - 10% Blowing, Speed Curve Fit

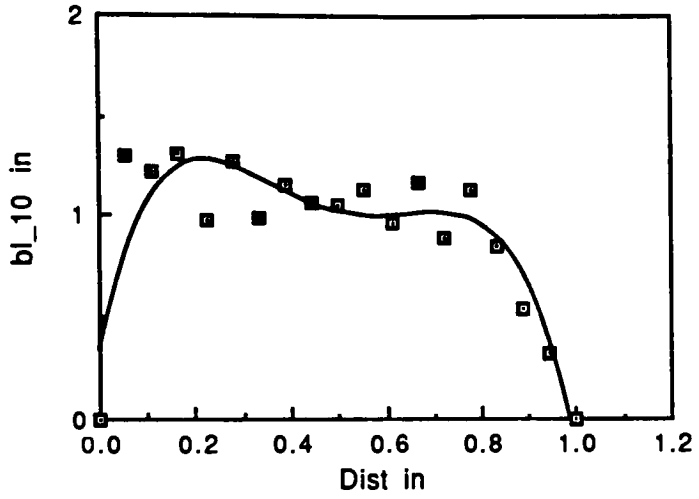

y = 0.33897 + 10.916x - 41.848x^2 + 60.515x^3 - 30.051x^4 R^2 = 0.790

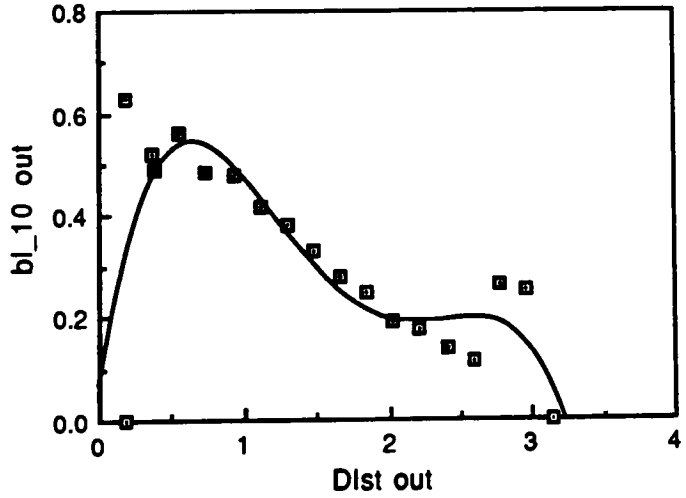

y = 6.5715e-2 + 1.7906x - 2.1434x^2 + 0.88478x^3 - 0.12221x^4 R^2 = 0

Figure D.9 - 15% Blowing, Speed Curve Fit

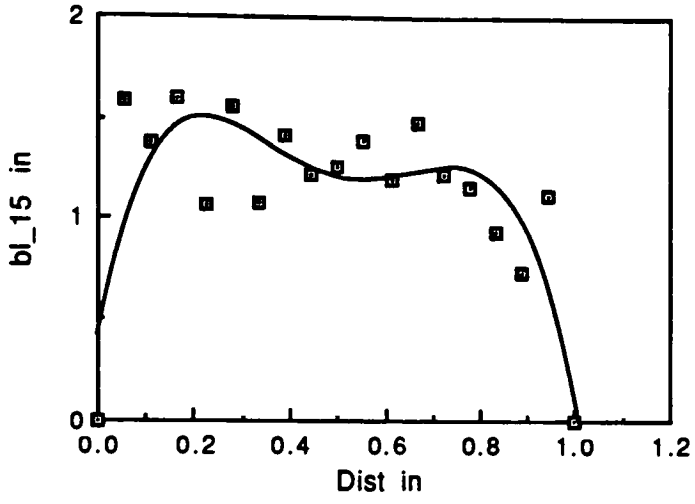

y = 0.41502 + 12.589x - 48.345x^2 + 69.951x^3 - 34.495x^4 R^2 = 0.642

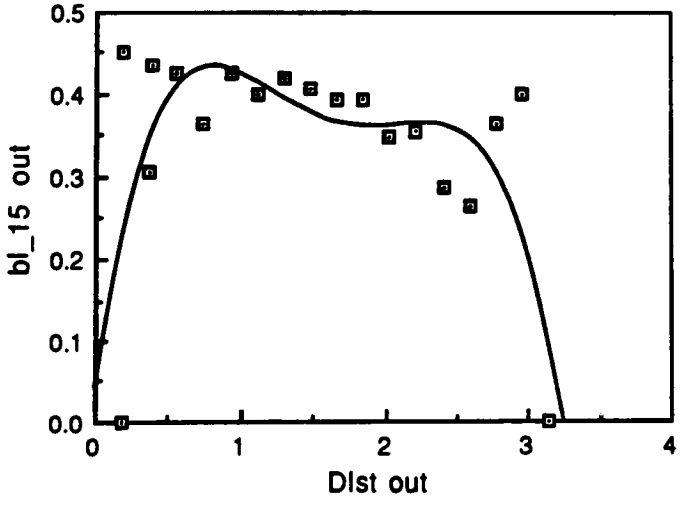

y = 4.0481e-2 + 1.2747x - 1.4037x^2 + 0.60478x^3 - 9.0763e-2x^4 R^2 =